國立臺灣大學理學院地質科學系
博士論文
Department of Geosciences
College of Science
National Taiwan University
Ph.D. Dissertation

過去三十六萬年來印度–太平洋暖池海水表面溫度與水文動態研究

Indo-Pacific Warm Pool Sea Surface Temperature and Hydrological Dynamics during the Past 360,000 Years

研究生：羅 立（Li Lo）撰

指導教授：沈川洲 博士

魏國彥 博士

Advisors: Chuan-Chou Shen, Ph.D.
Kuo-Yen Wei, Ph.D.

民國一百零三年六月
June 2014

ABSTRACT

In this study, we reconstructed the high resolution sea surface temperature (SST), and rain fall belt variations, and identified the non-linear relationship between low latitude Indo-Pacific warm pool (IPWP) and greenhouse gases radiative forcing during the past 360,000 years by using the marine sediment core, MD05-2925 (9.3^{o}S, 151.5^{o}E, water depth 1661 m), located in the Solomon Sea.

For the past few decades, global climate changes have raised popular awareness of the fact that the air-sea thermal-hydrological conditions are crucial to large population's lives and land management. However, the lack of long-term observation records and complex geography configuration hinder the understanding of the low latitude IPWP region. Here we attempt to reconcile the following: (1) teleconnections between both North and South Hemisphere (NH and SH) high latitude climate systems during the fast climate change period; (2) orbital configuration control to the rain fall belt, intertropical convergence zone (ITCZ) shifting; (3) greenhouses gases radiative forcing control to the IPWP surface thermal condition. To achieve these goals, we first reconstructed a well-constrained age model by using radiocarbon dates and composite benthic foraminiferal $\delta^{18}O$ stratigraphy. Surface dweller planktonic foraminifera, *Globigerinoides ruber* (white, *s.s.*, 250-300 μm), was used for measuring Mg, and REE/Ca ratios were applied to SST and precipitation conditions, respectively. Compilations of the previous studies were also applied for supporting regional climate interpretations.

The summary of the main results in this study are the following: first, during the last termination, South-IPWP SSTs were warmed earlier than those of North-IPWP, and during the NH cooling events (e.g. Heinrich event 1 and Younger Dryas,

H1 and YD), S-IPWP SSTs also warmed faster than the N-IPWP. For the precipitation pattern, N- and S-IPWP both show decreases during the H1 and YD. Southward shifting of ITCZ in the IPWP regions could be interpreted by the atmospheric teleconnection and/or the oceanic forcing from the relative warmer S-IPWP. Second, the orbital timescales of ITCZ shifting histories were reconstructed based in the *G. ruber* REE/Ca ratios generated from the site MD05-2925. REE/Ca in the Solomon Sea could be used as a new proxy related to the Papua New Guinea (PNG) precipitation/chemical weathering conditions. The basic climatic pattern reflected by REE/Ca record during the past 284,000 years from this study is opposite to that of the speleothem records from the East Asian. However, the obliquity cycle also plays an important role. The obliquity pacing in the IPWP ITCZ shifting could be interpreted as the atmospheric "pressure push" between the Asian-Australian continental heat differences, caused by differentiated solar energy under different obliquity degrees. Third, the non-linearity of S-IPWP SST responses to the greenhouse gases radiative forcing (ΔRF_{GHG}) has been identified for the past 360,000 years. By using the non-overlapping binned method, we proposed a threshold of the sensitive changes around pCO_2 220 ± 10 ppm. Below this threshold, the sensitive (0.5 ^{o}C/Wm-2) was lower than the pCO2 >220 ppmv (1.4 $^{o}C/Wm^{-2}$). Significant sensitivity changes around 220 ± 10 ppmv are also supported by the Eastern Equatorial Pacific sites, but not the N-IPWP sites. This suggests that the non-linearity may be affected by the SH forcing. According to the *Jaccard et al.* (2013), the threshold may relate to the re-organization of the sea-ice distribution and consequential intermediate/mode water masses production rate changes. Thus, the combination of atmospheric (radiative changes) and oceanic (intermediate/mode water masses) changes have caused the non-linear response in the S-IPWP and EEP regions.

In sum, we suggest future research is needed to provide high resolution (<1-kyr) proxies-inferred thermal and hydrological records in the critical path through the latitudinal and longitudinal site distributions. Further fully coupled and geographic resolution climate models are also required to reconcile the climate dynamics in IPWP. Finally, longer time span (cover at least 3-4 glacial/interglacial cycles) is also crucial to reconstruct the long term variability and teleconnection between high-low latitude and orbital configurations.

摘　要

本研究利用位於巴布亞新幾內亞(Papua, New Guinea)東側所羅門海(Solomon Sea)之海洋沈積物岩芯MD05-2925 (9.3°S, 151.5°E, 水深1661米) 重建了過去三十六萬年來高解析度(200-900年解析度) 之海水表面溫度(sea surface temperature, SST), 降雨帶遷徙以及對溫室氣體(greenhouse gases)造成之輻射熱的非線性反應。

在過去50-60年以來，快速的氣候變遷已在低緯度的印度-太平洋暖池(Indo-Pacific Warm Pool, IPWP)區域造成急遽的溫度以及降雨帶的遷徙變化，環境所帶來的衝擊影響許多鄰近區域國家人民的安全。但是在缺乏長期的觀測紀錄，以及複雜的島嶼地形影響下，目前為止仍無法對於此區域的氣候模式有充分的瞭解。本研究嘗試利用古氣候/古海洋學研究方法釐清：1. 快速氣候變遷事件時期低緯度地區與南北半球高緯度氣候系統之間的遙相關，2. 軌道力對於研究區域的主要降雨帶-間熱帶輻合帶(intertropical convergence zone, ITCZ)的南北遷徙影響，3. 溫室氣體濃度變化所造成的輻射熱對於本區域的海水表面溫度變化。為了達成以上目標，我們第一步利用了碳十四定年與底棲性有孔蟲氧同位素地層建立了過去36萬年來良好的年代模式，進一步利用了居住在海水表層的浮游性有孔蟲*Globigerinoides ruber* (white, *s.s.*, 250-300 μm)的鎂/鈣與稀土元素/鈣 (Mg/Ca, and Rare Earth Element/Ca, REE/Ca)的比值重建了海水表面溫度與降雨變化，並與過去已發表在鄰近區域的紀錄做整合性的比較與討論。

以下整理本研究所重要結果：1. 在上次冰消期時，南印度太平洋暖池(S-IPWP)升溫早於北印度太平洋暖池區域(N-IPWP)，並且在北半球冷卻事件 (如

Heinrich event 1與Younger dryas, H1 and YD)時，S-IPWP溫度上升較N-IPWP多。在降雨方面，整個印度太平洋暖池都在H1 and YD事件時有明顯的水體氧同位素增加增加，ITCZ的南移可以同時或是部份解釋為受到大氣的遙相關影響，或是來自於S-IPWP的暖化的海洋影響。2. 在軌道時間尺度下的ITCZ遷徙事件的研究，我們透過了浮游性有孔蟲的稀土元素/鈣比值成為所羅門海區域的新代用指標，REE/Ca可被解釋為PNG地區的降雨/化學風化代用指標。在過去28萬年來，ITCZ在PNG區域的降雨記錄正好與東亞夏季季風相反，但地軸傾角週期(obliquity)同時也在PNG地區的ITCZ降雨記錄上扮演重要的角色。如此顯著的obliquity週期可以藉擺盪在亞洲-澳洲大陸(Asia-Australia)之間的氣壓差所解釋，當地軸傾角改變時，因著亞洲與澳洲大陸的大小差異，會造成兩者陸地被加熱的程度差異，進一步影響到兩者之間的大氣壓力梯度。3. 我們發現在過去36萬年來的S-IPWP SST與溫室氣體所造成的輻射熱有非線性的關係，關鍵的閥值（threshold）位於二氧化碳濃度220 ± 10（pCO_2, ppmv)，當大氣二氧化碳濃度低於220 ppmv時，S-IPWP對於輻射熱改變的敏感度(sensitivity)較小(0.5 ℃/Wm^{-2}), 但當二氧化碳濃度高於220 ppm時，敏感度將顯著改變(1.4 ℃/Wm^{-2})。這樣的非線性關係在東赤道太平洋(eastern equatorial Pacific, EEP)地區的岩芯中也同樣被觀察到，但是在N-IPWP則區域缺乏類似的反應，這樣的現象暗示著南半球的影響。而根據 *Jaccard* 等人(2013)的研究顯示，當大氣二氧化碳濃度 220 ppmv, 過去一百萬年來同時也是南大洋海冰覆蓋以及相對應的中層水/模態水生產率改變的關鍵閥值。故此本研究推測S-IPWP SST的非線性變化是因為同時受到了直接來自於大氣的輻射熱改變，與海洋水團生產速率同時變化下的結果。

本研究建議未來在此區域仍須要更多高解析度的溫度與水文紀錄，特別是在重要的水文交界處，或是隨著經緯度分布的站位。更高空間解析度的大氣-海洋耦合模式的配合將更能幫助研究者瞭解此區域整合性的氣候動力學，最後至少涵蓋3-4個冰期間冰期的長時間尺度的研究對於瞭解低緯度地區與南北半球高緯度地區的遙相關也是非常重要的關鍵。

PUBLICATION LIST

1. Referred Papers

Min-Te Chen, Xiao-Pei Lin, Yuan-Pin Chang, Yi-Chi Chen, ***Li Lo***, Chuan-Chou Shen, Yusuke Yokoyama, Delia W. Oppo, W. G. Thompson, Rong Zhang
Dynamic millennial-scale climate changes in the northwestern Pacific over the past 40,000 years
Geophysical Research Letters *2010, 37, 2010GL045202* **(SCI IF: 3.792)**

Chuan-Chou Shen, Chung-Che Wu, Yi Liu, Jimin Yu, Ching-Chih Chang, Doan Dinh Lam, Jain-Ru Jhou, ***Li Lo***, Kuo-Yen Wei
Rapid and precise measurements of natural carbonate rare earth elements in fentogram quantities by inductive coupled plasma sector field mass spectrometry
Analytical Chemistry *2011, 83, 6842-6848* **(SCI IF: 5.856)**

Li Lo, Yung-Hsiang Lai, Kuo-Yen Wei, Yu-Shih Lin, Horng-Sheng Mii, Chuan-Chou Shen
Persistent sea surface temperature and declined sea surface salinity of Kuroshio Current over the past 7,500 years
Journal of Asian Earth Sciences *2013, 66, 234-239* **(SCI IF: 2.714*, top ten hottest paper, 2013*)**

Li Lo, Chuan-Chou Shen, Chia-Jumg Lu, Yi-Chi Chen, Ching-Chih Chang, Kuo-Yen Wei, Dingchuang Qu, Michael K. Gagan.
Determination of element/Ca ratios in foraminiferal and coral using cold- and hot-plasma techniques on inductively coupled plasma sector field mass spectrometry
Journal of Asian Earth Sciences *2014, 81, 115-122* (**SCI IF: 2.379**)

Liangcheng Tan, Chuan-Chou Shen, Yanjun Cai, ***Li Lo***, Zhisheng An

Paleoclimatic and paleoenvironmental implications of trace element variations in an annually layered stalagmite from central China

Quaternary Research (accepted) (**SCI IF: 2.204**)

T. Li, C.-C. Shen, L.-J. Huang, X. Jiang, X. Yang, H.-S. Mii, S.-Y. Lee, ***Li Lo***
Variability of Asian summer monsoon during the penultimate glacial/interglacial period inferred from stalagmite oxygen isotope records from Yangkou cave, Chongqing, southwestern China
Climate of the Past Discussion (accepted)

2. Manuscripts Submitted

Yi Liu, ***Li Lo***, Zhengguo Shi, Kuo-Yen Wei, Jain-Ru Jhou, Chung-Che Wu , Zicheng Peng, Chuan-Chou Shen
Evolution of Pacific Intertropical Convergence Zone over the past 280,000 years
(*submitted to Nature Geoscience*, co-first author)

3. Manuscripts in preparation

Li Lo, Chuan-Chou Shen, Kuo-Yen Wei, George S. Burr, Horng-Sheng Mii, Min-Te Chen, Shih-Yu Lee, Meng-Chieh Tsai
Millennial meridional dynamics of Indo-Pacific Warm Pool during the last deglaciation
(*to be submitted to Climate of the Past*)

Li Lo, Kuo-Yen Wei, Sheng-Pu Chang, Horng-Sheng Mii, George S. Burr, Shih-Yu Lee, Min-Te Chen, Yi-Chi Chen, Chih-Kai Chuang, Chuan-Chou Shen
Non-linear response of South-IPWP SST to greenhouse gases radio-forcing during the past 360,000 years
(*to be submitted to Nature*)

4. OTHER PUBLICATION:

Kuo-Yen Wei, Yu-Shih Lin, ***Li Lo***, Chuan-Chou Shen, In-Tien Lin, Horng-Sheng Mii
Sea-surface temperature and hydrological variations in Okinawa Trough during the last 10,000 years
Interactions of Nature and Humans: Perspectives of Environmental History, Linking Publishing, 2008, 33-53, (in Chinese with English abstract).

Kuo-Yen Wei, ***Li Lo***, Chih-Kai Chuang, Shao-Wei Huang, Jyh-Jaan Huang, Saul-Wood Lin
A short note on the extant Rhodoliths found on the continental shelf off Dong-He, eastern Taiwan
Western Pacific Earth Sciences 2009, (9), 99-118 (in Chinese with English abstract).

Li Lo, Yuan-Pin Chang, Chuan-Chou Shen, Min-Te Chen, Kuo-Yen Wei
Invasion of warm, saline, and well ventilated intermediate water in cold stadials during the last 30,000 years? Evidence from the middle Okinawa Trough Site MD01-2404
Minerlogical Magazine 2011, (75), 1352.

Li Lo
Footnote for the next generation's geologists.
Evolution (演化) *2010, (16), 101-105 (in Chinese)*

Li Lo
Thermalhaline circulation and its importance to the Paleoceanography studies.
Science Monthly (科學月刊) 2014, April *(in Chinese).*

5. CONFERENCE CONTRIBUTION:

Oral presentation:

Li Lo, Chung-Chou Shen, Kuo-Yen Wei, Meng-Yang Lee, Horng-Sheng Mii
High Resolution Sea Surface Temperature Records from the Southern Marginal Indo-Pacific Warm Pool: Deglaciation Timing and Inter-Basin Pattern Differences
2010 Western Pacific Geophysics Meeting Program

Li Lo, Yuan-Pin Chang, Chung-Chou Shen, Min-Te Chen, Kuo-Yen Wei
Invasion of Warm, Saline, and well Ventilated Intermediate Water in Cold Stadials during the Last 30,000 Years? Evidence from the Middle Okinawa Trough Site MD01-2404
2011 Goldschmidt Meeting

Li Lo, Yung-Hsiang Lai, Kuo-Yen Wei, Yu-Shih Lin, Horng-Sheng Mii, Chuan-Chou Shen
Persistent sea surface temperature and declined sea surface salinity in the northwestern tropical Pacific over the past 7,500 years
2013 The 13th symposium on Quaternary of Taiwan & 3rd International IMAGES/PAGES Workshop of PPP

Poster presentation:

Yin Lin, Yue-Gau Chen, Chuan-Chou Shen, Hong-Wei Chiang, ***Li Lo***, Ching-Chih Chang, and Doan Dinh Lam.
Rainfall fluctuation over the past 4,000 years in Northern Vietnam inferred from stalagmite geochemical data
2007 American Geophysics Union Fall Meeting Program

Li Lo, Yi-Chun Lin, Meng-Yang Lee, Kuo-Yen Wei, Chuan-Chou Shen, and Horng-Sheng Mii
Changes in vertical hydrological profile at the southern margin of the Western Pacific Warlm Pool (WPWP) during the past 168,000 years
2008 American Geophysics Union Fall Meeting Program

Yung-Hsiang Lai, Kuo-Yen Wei, Chuan-Chou Shen, Horng-Sheng Mii, and ***Li Lo***
Hydrographic changes of the Kuroshio Current in the upper reach area during the past 6,000 years
2008 American Geophysics Union Fall Meeting Program

Meng-Yang Lee, ***Li Lo***, Yi-Chun Lin, Horng-Sheng Mii, Kuo-Yen Wei, and Chuan-Chou Shen
Variability of thermocline hydrography at the southern margin of the Western PAcific Warm Pool during the last 170 ka
2009 General Assembly of European Geophysics Union Program

Yi-Chi Chen, Yuan-Pin Chang, Min-Te Chen, ***Li Lo***, Kuo-Yen Wei, and Chuan-Chou Shen
Intrusion of the Kuroshio Current to the Okinawa Trough during 40-100 thousand years before present?
2009 American Geophysics Union Fall Meeting Program

Li Lo, Kuo-Yen Wei, Chuan-Chou Shen, Meng-Yang Lee, Horng-Sheng Mii, and Chuan-Chou Shen
The formation of a permanent SST gradient at the Plio-Pleistocene boundary: Highlights from the Western Pacific Warm Pool periphery area.
2009 American Geophysics Union Fall Meeting Program
Jyh-Jaan Huang, Kuo-Yen Wei, Chuan-Chou Shen, ***Li Lo***, and Chi-Yu Huang
Thermal and hydrological variability in the southern South China Sea over the past 11,600 years
2009 American Geophysics Union Fall Meeting Program

Chuan-Chou Shen, Kuo-Yen Wei, Yung-Hsiang Lai, ***Li Lo***, Horng-Sheng Mii
Intensification of the Kuroshio Current and orbit-driven southward shifts of Intertropical Convergence Zone and Western Pacific Warm Pool in the western Pacific since 8 thousand years ago
2010 Western Pacific Geophysics Meeting Program

Yuan-Pin Chang, Yi-Chi Chen, ***Li Lo***, Chuan-Chou Shen, Min-Te Chen
The Last Interglacial-Glacial SST Records Derived from Foraminiferal Mg/Ca of the East China Sea (IMAGES core: MD012404) and the Implications on Hydrological Changes
2010 Western Pacific Geophysics Meeting Program

Yi-Chi Chen, Kuo-Yen Wei, ***Li Lo***, Chuan-Chou Shen, Meng Yang Lee
Magnitude and timing of thermocline changes in the southwest Pacific warm pool during the last two terminations
2010 Western Pacific Geophysics Meeting Program

Chih-Kai Chuang, Kuo-Yen Wei, Huei-Chin Ke, Meng Yang Lee, Horng Sheng Mii, ***Li Lo***
Upper Pliocene-Pleistocene Calcareous Nannofossil Biostratigraphy of ODP1115B in the Solomon Sea, Western Equatorial Pacific.
2010 Western Pacific Geophysics Meeting Program

Li Lo, Chung-Chou Shen, Kuo-Yen Wei, Meng-Yang Lee, Horng-Sheng Mii
High Resolution Sea Surface Temperature Records form the Southern Marginal Indo-Pacific Warm Pool: Deglacial Timing and Inter-Hemispheric Pattern Differences
2010 10th International Conference on Paleoceanography

Yi-Chi Chen, Kuo-Yen Wei, ***Li Lo***, Chuan-Chou Shen, Meng Yang Lee
Magnitude and timing of thermocline changes in the southwest Pacific warm pool during the last two terminations
2010 10th International Conference on Paleoceanography

Yin Lin, ***Li Lo***, Yue-Gau Chen, Chuan-Chou Shen, Doan Dinh Lam
The Holocene Monsoon discrepancy between Southwest China and Northern Vietnam
2010 American Geophysics Union Fall Meeting Program

Chien-Ju Chou, Yi Liu, ***Li Lo***, Kuo-Yen Wei, Chung-Chou Shen
Planktonic foraminifer rare earth elements as a potential new aeolian dust proxy
2012 American Geophysics Union Fall Meeting Program

Chih-Kai Chung, Kuo-Yen Wei, ***Li Lo***, Yuan-Pin Chang, Huei-Chin Ke, Chuan-Chou Shen, Horng-Sheng Mii, Meng-Yang Lee, Pin-Chuan Lin
Quaternary high resolution paleoceanography records in the south marginal of Western Pacific Warm Pool
2013 The 13th symposium on Quaternary of Taiwan & 3rd International IMAGES/PAGES Workshop of PPP

Meng-Ting Chiang, Kuo-Yen Wei, Chih-Kai Chung, ***Li Lo***
Pulleniatina coiling change events during early Pleistocene in ODP 1115B, western equatorial Pacific
2013 The 13th symposium on Quaternary of Taiwan & 3rd International IMAGES/PAGES Workshop of PPP

Li Lo, Kuo-Yen Wei, Sheng-Pu Chang, Horng-Sheng Mii, George S. Burr, Shih-Yu Lee, Min-Te Chen, Yi-Chi Chen, Chih-Kai Chuang, Chuan-Chou Shen
Non-linear response of S-IPWP SST to greenhouse gases radio-forcing during the past 360,000 years
2013 American Geophysics Union Fall Meeting Program

TABLE OF CONTENTS

TABLES AND FIGURES

Chapter 1.

Introduction

Chapter 1. Introduction

The Indo-Pacific Warm Pool (IPWP) is the largest marine warm water mass with an annual average sea surface temperature (SST) >28^{o}C [*Yan et al.*, 1992, Figure 1-1A, 1-1C]. Vigorous atmospheric circulation in the IPWP transports substantial latent heat and water moisture from the tropics to middle and high latitudes [*Yan et al.*, 1992]. Global climate changes have shown significant impacts to the IPWP thermal variation and precipitation changes.

Over the past five decades, the IPWP has been responsible for regional surface water freshening and westward movements of precipitation zones that have caused regional drought in East Africa and storm track changes in East Australia [*Cravatte et al.*, 2009; *Williams and Funk*, 2011].

The Intertropical Convergence Zone (ITCZ) migrates meridionally with the seasonal angle of the sun [*Waliser and Gautier*, 1993] and circles the globe in the tropics [Figure 1-1B, 1-1D]. The convergence of inter-hemispheric trade winds leads to strong convective clouds, heavy precipitation, and intense latent-heat transfer, altering rainfall patterns worldwide. Owing to its strong rainfall gradient, a small displacement in the position of the ITCZ can cause dramatic changes in hydrological conditions and the frequency of extreme weather events—like droughts, floods, and tropical cyclones [*Cai et al.*, 2012].

Furthermore, the rapid rise of anthropogenic CO_2 emission in the past six decades has posted a threat to human sustainability. A doubled CO_2 (560 ppmv) concentration of pre-industrial value is projected to occur in Years 2050-2100 and may cause global mean temperature warming for 2.0-4.5^{o}C by the end of 21st century, which may be accompanied by large-scale ice sheet melts, rainfall belt shifts, and a rise in sea level [*IPCC*, 2007].

However, modern climatology studies could only provide short-term data to try to reconstruct present interactions between the air-sea system in the IPWP region. Paleoclimatology studies are needed to test teleconnections between low and high latitude and radiative forcing variations to the sensitivity to the IPWP thermal and hydrological changes. To understand sea surface temperature (SST), ITCZ variations, and radiative forcing (RF) changes are crucial to make future predictions.

This study focuses on the reconstruction of the thermal and hydrological histories in the IPWP region, and further attempt to reveal the teleconnection between low and high latitudes, thermal variation accompanied with greenhouse gas concentrations, and precipitation belts shifting.

Since the early 2000s, intense paleoclimatology studies have been conducted to understand long-term thermal and hydrological changes in the IPWP during the glacial/interglacial (G/IG) cycles and to test the sensitivities of warm pool thermal and hydrological fluctuations to high latitude ice sheet coverage and greenhouse gas concentration variations through the late Pleistocene [e.g., *Lea et al.*, 2000; *Stott et al.*, 2002; *Visser et al.*, 2003; *Rosenthal et al.*, 2003; *Stott et al.*, 2004; *de Garidel-Thoron*

et al., 2005; *Steinke et al.*, 2006; *Levi et al.*, 2007; *Xu et al.*, 2008; *Linsley et al.*, 2010; *Bolliet et al.*, 2011, Figure 1-1, 1-2]. However, complicated ocean-island configuration and regional topography hinder the fidelity of detailed description of past climate changes [*Griffiths et al.*, 2009; *Mohtadi et al.*, 2011]. In particular, little is known about the meridional thermal-hydrological dynamics between the N-IPWP and S-IPWP during the last termination transition.

The lack of long-term records from the meteorological core of the ITCZ, in the low-latitude Pacific, severely hinders us from understanding its natural variability related to orbital forcings during the Quaternary. An understanding of ITCZ responses to orbital forcings has global significance because the region is the largest "heat engine" and moisture source in the world.

The sensitivity of tropical Pacific Ocean sea surface temperature to greenhouses gases radiative forcing (mainly contributed by CO_2) changes during the past four to five G/IG cycles have been previously addressed by *Lea*, [2004] and *Dyez and Ravelo*, [2012]. They performed linear regression analyses to estimate SST responses to changes in pCO_2. Based on the regression coefficients obtained from the paleoclimate records, they project a 33-36^{o}C tropical Pacific SST for the future doubling CO_2 scenario. Alternatively, the CO_2 radiative effect on SST may not be linear and the climate may switch non-linearly as suggested by other studies [*e.g.*, *Paillard*, 2001; *Peacock et al.*, 2006; *Carlson and Winsor*, 2012]. Linear versus non-linear regression differences would not only affect the accuracy of the prediction to future climate evolution but also challenge our knowledge of the interactions between climate components within the system.

Motivation and the structure of this dissertation:

To obtain better understanding of the tropical Pacific response to greenhouse gases and ice volumes changes, we need high-resolution SST and hydrological records to address changes during the G/IG cycles and spatial recovery to identify possible climate teleconnections. This study of IPWP focuses on the teleconnection between low and high latitudes, thermal variation accompanied with atmospheric greenhouse gases concentration, and precipitation belts shifting.

Research region:

Papua New Guinea (PNG), a mountainous terrain located at the southern border of the ITCZ [Figure 1-1], delivers a large amount of suspended sediments and solutes to the adjacent oceans as a result of the prodigious precipitation in the region [*Milliman et al.*, 1999; *Nittouer et al.*, 1995]. This transport occurs mostly in the wet season (>90% annual load) when the ITCZ is located over PNG [*Chappell et al.*, 2011]. Archives from nearby marine basins therefore reflect this sediment delivery and provide a direct record of precipitation influenced by the ITCZ position.

Solomon Sea, which is the passage of surface and subsurface water masses between low- and middle-latitude South Pacific Ocean gyre and cross equatorial currents [*Grenier et al.*, 2011; *Melet et al.*, 2010, Figure 1-2].

Structure of this dissertation and short summaries of results:

Material and methods are summarized in Chapter 2. We firstly present new oceanic proxy-inferred SST and ice volume-corrected surface seawater oxygen isotope $\delta^{18}O$ ($\delta^{18}O_{SW\text{-}IVC}$) records from the Solomon Sea near the Papua New Guinea (PNG) covering the past 23-10.5 thousand years ago (ka, before 1950 AD, Figure 1-3)

in Chapter 3. New SST and $\delta^{18}O_{SW\text{-}IVC}$ stacked records since the last termination are constructed for both N-IPWP and S-IPWP to understand regional thermal and hydrological changes and interhemispheric teleconnections [Figure 1-4]. Secondly, in chapter 4, we have established a 284-kyr record of rare earth elements (REEs) to Ca ratios in the planktonic foraminifer *Globigerinoides ruber* [Figure 1-5]. Furthermore, new calculations from a previous orbital-accelerated transient experiment using a coupled fast ocean-atmosphere model (FOAM, *Kutzbach et al.*, 2008; *Shi et al.*, 2011) forced by variations in orbital parameters is presented to clarify dynamical ITCZ migration processes in the western Pacific [Figure 1-6]. Thirdly, in chapter 5, we reconstruct a high resolution SST (200- to 900-yrs resolution) record from the Solomon Sea, on the S-IPWP, of the past four G/IG cycles during the past 360 thousand years (360 ka), and examine the non-linearity between the tropical Pacific SST and RF [Figure 1-7, 1-8].

We conclude that increasing IPWP thermal gradients during the Heinrich event 1 (H1) and Younger Dryas (YD) periods may alter the Hadley circulation and consequently reducing monsoon region precipitation. For the orbital timescale ITCZ shifting in the Solomon Sea region, obliquity can shift the position of the ITCZ and operates in tandem with precessional forcing. Given that the obliquity signal is stronger in the Nd/Ca-inferred precipitation record than in the simulation, our proposed obliquity-induced "pressure-push" mechanism might be more significant for both PNG and North Australia. We also propose that the SST is in fact nonlinear to RF and after a major threshold level at 220 ± 10 ppmv, which S-WPWP SST linearly increases ~1.9 ± 0.4 ^{o}C (by the sensitivity changes from 0.5 to 1.4 $^{o}C/Wm^{-2}$, when $pCO_2 \geq 220 \pm 10$ ppmv). Potential mechanism to explain this non-linearity of S-

WPWP SST changes are the results of the combination of the Southern Ocean sea ice induced intermediate/mode water formations and the greenhouse gases changes.

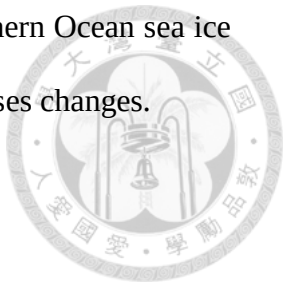

References

Bolliet, T., Holbourn, A., Kuhnt, W., Laj, C., Kissel, C., Beaufort, L., Kienast, M., Andersen, N., and Garbe-Schönberg, D., (2011), Mindanao Dome variability over the last 160 kyr: Episodic glacial cooling of the West Pacific Warm Pool. *Paleoceanography* **26**, PA1208, doi: 10.1029/2010PA001966.

Cai, W., Lengaigne, M., Borlace, S., Collions, M., Cowan, T., McPhaden, M. J., Timmermann, a., Power, S., Brown, J., Menkes, C., Ngari, A., Vincent, E. M., and Widlansky, M. J., (2012), More extreme swings of the South Pacific convergence zone due to greenhouse warming. *Nature* **488,** 365-369.

Carlson, A. E., and Winsor, K., (2012), Northern Hemisphere ice-sheet responses to past climate warming. *Nature Geoscience* **5**, 607-613.

Chappell, N. A., Tych, W., Shearman, P., Lokes, B. & Chitoa, J. in *Sediment Problems and Sediment Management in Asian River Basins* (eds. Walling, D. E.) 92-102 (IAHS Press, Wallingford, 2011)

Cravatte, S., Delcroix, T., Zhang, D., McPhaden, M., and Leloup, J., (2009), Observed freshening and warming of the western Pacific Warm Pool. *Climate Dynamics* **33**, 565 – 589.

de Garidel-Thoron, T., Rosenthal, Y., Bassinot, F., and Beaufort, L., (2005), Stable sea surface temperatures in the western Pacific warm pool over the past 1.75 million years. *Nature* **433**, 294 – 298.

Dyez, K. A., and Ravelo, A. C., (2012), Late Pleistocene tropical Pacific temperature sensitivity to radiative greenhouse gas forcing. *Geology* **41**, 23-26.

Grenier, M., Cravatte, S., Blanke, B., Menkes, C., Joch-Larrouy, A., Durand, F., Melet, A., and Jeandel, C., (2011), From the western boundary currents to the Pacific Equatorial Undercurrent: Modeled pathways and water mass evolutions. *Journal of Geophysical Research* **116**, C12044, doi: 10.1029/JC007477.

Griffiths, M. L., Drysdale, R. N., Gagan, M. K., Zhao, J.-X., Ayliffe, L. K., Hellstrom, J. C., Hantoro, W. S., Frisia, S., Feng, Y.-X., Cartwright, I., St. Pierre, E., Fischer, M., J., and Suwargadi, B. W., (2009), Increasing Australian-Indonesian monsoon rainfall linked to early Holocene sea-level rise. *Nature Geoscience* **2**, 636 – 639.

IPCC AR4 report. (2007), Contribution of Working Groups I, II and III to the Fourth Assessment Report of the Intergovernmental Panel on Climate Change. Core Writing Team, Pachauri, R.K. and Reisinger, A. (Eds.). IPCC, Geneva, Switzerland. pp. 104.

Kutzbach, J. E., Liu, X., Liu, Z. and Chen, G., (2008), Simulation of the evolutionary response of global summer monsoons to orbital forcing over the past 280,000 years. *Climate Dynam*ics **30,** 567-579.

Lea, D. W., Pak, D. K., and Spero, H. J., (2000), Climate impact of late Quaternary equatorial Pacific sea surface temperature variations. *Science* **289**, 1719 – 1724.

Lea, D. W., (2004), The 100,000-yr cycle in tropical SST, greenhouse forcing, and climate sensitivity. *Journal of Climate* **17**, 2170-2179.

Levi, C., Labeyrie, L., Bassinot, F., Guichard, F., Cortijo, E., Waelbroeck, C., Caillon, N., Duprat, J., de Garidel-Thoron, T., and Elderfield, H., (2007), Low-latitude hydrological cycle and rapid climate changes during the last deglaciation. *Geochemistry, Geophysics, Geosystems* **8**, Q05N12, doi: 10.1029/2006GC001514.

Linsley, B. K., Rosenthal, Y., and Oppo, D. W., (2010), Holocene evolution of the Indonesian throughflow and the western Pacific warm Pool. *Nature Geoscience* **3**, 578 – 583.

Milliman, J. D., Farnsworth, K. L., and Albertin, C. S., (1999), Flux and fate of fluvial sediments leaving large islands in the East Indies. *Journal of Sea Research* **41,** 97-107.

Melet, A., Gourdeau, L., and Verron, J., (2010), Variability in Solomon Sea circulation derived from altimeter sea level data. *Ocean Dynamics* **60**, 883-900.

Mohtadi, M., Oppo, D. W., Steinke, S., Stuut, J.-B. W., De Pol-Holz, R., Hebbeln, D., and Lückge, A., (2011), Glacial to Holocene swings of the Australian-Indonesian monsoon. *Nature Geoscience* **4**, 540 – 544.

Nittrouer, C. A., Brunskill, G. J., and Figueiredo, A. G., (1995), Importance of tropical coastal environments. *Geo-Ma*rine *Lett*ers **15**, 121-126.

Northern Greenland Ice Core Project Members, (2004), High-resolution record of Northern Hemisphere climate extending into the last interglacial period. *Nature* **431**, 147 – 151.

Oppo, D. W., Rosenthal, Y., and Linsley, B. K., (2009), 2,000-year-long temperature and hydrology reconstructions from the Indo-Pacific warm pool. *Nature* **460**, 1113 – 1116.

Paillard, D., (2001), Glacial cycles: toward a new paradigm. *Reviews of Geophysics* **39**, 325-346.

Peacock, S., Lane, E., and Restrepo, J. M., (2006), A possible sequence of events from the generalized glacial-interglacial cycle. *Global Biogeochemical Cycles* **20**, GB2010.

Pena, L. D., Cacho, I., Ferretti, P., and Hall, M. A., (2008), El Niño-Southern Oscillation-like variability during glacial terminations and interlatitudinal teleconnections. *Paleoceanography* **23**, PA3101.

Pena, L. D., Goldstein, S. L., Hemming, S. R., Jones, K. M., Calvo, E., Pelejero, C., and Cacho, I., (2013), Rapid changes in meridional advection of Southern Ocean intermediate waters to the tropical Pacific during the last 30 kyr. *Earth and Planetary Science Letters* **368**, 20-32.

Qu, T., Gao, S., and Fine, R. A., (2013), Subduction of South Pacific tropical water and its equatorward past way shown by a simulated passive tracer. *Journal of Physical Oceanograohy* **43**, 1551-1656.

Reynolds, R. W., Rayner, N. A., Smith, T. M., and Stokes, D. C., (2002), An improved in situ and satellite SST analysis for climate. *Journal of Climate*, 15, 1609 – 1625.

Rosenthal, Y., Oppo, D. W., and Linsley, B. K., (2003), The amplitude and phasing of climate change during the last deglaciation in the Sulu Sea, western equatorial Pacific. *Geophysical Research Letters* **30**, 1428, doi: 10.1029/2002GL016612.

Schulz, M., and Mudelsee, M., (2002), REDFIT: estimating red-noise spectra directly from unevenly spaced paleoclimatic time series. *Computers and Geosciences* **28**, 421-426.

Shi, Z. G., Liu X. D., Sun, Y. B., An, Z. S., Liu, Z., and Kutzbach, J., (2011), Distinct responses of East Asian summer and winter monsoons to astronomical forcing. *Climate of the Past* **7,** 1363-1370.

Steinke, S., Chiu, H.-I., Yu, P.-S., Shen, C.-C., Erlenkeuser, H., Löwemark, L., and Chen, M.-T., (2006), On the influence of sea level and monsoon climate on the southern South China Sea freshwater budget over the past 22,000 years. *Quaternary Science Reviews* **25**, 1475 – 1488.

Stenni, B., Jouzel, J., Masson-Delmotte, V., Röthlisberger, R., Castellano, E., Cattani, O., Falourd, S., Johnsen, S. J., Longinelli, A., Sachs, J. P., Selmo, E., Souchez, R., Steffensen, J. P., Udisti, R., (2003), A late-glacial high-resolution site and source temperature record derived from EPICA Dome C isotope records (East Antarctica). *Earth and Planetary Science Letters* **217**, 183 – 195.

Stott, L., Cannariato, K., Thunell, R., Haug, G. H., Koutavas, A., and Lund, S., (2004), Decline of surface temperature and salinity in the western tropical Pacific Ocean in the Holocene epoch. *Nature* **431**, 56 – 59.

Stott, L., Poulsen, C., Lund, S., and Thunell, R., (2002), Super ENSO and global climate oscillations at millennial time scales. *Science* **297**, 222-226.

Visser, K., Thunell, R., and Stott, L., (2003), Magnitude and timing of temperature change in the Indo-Pacific warm pool during deglaciation. *Nature* **421**, 152 – 155.

Waliser, D. E., and Gautier, C. A., (1993), Satellite-derived climatology of the ITCZ. *J*ournal of *Clim*ate **6,** 2162-2174.

Williams, A. P, and Funk, C., (2011), A westward extension of the warm pool leads to a westward extension of the Walker circulation, drying eastern Africa. *Climate Dynamics* **37**, 2417 – 2435.

Xu, J., Holbourn, A., Kuhnt, W., Jian, Z., and Kawamura, H., (2008), Changes in the thermocline structure of the Indonesian outflow during Terminations Ⅰ and Ⅱ. *Earth and Planetary Science Letters* **273**, 152 – 162.

Yan, X.-H., Ho, C.-R., Zheng, Q., and Klemas, V., (1992), Temperature and size variabilities of the western Pacific warm pool. *Science* **258**, 1643-1645.

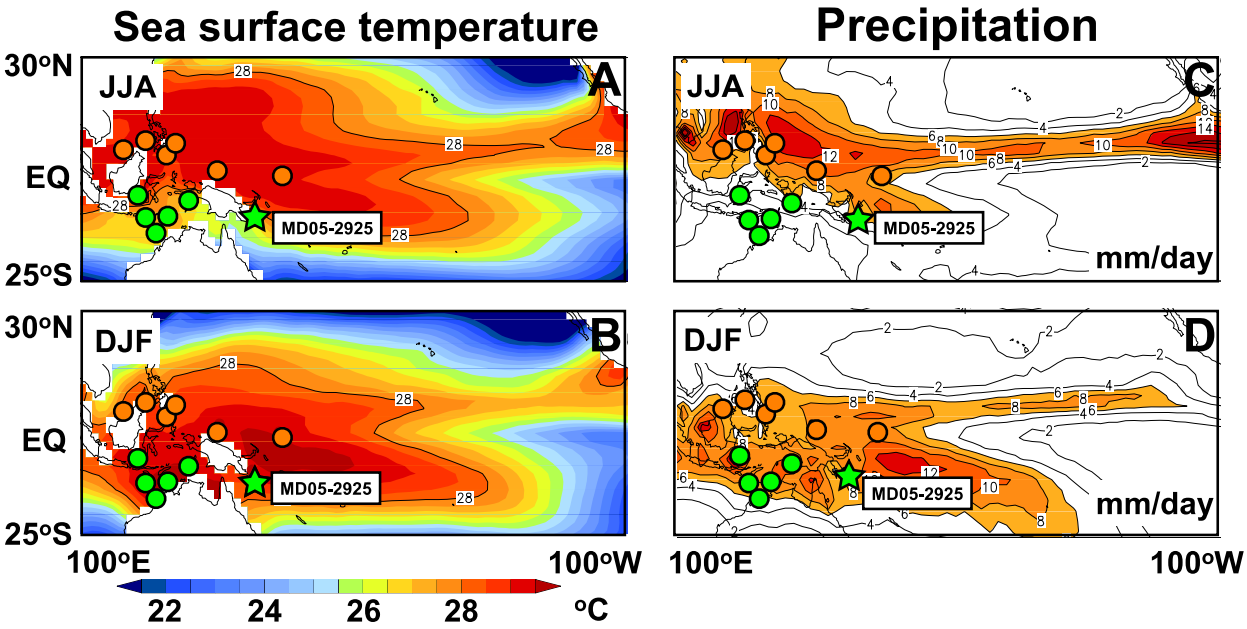

Figure 1-1. Climatological map of the Indo-Pacific Warm Pool (IPWP) sea surface temperature (SST, left) and precipitation (right) during 1950-2004 AD [*Reynolds et al.*, 2002]. Upper panels are from the June-July-August (JJA), and lower panels are from December-January-February (DJF) averages of (A, C) SSTs and (B, D) precipitation distribution maps. SST and precipitation are at 0.5 ^{o}C and 2 mm/day intervals. Green star is the study site MD05-2925. Orange and green dots are the previous study sites [Table 2-3] in IPWP region for reconstruction of meridional thermal and precipitation variations during the glacial/interglacial change [Chapter 3].

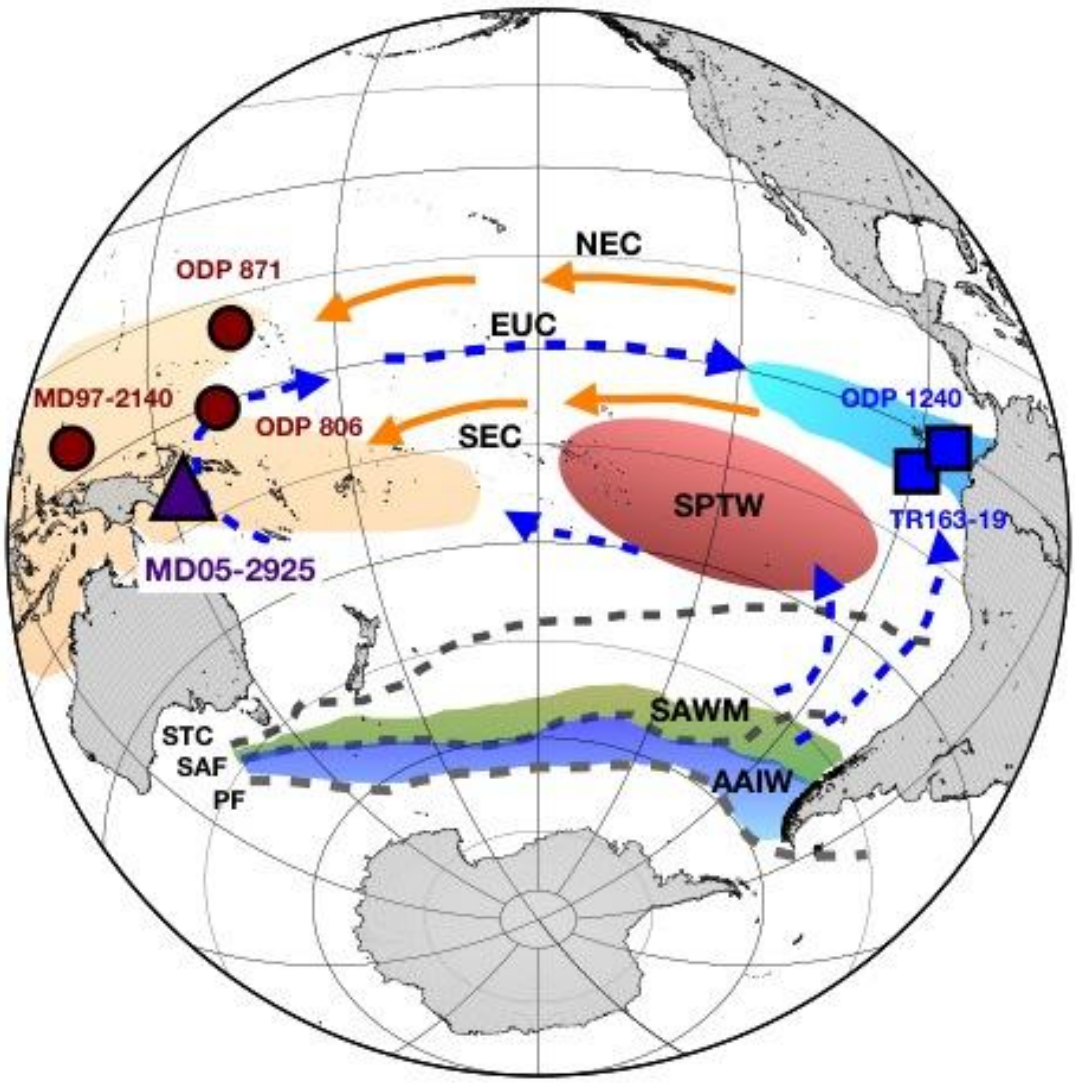

Figure 1-2. Schematic circulation, water masses distribution, and site location map. Purple triangle represents site MD05-2925 (9.3°S, 151.5°E) in this study, and red circles and blue squares are selected sites in the equatorial Pacific [Table 2-4]. Gray dashed lines show the Polar Front (PF), Subanatarctic Front (SAF), and Subtropical convergence zone (STC), respectively. Blue and green shadings indicate the formation region of Subanatarctic Mode Water (SAMW), and Antarctic Intermediate Water (AAIW), respectively. Dark red, orange, and blue shadings represent South Pacific Tropical Water (SPTW), Indo-Pacific Warm Pool (IPWP), and Eastern Equatorial Pacific (EEP) cold tongue regions, respectively. Blue dashed arrays represent the undercurrent pathways, (Equatorial Under Current, EUC, and orange solid ones represent surface current systems, South Equatorial Current (SEC) and North Equatorial Current (NEC). SAMW/AAIW transport Southern hemisphere (SH) high latitude to the SPTW, and then spread out the South Pacific Ocean through the EUC and EEP wind-driven upwelling [*Pena et al.*, 2013] system and resurfacing process through water masses mixing [*Qu et al.*, 2013] within decades.

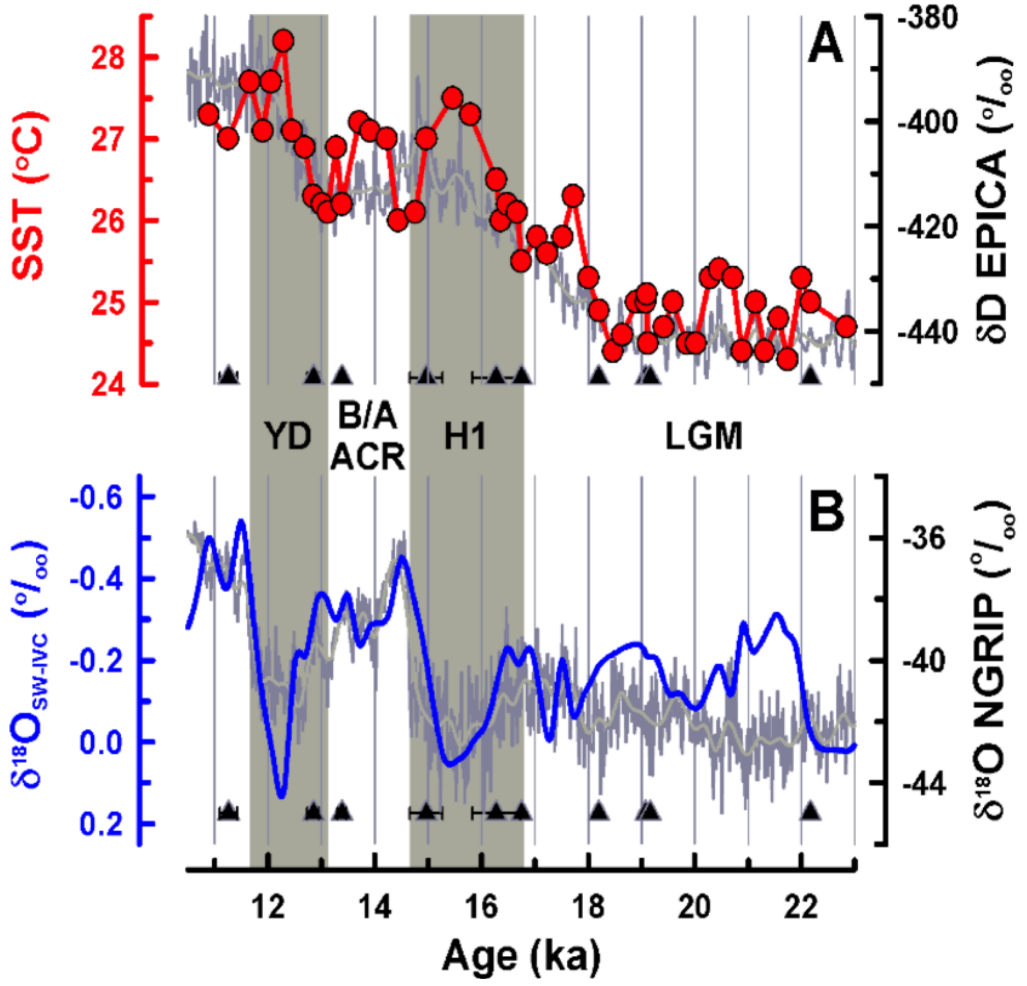

Figure 1-3. Geochemical proxies from site MD05-2925. (A) $\delta^{18}O_{SW\text{-}IVC}$ (blue line) and (B) SST (red dots and line) were reconstructed with *G. ruber* Mg/Ca ratios and $\delta^{18}O_C$. Gray line is the Greenland ice core NGRIP oxygen isotope record [*Northern Greenland Ice Core Project Members*, 2004]. Dark gray line denotes the Antarctica EPICA deuterium isotope record [*Stenni et al.*, 2003]. The superimposed black lines are the 200-yr smoothed records. Black triangles are accelerator mass spectrometry (AMS) ^{14}C dates [Table 2-1]. Vertical bars denote the H1 and YD periods.

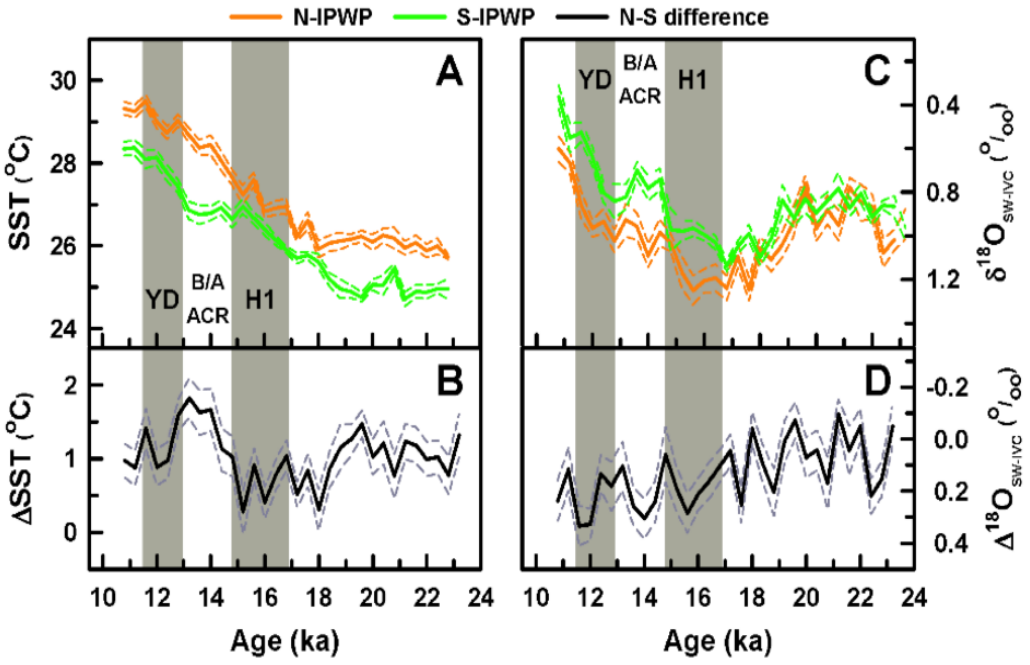

Figure 1-4. Four-hundred-year non-overlapping binned (A) SST and (C) $\delta^{18}O_{SW\text{-}IVC}$ of N- (orange solid lines) and S-IPWP (green solid lines). Lower panel are the differences of (B) SST and (D) $\delta^{18}O_{SW\text{-}IVC}$ between N- and S-IPWP, respectively. The compilations of N- and S-IPWP surface water thermal and hydrological records were calculated with a non-overlapping binned method [*Oppo et al.*, 2009; *Linsley et al.*, 2010, Chapter 2]. All dashed lines represent 1-sigma uncertainty range. Gray bars represent the H1 and YD events.

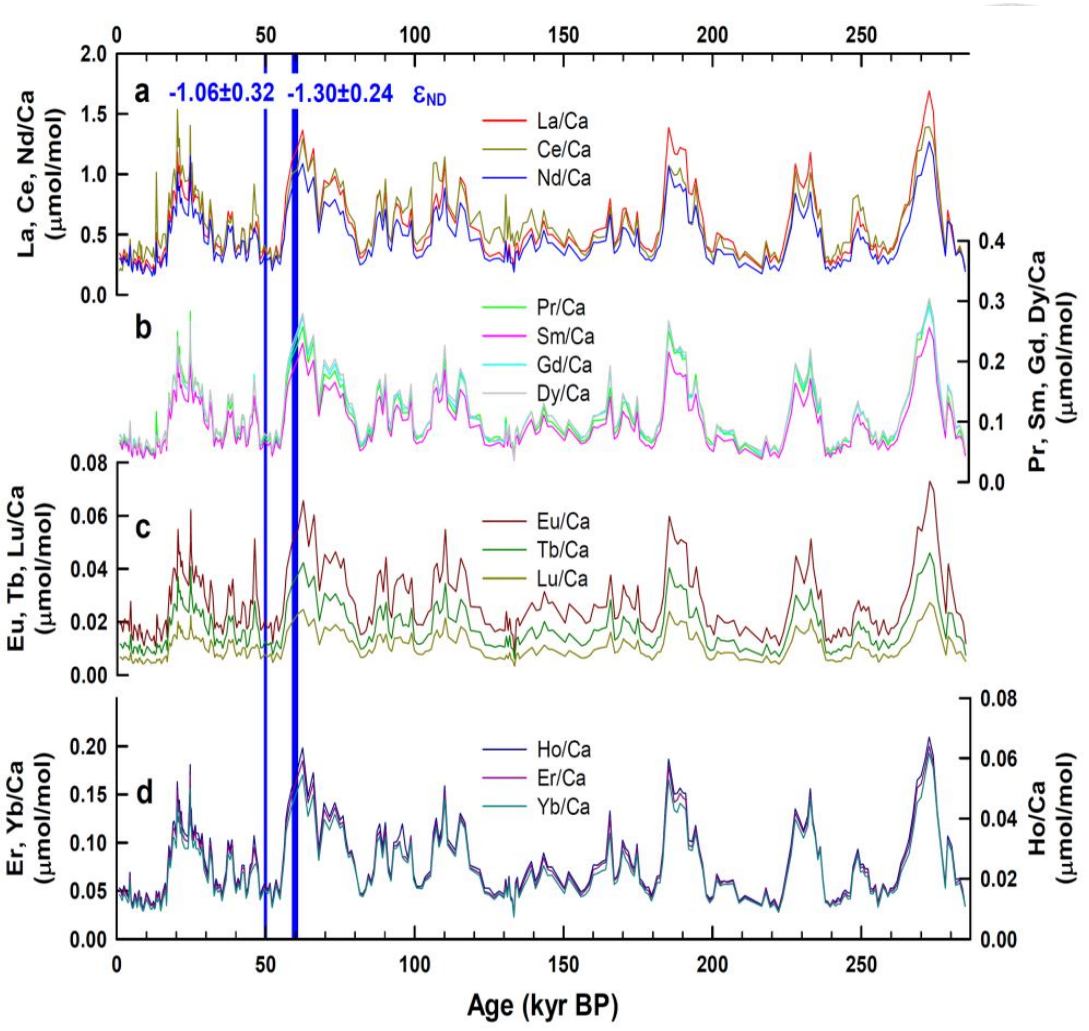

Figure 1-5. Time series of REE/Ca of planktonic foraminifera *G. ruber*. (a) La/Ca, Ce/Ca and Nd/Ca. (b) Pr/Ca, Sm/Ca, Gd/Ca and Dy/Ca. (c) Eu/Ca ,Tb/Ca and Lu/Ca. (d) Ho/Ca, Er/Ca and Yb/Ca. ε_{Nd} values at ages of 49.5-50.1 and 58.8-60.6 kyr BP are given in panel (a).

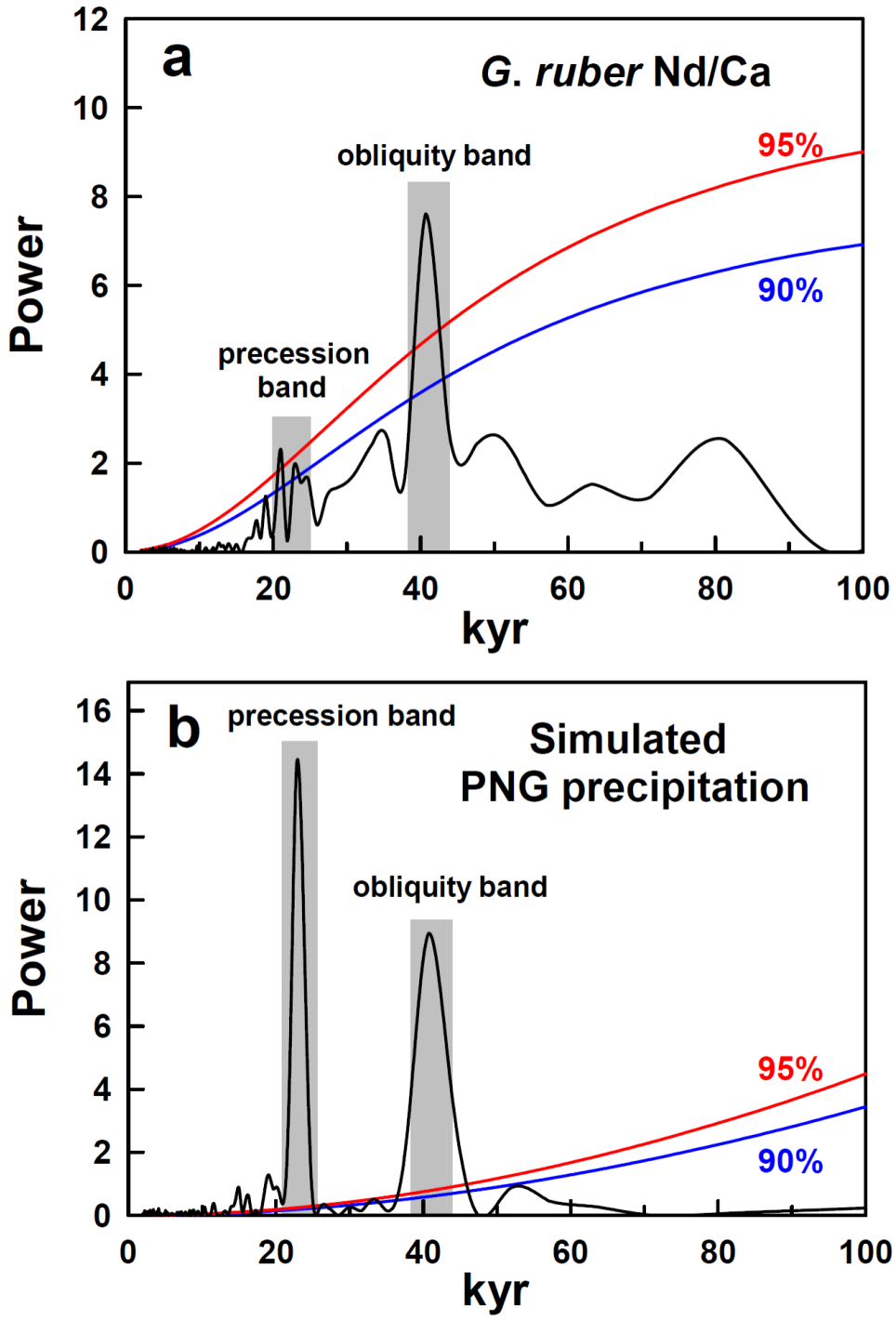

Figure 1-6. Spectral power analysis results. (a) MD 05-2925 planktonic foraminifer *G. ruber* Nd/Ca record. (b) Simulated PNG precipitation (5-12°S and 130-160°E) over the past 284 kyr. We used REDFIT v 3.8 [*Schulz and Mudelsee*, 2002] to perform spectral analyses. Red and blue lines respectively denote 95% and 90% significance levels of coherence. Vertical bars are the significant precession and obliquity bands.

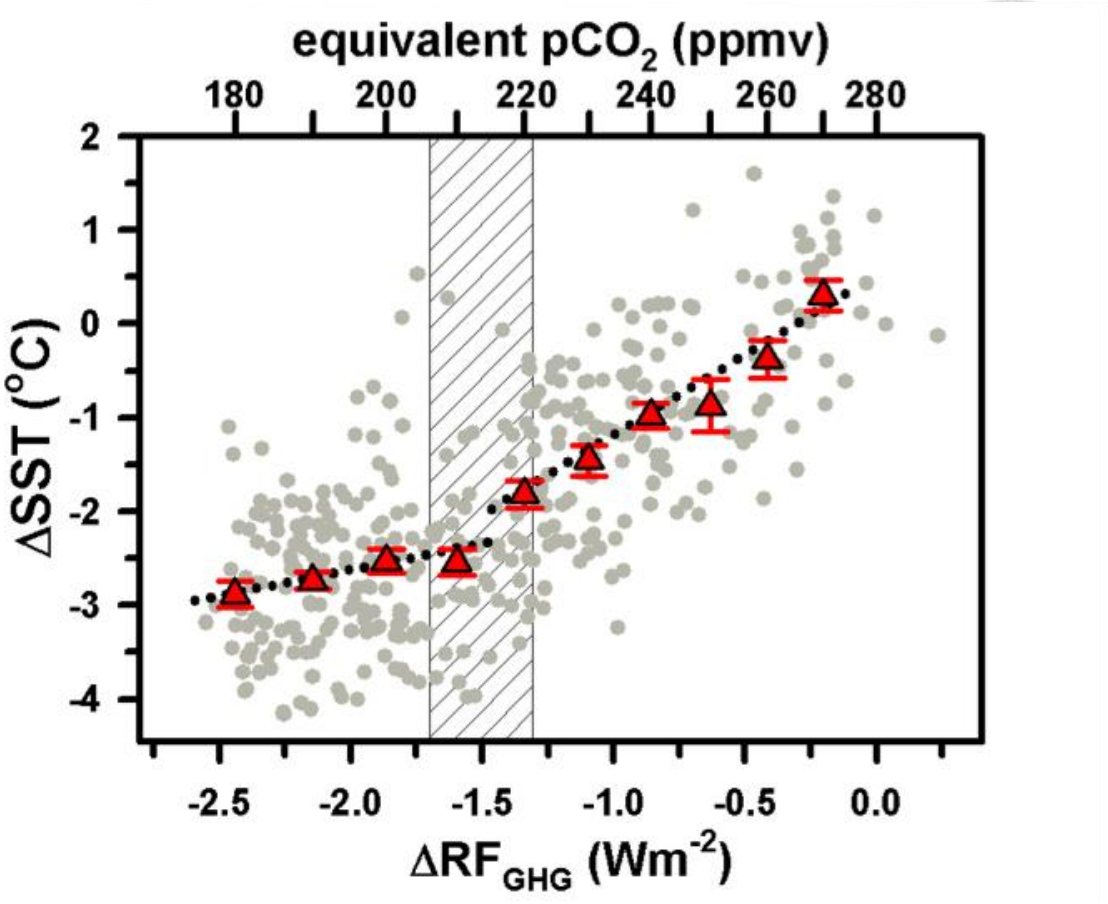

Figure 1-7. Non-linear climate sensitivity. Past Solomon SST changes (ΔSST) to changes in greenhouse gas radiative forcing (ΔRF_{GHG}). Both ΔRF_{GHG} and ΔSST dataset has been interpolated to 1-kyr interval. Standard deviation of mean for every 10 ppmv equivalent pCO_2 has been calculated by non-overlapping binned method (red triangles, *Oppo et al.*, 2009; *Linsley et al.*, 2010). The dark bar represents the significant difference threshold for the non-linear SST changes around 220 ± 10 ppmv.

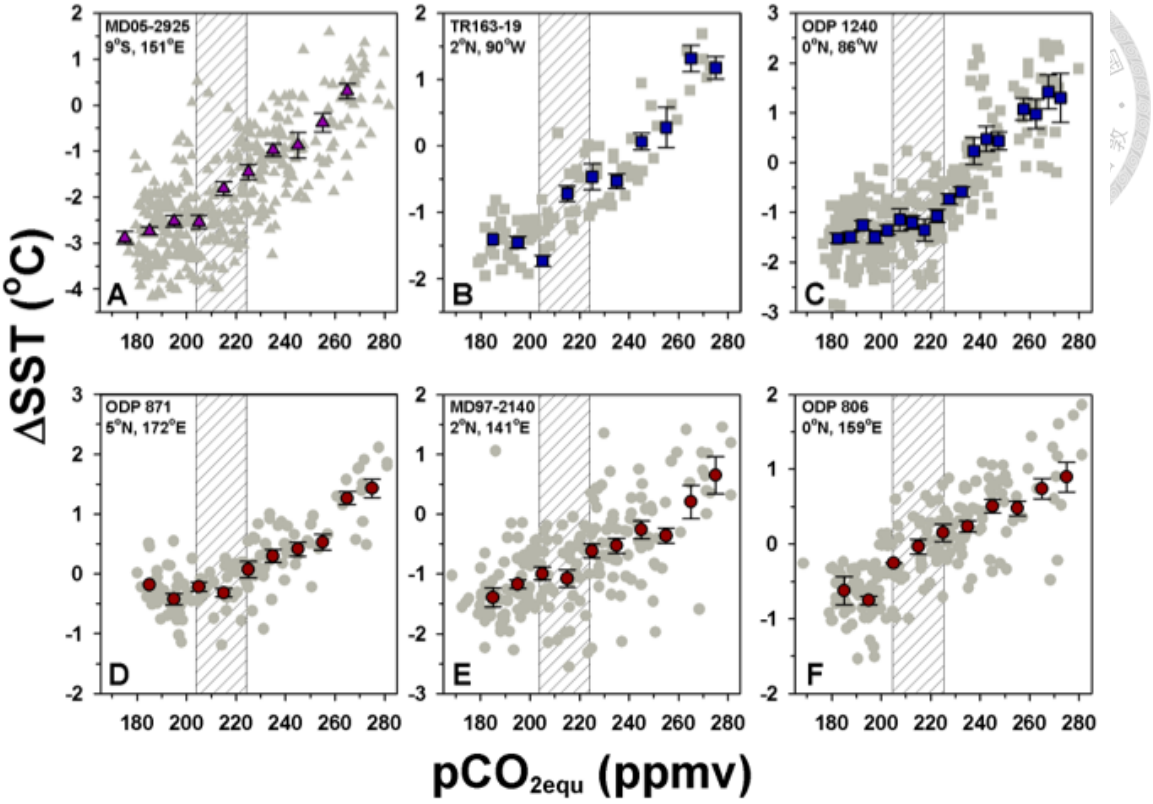

Figure 1-8. Tropical Pacific SST sensitivity. The SST sensitivity of (A) Solomon Sea (MD05-2925, purple triangles, this study), (B, C) eastern equatorial Pacific (TR163-19, and ODP 1240, blue squares, *Lea et al.*, 2000; *Pena et al.*, 2008, respectively), and (D-F) western Pacific (ODP 871, MD97-2140, and ODP 806, dark red circles, *Dyez and Ravelo*, 2012, *de Garidel-Thoron et al.*, 2005; and *Lea et al.*, 2000, respectively). Only the MD05-2925 and ODP 1240 SST were resampled into 1-kyr resolution, the others were resampled into 4-kyr resolution. Gray circles, squares, and triangles represent the raw dataset for each site.

Chapter 2.

Material and Methods Summary

Chapter 2. Material and Methods Summary

MD05-2925

Site MD05-2925 (9.3^{o}S, 151.5^{o}E, water depth 1661 m) was collected during the 2005 PECTEN (Past Equatorial Climate: Tracking El Niño) cruise which supported by International Marine and Climate Changes (IMAGES) Project on the research vessel Marion Dufresen. MD05-2925 is located at the northern slope of Woodlark Basin in the Solomon Sea, which is the passage of surface and subsurface water masses between low- and middle-latitude South Pacific Ocean gyre and cross equatorial currents. The New Guinea Counter Current and South Equatorial Current, as low-level western boundary currents, flow northwest through the Solomon Sea, transporting southern subtropical waters to the equatorial region via Vitiaz Strait [*Melet et al.*, 2010a; *Melet et al.*, 2010b; *Cravatte et al.*, 2011; *Grenier et al.*, 2011; *Melet et al.*, 2011]. The average sea surface temperature (SST) is 28.5 ^{o}C [*Locarnini et al.*, 2010], with seasonally apart from the core region of the warm surface water mass in the Indo-Pacific warm pool (IPWP).

The precipitation sources are mainly comes from the south Indian Ocean and the Coral Sea [*Gimeno et al.*, 2012], and are focused during the July-August-September (JAS). Intertropical convergence zone (ITCZ) and the South Pacific Convergence (SPCZ) are integrated here, which resulting as a bridging from the southwester equator to the middle latitude Pacific Ocean [*Shiau et al.*, 2012, and references therein].

The total length of MD05-2925 is 2843 cm, and the upper 1882 cm was used in this study. The MD05-2925 core sediment is composed of a mixture of biogenic carbonate and silty clay [*Beaufort et al.*, 2005]. The depth of core is well above the regional Carbonate Compensation Depth (CCD). The chlorophyll level of

0.2 mg/m^3 [*Radenac et al.*, 2012] for surrounding surface water in eastern Papua New Guinea (PNG) suggests low regional productivity. The dissolved-oxygen concentrations are high (>3 mL/L) through the whole water column including bottom waters of the eastern PNG [*Garcia et al.*, 2010]. The local benthic oxygen flux, reflecting organic matter remineralization, is only 0.1 mol/m^2/yr [*Jahnke*, 2003]. It is lower than the values of 0.8 mol/m^2/yr for the reducing margins [notably in the eastern boundary upwelling systems (EUBS) and North Indian Ocean, *Jahnke*, 2003]. These data indicates an oxidative sea floor condition at this study site.

Oxygen isotope

Planktonic foraminifera, *Globigerinoides ruber* (white, *s.s.*, 250-300 μm), were hand picked under microscope for the oxygen isotope measurement. Each samples contained 7-10 individuals and were immersed with methanol and ultrasonicated for 10 seconds, and rinsed with deionized water 5 times. Samples were immersed afterward in the hyperchloride sodium (NaOCl) for 24 hours, and then measured by an isotopic ratio mass spectrometer (IRMS), Micromass IsoPrime, housed in the National Taiwan Normal University. Long-term precision is 0.10‰ (2RSD, N = 701) with respect to Vienna Pee Dee Belemnite (VPDB) [*Lo et al.*, 2013].

Trace elements/Ca (TE/Ca) measurements

For TE/Ca (mainly Mg and REEs) ratio measurements, 20-30 individuals were gently crushed and transported into 1.5 mL Teflon vial. The clean procedure is as follows: (1) Foraminiferal fragments were immersed with ethanol, ultrasonicated for 20 minutes, and then rinsed by Milli-Q ultra-pure water 3 times. (2) An aliquot of 0.45 mL 3% H_2O_2 was added for 2 hours to decompose organic material. (3) NH_4Cl

(0.45 mL, 1.0 N) was added for 20 minutes to adsorb cations on chamber surface. (4) NH_2OH (0.45 mL, 0.01 N) was added for 3 hours to dissolve metallic oxides. (5) Diluted nitric acid (1 mL, 0.005 N) was added to polish the high-Mg content surface. A sector field inductive coupled plasma mass spectrometer (SF-ICP-MS), Thermo Electron Element II, housed at the High-Precision Spectrometry and Environment Change Laboratory (HISPEC), Department of Geosciences, National Taiwan University, was used to determine trace element/Ca ratios following the methodology developed by *Lo et al.*, [2014]. Two-year reproducibility for Mg/Ca analysis is ±0.21% (1 RSD).

We measured REE/Ca records of the planktonic foraminifer *G. ruber* (white, *s.s.* 250-300 μm). REE/Ca ratios were calculated using the ion beams of ^{46}Ca, ^{139}La, ^{140}Ce, ^{141}Pr, ^{146}Nd, ^{147}Sm, ^{153}Eu, ^{160}Gd, ^{159}Tb, ^{163}Dy, ^{165}Ho, ^{166}Er, ^{172}Yb and ^{175}Lu, detected on an inductively coupled plasma sector field mass spectrometer (ICP-SF-MS), Thermo Fisher ELEMENT II, equipped with a dry introduction Cetac ARIDUS [*Shen et al.*, 2011] system. Two-month 2-sigma reproducibility is ±1.9-6.5%. The detailed instrumental settings and analytical methodology are described in *Shen et al.* [2001].

Nd isotope:

Planktonic foraminifer *G. ruber* and sediment (<63 ⌈m) samples were collected from two depths of 472-477 cm (49.5-50.1 kyr BP, 580 individuals, >250 μm) and 537-542 cm (58.8-60.6 kyr BP, 250 individuals, >250 μm) of core MD05-2925. The picked planktonic foraminifer samples were cleaned with the same protocol for REE/Ca ratio analysis and then dissolved in 2 M HNO_3. The sediment samples were first cleaned with 10% CH_3COOH to remove carbonate, and

subsequently cleaned with a reductive reagent (1 M $NH_2OH \cdot HCl$ in 25% CH_3COOH) to remove Fe-Mn phases on the sample surface [*Bayon et al.*, 2004]. The cleaned sediment samples were decomposed in a mixed solution of HF, $HClO_4$, and HNO_3, and then dissolved in 2 M HNO_3.

Neodymium in the 2 M HNO_3 dissolved samples was extracted by a two-stage column separation [*Pin and Zalduegui*, 1997]. The REE fraction in the solution was purified from the remaining major and trace elements using Eichrom RE resin. Neodymium was subsequently separated from the other REE with Eichrom Ln resin.

Neodymium isotopic compositions were measured by a multi-collector ICP-MS (MC-ICP-MS), Thermo Fisher Neptune, in the HISPEC. The measured $^{143}Nd/^{144}Nd$ ratios were normalized to $^{146}Nd/^{144}Nd = 0.7219$ using an exponential law. La Jolla standard was measured at 0.511811±0.000014 (2σ, n = 13). All $^{143}Nd/^{144}Nd$ ratios were calibrated to the reported value relative to the La Jolla standard value of 0.511858 [*Lugmair et al.*, 1983]. Sample $^{143}Nd/^{144}Nd$ ratios [$(^{143}Nd/^{144}Nd)_{sample}$] are expressed as ε notation defined by an equation of $\varepsilon_{Nd} = [(^{143}Nd/^{144}Nd)_{sample/}(^{143}Nd/^{144}Nd)_{CHUR}-1]\times10^4$, where the $^{143}Nd/^{144}Nd$ ratio of CHUR standard for Chondritic Uniform Reservoir [$(^{143}Nd/^{144}Nd)_{CHUR}$] is 0.512638 [*Jacobsen and Wassergurg*, 1980].

$\delta^{18}O_{SW\text{-}IVC}$ calculation

To extract seawater $\delta^{18}O$ ($\delta^{18}O_{SW}$) values, we used a cultural based equation, $SST = 16.5 - 4.8 \times (\delta^{18}O_C - \delta^{18}O_{SW})$ [*Bemis et al.*, 1998] and a constant offset of 0.27‰ between carbonate VPDB and Vienna Standard Ocean Water (VSMOW) scales. Ice volume corrected $\delta^{18}O_{SW}$ ($\delta^{18}O_{SW\text{-}IVC}$) was calculated using the method proposed by *Waelbroeck et al.* [2002]. We only calculated $\delta^{18}O_{SW\text{-}IVC}$ for the last

termination, because the complication of long-term sea level reconstruction.

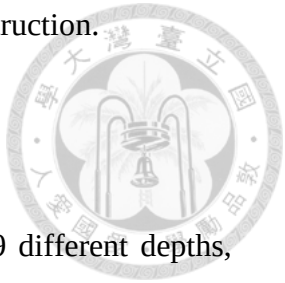

Age model

A series of planktonic foraminiferal AMS ^{14}C dates at 19 different depths, including 200 individuals of *Globigerinoides sacculifer* (>500 μm) each, from the upper 292 cm of the core were measured. Dates were calibrated to calendar ages (before 1950 AD) using CALIB 6.0.1 software [*Stuiver et al.*, 2010] with a reservoir age difference (ΔR) estimated from the Marine Reservoir Correction Database (http://calib.qub.ac.uk/marine/). The calculated weighted mean ΔR value is 64 ± 23 years for the selected four sites around the Solomon Sea [*Petchey et al.*, 2004]. The chronology was based on linear interpolation between calibrated ^{14}C dates [Figure 2-1, Table 2-1].

Composite benthic foraminiferal oxygen isotope data are established with benthic foraminifera (>250 μm, 2-4 individuals each depth), including the *Uvigerina spp.* (171 samples), *Cibicidoides wuellerstorfi* (9 samples), and *Bulimina spp.* (6 samples) [Figure 2-2]. The $\delta^{18}O$ offset calibration between *Uvigerina spp.* and *C. wuellerstorfi* is +0.64‰ [*Shackleton and Opdyke*, 1973], and between *Uvigerina spp.* and *Bulimina spp.* is -0.11‰ [*Oba et al.*, 2006].

For core samples below 292 cm, the age model was constructed by correlating the composite benthic foraminiferal oxygen isotopic data of core MD05-2925 to the LR04 stack record [*Lisiecki and Raymo*, 2005]. All age control points are summarized in Table 2-2 In addition, the age model is supported by two planktonic/nannofossil biostratigraphic events. The last occurrence (LO) of *G. ruber* (pink) occurred between the depth of 830 and 835 cm, average dated 126.8 kyr, which is consistent with the observation in the southern South China Sea [*Lee et al.*, 1999].

The first occurrence (FO) of *Emiliania huxleyi* was observed between the depth of 1550 and 1580 cm, with an age estimate of about 293-299 kyr and within Marine Isotope Stage (MIS) 8. The overall sedimentation rate is ~10 cm/kyr. The relatively high sedimentation rates ranged from 10-40 cm/kyr occurred at upper section of MD05-2925 from the depth of 0-300 cm which represents ~170 years per sample. For lower section, each sample represents ~906 years.

Radiative forcing calculation

Details of the ΔRF_{GHG} calculation should consider all the major greenhouse gases, and calculate the differences between certain past time and the pre-industrial greenhouse gases level ($[CO_2]_0$ = 280 ppm, $[CH_4]_0$ = 700 ppb, and $[N_2O]_0$ = 720 ppb, *Ramaswamy et al.*, 2001). The full equations to determine ΔRF_{GHG} are listed below:

$$\Delta RF_{CO2} = 4.841 \ln ([CO_2]/[CO_2]_0) + 0.0906 (\sqrt{[CO_2]} - \sqrt{[CO_2]_0})$$

EQ1

$$\Delta RF_{CH4} = 0.036 (\sqrt{[CH_4]} - \sqrt{[CH_4]_0}) - [0.47 \ln\{1 + 2.01x10^{-5} ([CH_4] [N_2O]_0)^{0.75} + 5.31x10^{-15} [CH_4] ([CH_4] [N_2O]_0)^{1.52}\}] - [0.47 \ln\{1 + 2.01x10^{-5} ([CH_4]_0 [N_2O]_0)^{0.75} + 5.31x10^{-15} [CH_4]_0 ([CH_4]_0 [N_2O]_0)^{1.52}\}]$$

EQ2

The contribution of N_2O to CH_4-induced radio forcing, however, is too small, and the EQ2 could be simplified as:

$$\Delta RF_{CH4} = 0.036 (\sqrt{[CH_4]} - \sqrt{[CH_4]_0})$$

EQ3

The sum of EQ1 and EQ3 is the total ΔRF_{GHG} during the past 360 kyrs, however, the CH_4 only contribute <5% of the RF. Thus in this study we only consider the RF contributed by CO_2 (EQ1).

Non-overlapping binned method

To build stacked N- and S-IPWP records, we followed the suggestions by *Leduc et al.* [2010] and considered three criteria for this dataset: (1) sites location within 12°N to 15°S, which is the main IPWP range [*Yan et al.*, 1992; *Gagan et al.*, 2004], (2) little or no influence by coastal upwelling, and (3) usage of specific proxies, Mg/Ca-derived SST and $\delta^{18}O_C$ records, of planktonic foraminifer, *G. ruber* (white, *s. s.*). We adopted the age model for sites, ODP 806, MD97-2140, MD97-2141, MD98-2162, MD98-2170, MD98-2176, and MD98-2181. For records with available original radiocarbon ages from sites, including MD01-2378, MD01-2390, MD98-2165, and MD06-3067, we recalculated the age models using new CALIB 6.0.1 program [*Stuvier et al.*, 2010]. The sea level change effect on $\delta^{18}O_{SW}$ was also corrected. The MATLAB code of a non-overlapping binned method was provided by Dr. D. W. Oppo and Dr. B. K. Linsley [*Oppo et al.*, 2009; *Linsley et al.*, 2010]. We divided the total data into every 400-yr window and calculated the mean and standard error of mean for each time window.

ODP 806 (0.3°N, 159.4°E, water depth 2520 m, *Lea et al.*, 2000), MD97-2140 (2.0°N, 141.7°E, water depth 2547 m, *de Garidel-Thoron et al.*, 2005), ODP 871 (5.6°N, 172.3°E, water depth 1255 m, *Dyez and Ravelo*, 2012), TR163-19 (2.3°N, 91°W, water depth 2348 m, *Lea et al.*, 2000), and ODP 1240 (0.0°N, 86.5°E, water depth 2921 m, *Pena et al.*, 2008) have also been collected to calculate the average climatic sensitivity [Table 2-4]. Due to the effect of time resolution, we resampled

ODP 806, ODP 871, TR163-19, and MD97-2140 into 4-kyr, and ODP 1240 into 1-kyr time resolution and then compared to the same time resampled Antarctica ΔT and pCO_2 records to calculated ΔRF_{GHG}.

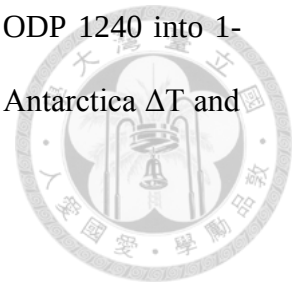

EOF analysis

We applied an empirical orthogonal function (EOF) analysis of modern SST dataset [1950-2004 AD, *Reynolds et al.*, 2002] for a sector from 20^oS – 20^oN, and 100^oE- 180^oE to determine the boundary between North- and South-IPWP [Chapter 3]. EOF1 factor identified clearly different SST variation groups between equator. EOF2 shows minor (9.7%) but significant inter-annual zonal (ENSO) control on the SST patterns.

FOAM

The simulated precipitation and other climatological records [Chapter 4] were calculated from an orbital-accelerated transient run using the coupled fast ocean-atmosphere model (FOAM, *Kutzbach et al.*, 2008; *Shi et al.*, 2011). With a factor of 100, the experiment was integrated for 2840 years under the orbital forcing only to obtain the climate evolution during the past 284 kyr. Changes in global ice volume/sea level and greenhouse gases were neglected. The spatial resolution was set to 4°×7.5° for atmosphere and 1.4°×2.8° for the ocean. A detailed description is available in *Kutzbach et al.* [2008], and *Shi et al.* [2011].

References

Bayon, G., German, C. R., Boella, R. M., Milton, J. A., Taylor, R. N., and Nesbitt, R. W., (2002), An improved method for extracting marine sediment fractions and its application to Sr and Nd isotopic analysis. *Chemical Geology* **187**, 179-199.

Beaufort, L., Chen, M.-T., Droxler, A. W., Shipboard scientific party, (2005), MD148- PECTEN IMAGES XIII cruise report, Institut Polire Francais Paul Emile Victor, Plouzaně, France.

Bemis, B. E., Spero, H. J., Bijima, J., and Lea, D. W., (1998). Revealuation of the oxygen isotopic composition of planktonic foraminifera: Experiomental results and revised paleotemperature equations. *Paleoceanography* **12**, 150-160.

Bolliet, T., Holbourn, A., Kuhnt, W., Laj, C., Kissel, C., Beaufort, L., Kienast, M., Andersen, N., and Garbe-Schönberg, D., (2011), Mindanao Dome variability over the last 160 kyr: Episodic glacial cooling of the West Pacific Warm Pool. *Paleoceanography* **26**, PA1208, doi: 10.1029/2010PA001966.

Cravatte, S., Ganachaud, A., Duong, Q. P., Kessler, W. S., Eldin, G., and Dutrieux, P., (2011), Observed circulation in the Solomon Sea from SADCP data. *Progress in Oceanography* **88**, 116-130.

de Garidel-Thoron, T., Rosenthal, Y., Bassinot, F., and Beaufort, L., (2005), Stable sea surface temperatures in the western Pacific warm pool over the past 1.75 million years. *Nature* **433**, 294 – 298.

Dyez, K. A., and Ravelo, A. C., (2012), Late Pleistocene tropical Pacific temperature sensitivity to radiative greenhouse gas forcing. *Geology* **41**, 23-26.

Gagan, M. K., Hendy, E. J., Hagerle, S. G., and Hantoro, W. S., (2004), Post-glacial evolution of the Indo-Pacific Warm Pool and El Nino-Southern oscillation. *Quaternary International* **118-119**, 127-143.

Garcia, H. E., Locarnini, R. A., Boyer, T. P., Antonov, J. I., Baranova, O. K., Zweng, M. M., and Johnson, D. R., (2010), *World Ocean Atlas 2009, Volume 3: Dissolved Oxygen, Apparent Oxygen Utilization, and Oxygen Saturation* (eds. Levitus, S.) NOAA Atlas NESDIS 70, U.S. Government Printing Office, Washington, D.C., 344 pp.

Gimeno, L., Stohl, A., Trigo, r. M., Dominguez, F., Yoshimura, K., Yu, L., Drumond, A., Duran-Quesada, A. M., and Nieto, R., (2012), Oceanic and terrestrial sources of contiental precipitation. *Reviews of Geophysics* **50**, RG4003.

Grenier, M., Cravatte, S., Blanke, B., Menkes, C., Joch-Larrouy, A., Durand, F., Melet, A., and Jeandel, C., (2011), From the western boundary currents to the Pacific Equatorial Undercurrent: Modeled pathways and water mass evolutions. *Journal of Geophysical Research* **116**, C12044, doi: 10.1029/JC007477.

Jacobsen, S. B. and Wasserburg, G. J., (1980), Sm–Nd isotopic evolution of chondrites. *Earth and Planetary Science Letters* **50**, 139–155.

Jahnke, R.A., (2003), Benthic oxygen fluxes. *JGOFS Report*, **38**, pp17.

Kutzbach, J. E., Liu, X., Liu, Z. and Chen, G., (2008), Simulation of the evolutionary response of global summer monsoons to orbital forcing over the past 280,000 years. *Climate Dynam*ics **30,** 567-579.

Lea, D. W., Pak, D. K., and Spero, H. J., (2000), Climate impact of late Quaternary equatorial Pacific sea surface temperature variations. *Science* **289**, 1719 – 1724.

Leduc, G., Schneider, R., Kim, J. H., and Lohmann, G., (2010), Holocene and Eemian sea surface temperature trends as revealed by alkenone and Mg/Ca paleothermometry. *Quaternary Science Reviews* **29**, 989 – 1004.

Lee, M. Y., Wei, K. Y., and Chen Y. G., (1999), High resolution oxygen isotope stratigraphy for the last 150,000 years in the southern South China Sea: Core MD972151. *Terrestrial, Atmospheric, and Ocean Sciences* **10**, 239-254.

Levi, C., Labeyrie, L., Bassinot, F., Guichard, F., Cortijo, E., Waelbroeck, C., Caillon, N., Duprat, J., de Garidel-Thoron, T., and Elderfield, H., (2007), Low-latitude hydrological cycle and rapid climate changes during the last deglaciation. *Geochemistry, Geophysics, Geosystems* **8**, Q05N12, doi: 10.1029/2006GC001514.

Linsley, B. K., Rosenthal, Y., and Oppo, D. W., (2010), Holocene evolution of the Indonesian throughflow and the western Pacific warm Pool. *Nature Geoscience* **3**, 578 – 583.

Lisiecki, L. E., and Raymo, M. E., (2005), A Pliocene-Pleistocene stack of 57 globally distributed benthic $\delta^{18}O$ records. *Paleoceanography* **20**, PA1003.

Lo, L., Lai, Y.-H., Wei, K.-Y., Lin, Y.-S., Mii, H.-S., and Shen, C.-C., (2013), Persistent sea surface temperature and declined sea surface salinity in the northwestern tropical Pacific over the past 7500 years. *Journal of Asian Earth Sciences* **66**, 234-239.

Lo, L., Shen, C.-C., Lu, C.-J., Chen, Y.-C., Chang, C.-C., Wei, K.-Y., Qu, D., and Gagan, M. K., (2014), Determination of element/Ca ratios in foraminifera and corals using cold- and hot-plasma techniques in inductively coupled plasma sector field mass spectrometry. *Journal of Asian Earth Sciences* **81**, 115-122.

Locarnini, R. A., Mishonov, A. V., Antonov, J. I., Boyer, T. P., Garcia, H. E., Baranova, O. K., Zweng, M. M., and Johnson, D. R., (2010), World Ocean Atlas 2009, in Levitus, S. ed. *NOAA Atlas NESDIS 68*, U.S. Government Printing Office, Washington, D.C..

Lugmair, G. W., Shimamura, T., Lewis, R. S., and Anders, E., (1983), Samarium-146 in the early solar system: evidence from neodymium in the Allende meteorite. *Science* **222**, 1015-1018.

Milliman, J. D., Farnsworth, K. L., and Albertin, C. S., (1999), Flux and fate of fluvial sediments leaving large islands in the East Indies. *Journal of Sea Research* **41,** 97-107.

Melet, A., Gourdeau, L., and Verron, J., (2010a), Variability in Solomon Sea circulation derived from altimeter sea level data. *Ocean Dynamics* **60**, 883-900.

Melet, A., Gourdeau, L., Kessler, W. S., Verron, J., and Molines, J.-M., (2010b), Thermocline Circulation in the Solomon Sea: A Modeling Study. *Journal of Physical Oceanography* **40**, 1302-1319.

Melet, A., Verron, J., Gourdeau, L., and Koch-Larrouy, A., (2011), Equatorial pathways of Solomon Sea water masses and their modification. *Journal of Physical Oceanography* **40**, 810 – 826.

Oba, T., Irino, T., Yamamoto, M., Murayama, M., Takamura, A., and Aoki, K., (2006), Paleoceanographic change off central Japan since the last 144,000 years based on high-resolution oxygen and carbon isotope records. *Global and Planetary Change* **53**, 5-20.

Oppo, D. W., Rosenthal, Y., and Linsley, B. K., (2009), 2,000-year-long temperature and hydrology reconstructions from the Indo-Pacific warm pool. *Nature* **460**, 1113 – 1116.

Pena, L. D., Cacho, I., Ferretti, P., and Hall, M. A., (2008), El Niño-Southern Oscillation-like variability during glacial terminations and interlatitudinal teleconnections. *Paleoceanography* **23**, PA3101.

Petchey, F., Phelan, M., and White, J. P., (2004), New ΔR values for the Southwest Pacific Ocean. *Radiocarbon* **46,** 1005-1014.

Pin, C., and Zalduegui, J. F. S., (1997), Sequential separation of light rare-earth elements, thorium and uranium by miniaturized extraction chromatography: Application to isotopic analyses of silicate rocks. *Analytica Chimica Acta* **339**, 79-89.

Radenac, M., Léger, F., Singh, A., and Delcroix T., (2012), Sea surface chlorophyll signature in the tropical Pacific during eastern and central Pacific ENSO events. *J*ournal of *Geophys*ics *Res*earch **117**, C04007, doi: 10.1029/2011JC007841.

Ramaswamy, V., Boucher, O., Haigh, J., Hauglustaine, D., Haywood, J., Myhre, G., Nakajima, T., Shi, G., Solomon, S., and Betts, R., (2001), Radiative forcing of climate change in, *Climate Change 2001: The Scientific Basis*, Houghton, J. T., *et al.* eds., Cambridge University Press, 319-416.

Reynolds, R. W., Rayner, N. A., Smith, T. M., and Stokes, D. C., (2002), An improved in situ and satellite SST analysis for climate. *Journal of Climate* **15**, 1609 – 1625.

Rosenthal, Y., Oppo, D. W., and Linsley, B. K., (2003), The amplitude and phasing of climate change during the last deglaciation in the Sulu Sea, western equatorial Pacific. *Geophysical Research Letters* **30**, 1428, doi: 10.1029/2002GL016612.

Shackleton, N. J., and Opdyke, N. D., (1973), Oxygen isotope and palaeomagnetic stratigraphy of equatorial Pacific core V28-238: Oxygen isotope temperatures and ice volumes on a 10^5 year and 10^6 year Scale. *Quaternary Res*earch **3**, 39-55.

Shen, C.-C., Hastings, D. W., Lee, T., Chiu, C.-H., Lee, M.-Y., Wei, K.-Y., Edwards, R. L., (2001), High precision glacial–interglacial benthic foraminiferal Sr/Ca records from the eastern equatorial Atlantic Ocean and Caribbean Sea. *Earth and Planet*ary *Sciences Letters* **190**, 197-209.

Shen, C.-C., Wu, C.-C., Liu, Y., Yu, J., Chang, C.-C., Lam, D. D., Chou, C.-J., Lo, L., and Wei, K.-Y., (2011), Measurements of natural carbonate rare earth elements in femtogram quantities by inductive coupled plasma sector field mass spectrometry. *Analytical Chemistry* **83,** 6842-6848.

Shi, Z. G., Liu X. D., Sun, Y. B., An, Z. S., Liu, Z., and Kutzbach, J., (2011), Distinct responses of East Asian summer and winter monsoons to astronomical forcing. *Climate of the Past* **7,** 1363-1370.

Shiau, L.-J., Chen, M.-T., Huh, C.-A., Yamamoto, M., and Yokoyama, Y., (2012), Insolation and cross-hemispheric controls on Australian monsoon variability over the past 180 ka: new evidence from off shore southeastern Papua New Guinea. *Journal of Quaternary Science* **27**, 911-920.

Steinke, S., Chiu, H.-I., Yu, P.-S., Shen, C.-C., Erlenkeuser, H., Löwemark, L., and Chen, M.-T., (2006), On the influence of sea level and monsoon climate on the southern South China Sea freshwater budget over the past 22,000 years. *Quaternary Science Reviews* **25**, 1475 – 1488.

Stott, L., Cannariato, K., Thunell, R., Haug, G. H., Koutavas, A., and Lund, S., (2004), Decline of surface temperature and salinity in the western tropical Pacific Ocean in the Holocene epoch. *Nature* **431**, 56 – 59.

Stott, L., Poulsen, C., Lund, S., and Thunell, R., (2002), Super ENSO and global climate oscillations at millennial time scales. *Science* **297**, 222-226.

Stuiver, M., Reimer, P. J., and Reimer, R. W., (2010), CALIB 6.0. [WWW program and documentation].

Visser, K., Thunell, R., and Stott, L., (2003), Magnitude and timing of temperature change in the Indo-Pacific warm pool during deglaciation. *Nature* **421**, 152 – 155.

Waelbroeck, C, Labeyire, L., Michel, E., Duplessy, J. C., McManus, J. F., Lambeck K., Balbon, E., and Labracherie, M., (2002), Sea-level and deep water temperature changes derived from benthic foraminifera isotopic records. *Quaternary Science Reviews* **21**, 295-305.

Xu, J., Holbourn, A., Kuhnt, W., Jian, Z., and Kawamura, H., (2008), Changes in the thermocline structure of the Indonesian outflow during Terminations Ⅰ and Ⅱ. *Earth and Planetary Science Letters* **273**, 152 – 162.

Yan, X.-H., Ho, C.-R., Zheng, Q., and Klemas, V., (1992), Temperature and size variabilities of the western Pacific warm pool. *Science* **258**, 1643-1645.

Table 2-1. AMS ^{14}C dates of core MD05-2925

Depth (cm)	Conventional ages ^{14}C age (yr) ± error		Calendar ages Dates ± error (2σ)		AMS Lab
2	1516	58	1022.5	140.5	U. Arizona[1]
5	1737	30	1223	79	GNS[2]
22	3534	41	3345	104	U. Arizona
35	4068	30	4013	123	GNS
72	6588	47	7027	138	U. Arizona
90	7751	35	8149.5	124.49	GNS
102	8030	65	8441	139	U. Arizona
117	8823	50	9413.5	110.5	GNS
127	10306	70	11258.5	158.5	U. Arizona
147	10411	70	12854	109.99	U. Arizona
157	12066	60	13392	83.99	GNS
172	13117	71	14972.5	308.5	U. Arizona
180	13748	35	16283	453	GNS
192	14080	74	16745.5	222.5	U. Arizona
207	15616	75	18200.5	174.5	GNS
217	16470	81	19082.5	89.5	U. Arizona
262	18985	94	22166.5	180.49	U. Arizona
272	20960	150	24411	167	U. Arizona
292	24650	78	25303.5	338.5	U. Arizona

[1] NSF-Arizona AMS Laboratory in University of Arizona (U. Arizona), Tucson, USA.
[2] Rafter Radiocarbon Laboratory, Institute of Geological and Nuclear Science (GNS), New Zealand.

Table 2-2. Depth-age pairs of control points by $\delta^{18}O$ graphic fitting to LR04 stack [*Lisiecki and Raymo*, 2005].

Depth (cm)	Age (kyr)
389	35.7
489	54.4
568	72.2
651	84.9
739	100.6
803	118.3
844	129.1
883	141.6
997	165.2
1112	192.0
1320	244.6
1432	260.6
1525	287.8
1702	324.4
1767	334.4
1866	358.6

Table 2-3. Selected sites for stacked N- and S-IPWP records.

Core	Location (Latitude, and Longitude)	References
North-IPWP group (orange circles in Figure 3-1 and 3-S2)		
ODP 806	0.3°N, 159.4°E	*Lea et al.*, 2000
MD97-2140	2.0°N, 141.7°E	*de Garidel-Thoron et al.*, 2005
MD98-2181	6.3°N, 125.83°E	*Stott et al.*, 2002; 2004
MD06-3067	6.5°N, 126.5°E	*Bolliet et al.*, 2011
MD97-2141	8.8°N, 121.3°E	*Rosenthal et al.*, 2003
MD01-2390	12.1°N, 113.24°E	*Stenike et al.*, 2006
South-IPWP group (green circles and star in Figure 3-1 and 3-S2)		
MD98-2162	4.4°S, 117.5°E	*Visser et al.*, 2003
MD98-2176	5.0°S, 133.4°E	*Stott et al.*, 2004
MD05-2925	9.3°S, 151.5°E	This Study
MD98-2165	9.7°S, 118.3°E	*Levi et al.*, 2007
MD98-2170	10.6°S, 125.4°E	*Stott et al.*, 2004
MD01-2378	13.1°S, 121.7°E	*Xu et al.*, 2008

Table 2-4. Selected sites for greenhouse gases radiative forcing calculation.

Core	Location (Latitude, and Longitude)	References
North-IPWP group		
ODP 806	0.3°N, 159.4°E	*Lea et al.*, 2000
MD97-2140	2.0°N, 141.7°E	*de Garidel-Thoron et al.*, 2005
ODP 871	5.6°N, 172.3°E	*Dyez and Ravelo.*, 2012
South-IPWP and EEP group		
TR163-19	2.3°N, 91°W	*Lea et al.*, 2000
ODP 1240	0.0°N, 86.5°E	*Pena et al.*, 2008
MD05-2925	9.3°S, 151.5°E	This Study

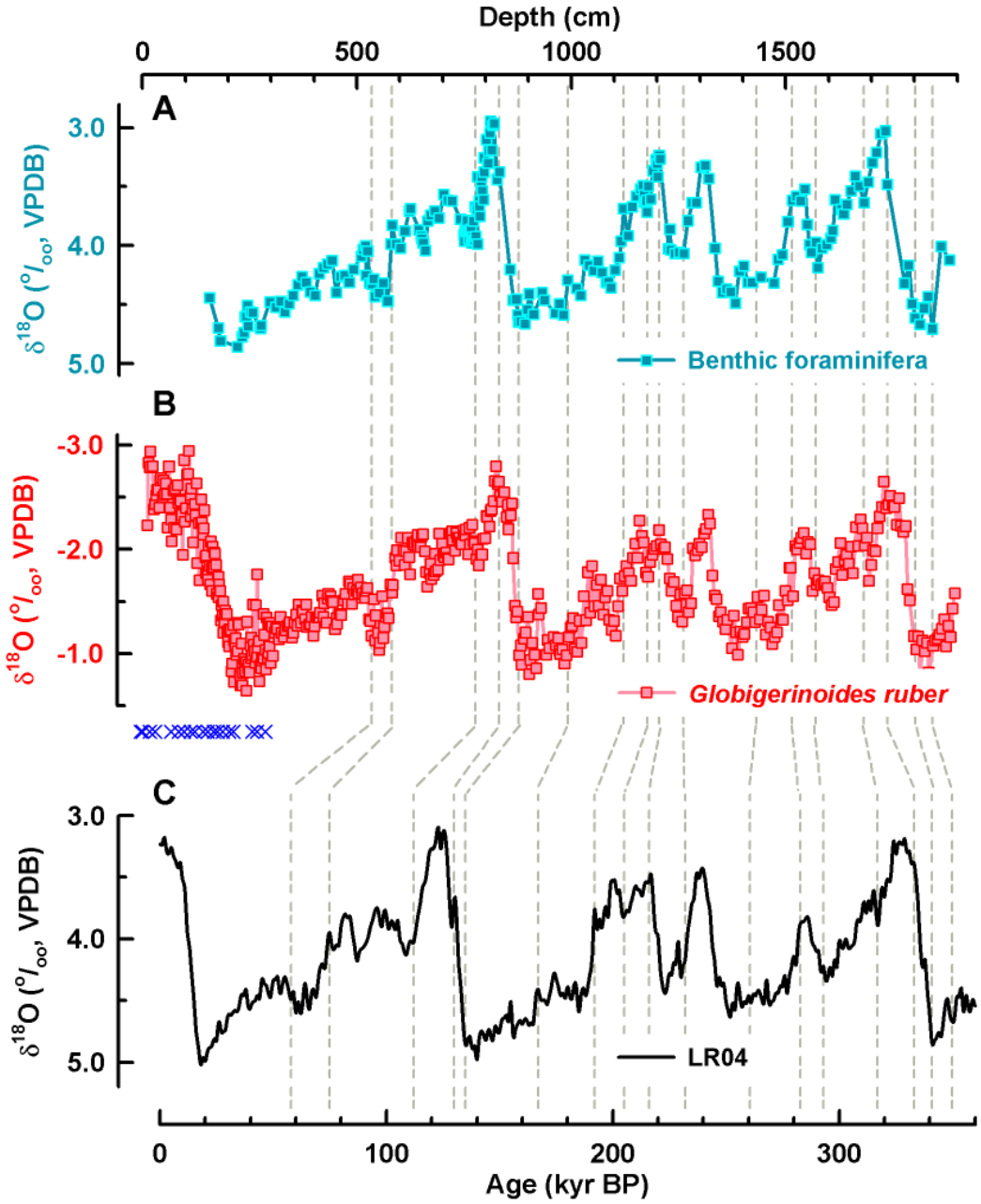

Figure 2-1. Age model of core MD05-2925. Blue cross symbols denote calibrated AMS ^{14}C dates used for upper 292 cm. (A) a composite MD05-2925 benthic foraminiferal $\delta^{18}O$ record, (B) MD05-2925 *G. ruber* $\delta^{18}O$ record. Dashed lines are the age control points by comparing with (C) global composite LR04 [*Lisiecki and Raymo*, 2005].

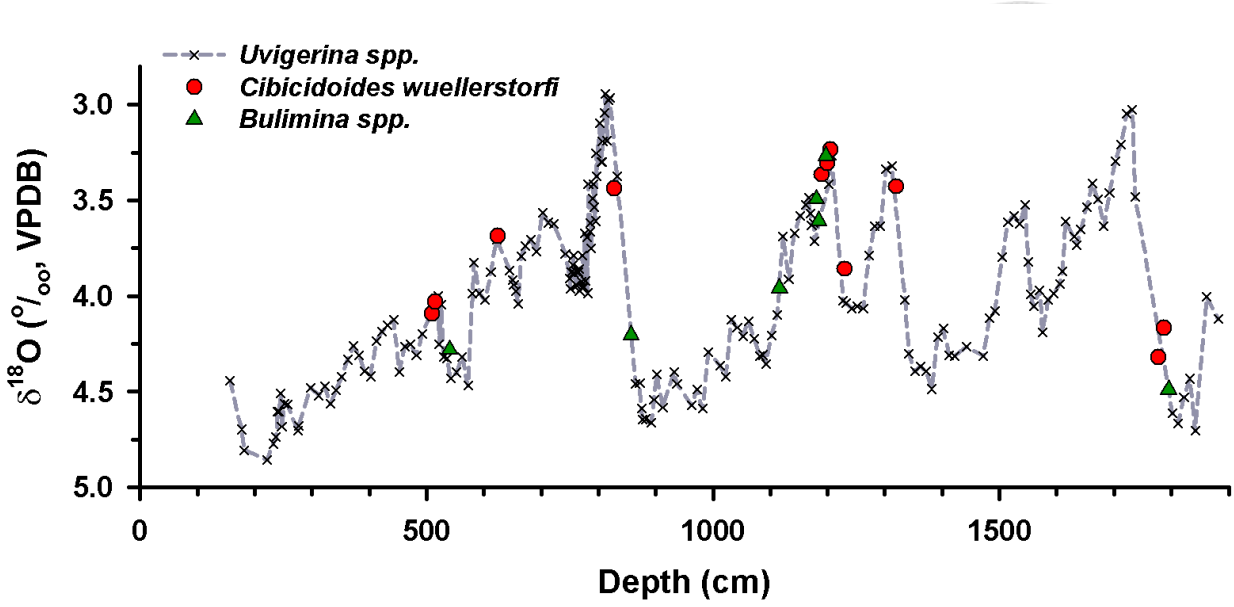

Figure 2-2. Composite benthic foraminiferal oxygen isotope record of core MD05-2925. Cross symbols with dark gray dashed line denote the oxygen isotope data for *Uvigerina spp.* Red dots and green triangles are the corrected $\delta^{18}O$ data of *C. wuellerstorfi* [*Shackleton and Opdyke*, 1973] and *Bulimina spp.* [*Oba et al.*, 2006], respectively.

Chapter 3.

Millennial meridional dynamics of Indo-Pacific Warm Pool during the last deglaciation

In Manuscript as **Li Lo**, Chuan-Chou Shen, Kuo-Yen Wei, George S. Burr, Horng-Sheng Mii, Min-Te Chen, Shih-Yu Lee, Meng-Chieh Tsai. Millennial meridional dynamics of Indo-Pacific Warm Pool during the last deglaciation

Millennial meridional dynamics of Indo-Pacific Warm Pool during the last deglaciation

Li Lo[1], Chuan-Chou Shen[1,*], Kuo-Yen Wei[1], George S. Burr[2], Horng-Sheng Mii[3], Min-Te Chen[4], Shih-Yu Lee[5], Meng-Chieh Tsai[1]

1. High-Precision Mass Spectrometry and Environment Change (HISPEC) Laboratory, Department of Geosciences, National Taiwan University, Taipei 10617, Taiwan, R.O.C.

2. NSF-Arizona Accelerator Mass Spectrometry Facility, Department of Physics, University of Arizona, Tucson, AZ 85721, USA

3. Department of Earth Sciences, National Taiwan Normal University, Taipei 11677, Taiwan, R.O.C.

4. Institute of Applied Geosciences, National Taiwan Ocean University, Keelung 20224, Taiwan, R.O.C.

5. Research Center for Environmental Changes, Academia Sinica, Taipei 11529, Taiwan, R.O.C.

To be submitted to *Climate of the Past*

2014

*Corresponding Author: Chuan-Chou Shen

Email: river@ntu.edu.tw; Tel: 886-2-3366-5878

Abstract

To in-depth understand the natural dynamics of the Indo-Pacific Warm Pool (IPWP) during the last deglaciation, stacked North- (N-) and South-IPWP (S-IPWP) thermal and hydrological records over the past 23-10.5 thousand years were built using planktonic foraminiferal geochemistry data from core MD05-2925 (9.3^{o}S, 151.5^{o}E, water depth 1661 m) in the Solomon Sea and eleven previous studied sites. Ice-volume corrected seawater $\delta^{18}O$ stacks show that S-IPWP $\delta^{18}O$ value is indistinguishable from its north counterpart through the glacial time. The N-IPWP SST stacked record is featured with an increase trend of 0.5 ^{o}C/kyr since ~18 ka. Its counterpart record in the S-IPWP shows an early onset of temperature increase at ~19 ka and a strong teleconnection to the high-latitude climate in south hemisphere. Meridional SST gradients between N- and S-IPWP were 1.5^{o}C during the Bølling/Allerød (B/A) period and only ~1^{o}C during the Heinrich event 1 (H1) and Younger Dryas (YD). The warm S-IPWP during the two events could weaken the northern hemispheric convection branch of the Hadley Cell and further reduce precipitation in the Asian Monsoon region.

1. Introduction

Indo-Pacific Warm Pool (IPWP) is the largest warm water mass with annual average sea surface temperature (SST) higher than 28^{o}C [*Yan et al.*, 1992]. The regional vigorous atmosphere circulation transports most profound latent heat and water moisture to the middle and high latitudes [*Yan et al.*, 1992]. For the past five decades, expended IPWP has caused the regional surface water freshening and the westward movement of precipitation zone, resulting in regional drought in the East Africa and storm track changes in East Australia [*Cravatte et al.*, 2009; *Williams and*

Funk, 2011]. Since the early 2000s, intense paleoclimatology studies have been conducted to understand IPWP long-term thermal and hydrological changes during the glacial/interglacial (G/IG) cycles and to test the sensitive of warm pool thermal and hydrological fluctuations to the high latitude ice sheet and greenhouse gases concentration variations through the late Pleistocene [e.g., *Lea et al.*, 2000; *Stott et al.*, 2002; *Visser et al.*, 2003; *Rosenthal et al.*, 2003; *Stott et al.*, 2004; *de Garidel-Thoron et al.*, 2005; *Steinke et al.*, 2006; *Levi et al.*, 2007; *Xu et al.*, 2008; *Linsley et al.*, 2010; *Bolliet et al.*, 2011].

Multi-sites stacked IPWP SST and seawater oxygen isotope ($\delta^{18}O_{SW}$) records since the last glacial to Holocene clearly show a close link of IPWP SST and hydrological with Asian-Australian Monsoon (AAM) system and sea level change [*Stott et al.*, 2004; *Oppo et al.*, 2009; *Linsley et al.*, 2010]. However, complicated ocean-island configuration and regional topography hinder the fidelity of detailed describing its past climate changes [*Griffiths et al.*, 2009; *Mohtadi et al.*, 2011]. Especially, little is known about its meridional thermal-hydrological dynamics between North- (N-) and South-IPWP (S-IPWP) during the last termination transition.

Here we present new oceanic proxy-inferred SST and ice volume corrected surface seawater oxygen isotope $\delta^{18}O$ ($\delta^{18}O_{SW\text{-}IVC}$) records from the Solomon Sea, Papua New Guinea (PNG) over the past 23-10.5 thousand years ago (ka, before 1950 AD). New SST and $\delta^{18}O_{SW\text{-}IVC}$ stacked records since the last termination are built for both N- and S-IPWP to understand their regional thermal and hydrological change and teleconnection with interhemispheric high-latitudes.

All the materials and methods are stated in Chapter 2. Site locations, geochemical proxies results, and modern climatological figures are in the Figures 3-1, 3-S1, and 3-S2, respectively.

2. Results and Discussion

2.1 Solomon SST and $\delta^{18}O_{W\text{-}IVC}$ records during the last termination

The Mg/Ca-inferred SST record reveals a stable glacial thermal condition during 23.0-18.5 ka with a variation less than 1^{o}C and a glacial-interglacial difference of ~3^{o}C between the last glacial maximum (LGM) and the end of Younger Dryas (YD) [Figure 3-2A]. This record is characterized by (i) the ending of glacial time at 18.5 ka, and (ii) rapid SST increases of 1-2^{o}C at time windows of 18.5-18.0, 17.0-16.0, 15.0-14.5, and 13.0-12.5 ka.

The onset of deglacial SST increase at this study site is consistent with the timing of thermal change in the southern ocean shown in the Antarctica ice core δD records [*Stenni et al.,* 2003, Figure 3-2A]. This agreement indicates a strong climatic teleconnection between low- and high-latitude realms in the Southern Hemisphere (SH). There is a significant SST increase of 1-2^{o}C during Heinrich event (H1) and YD. Previous studies from the Eastern Equatorial and South Pacific reveal the mechanism by the early warming of South Pacific subtropical mode water [*Pahnke et al.*, 2003; *Lamy et al.*, 2004; *Pena et al.*, 2008]. The warming signal was transported through the gyre circulation to the east equatorial Pacific and eventually to the west Pacific [Figure 3-2A]. However, except for the Cariaco Basin, there is no significant millennial timescales SST perturbations have been reported in the tropical Atlantic, and tropical Pacific [*Stott et al.*, 2002; *Lea et al.*, 2003; *Rosenthal et al.*, 2003; *Stott et al.*, 2004; *Weldeab et al.*, 2005, 2006, 2007; *Ziegler et al.*, 2008; *Bolliet et al.*, 2011].

The Solomon Sea $\delta^{18}O_{SW\text{-}IVC}$ record is given in Figure 3-2B. It varies from -0.5 to 0.1‰ during 23.0-10.5 ka. A relative stable condition with 1-sigma variability of 0.1‰ occurred from 23.0-16.0 ka. Two significant positive excursions with 0.2-0.5‰ enrichment in $\delta^{18}O$ are observed at intervals of 16.8-15.0, and 13.8-11.8 ka.

Two stable periods with low$\delta^{18}O_{SW\text{-}IVC}$ of about -0.4‰ are during 15.0-13.0 ka and younger than 11.8 ka.

The dramatic $\delta^{18}O_{SW\text{-}IVC}$ increasing anomalies during the H1 and YD periods likely result from a weakening and/or southward shifting ITCZ at this region [*Chiang and Bitz*, 2005; *Broccoli et al.*, 2006]. Agreement of $\delta^{18}O$ sequences of Greenland NGRIP ice core and the Solomon Sea $\delta^{18}O_{SW\text{-}IVC}$ indicates that an imprint from high northern hemisphere (NH) during the deglacial periods [Figure 3-2B].

2.2 Millennial timescales variations of N- and S-IPWP SST stacks

Both N- and S-IPWP stacked SSTs show the same temperature difference of ~3^{o}C between the last glacial and interglacial states [Figure 3-3A]. However, there are two significant dissimilarities between the two records. The onset of termination in S-IPWP at ~19 ka, consistent with temperature increase in the Antarctica [*Stenni et al.*, 2003], is 1 kyr earlier than that in N-IPWP [Figure 3-3A]. After 18 ka, the N-IPWP stacked SST increased steadily through the termination with a rate of 0.5 ^{o}C/kyr. Millennial-timescale variability is absent in this record [Figure 3-3A]. The S-IPWP one is however, characterized by a warming trend during H1 and YD periods, similar to Antarctic ice core temperature record [*Stenni et al.*, 2003], and a steady thermal condition at ~27^{o}C during Bølling/Allerød [B/A, or Antarctic Cold Reversal (ACR)] period [Figure 3-3A]. The thermal gradient between N- and S-IPWP is <0.5^{o}C for the two NH cooling events, H1 and YD, smaller than 1-1.5^{o}C for the other stages [Figure 3-3B]. The evidence indicates that the meridional SST gradient between N- and S-IPWP varied over the last termination. S-IPWP SST compilation shows a good correlation with southern high latitude climate system. Persistent N-IPWP with fluctuated S-IPWP may imply a meridional extent dynamic IPWP through the last

deglacial period.

2.3 N- and S-IPWP $\delta^{18}O_{SW\text{-}IVC}$ records

Both N- and S-IPWP $\delta^{18}O_{SW\text{-}IVC}$ compilations feature with (i) high values of 0.8-1.2‰ at the glacial time, (ii) a decreasing trend after 17-16 ka, and (iii) a remarkable fast decrease of 0.2-0.4‰ during the H1 and YD periods [Figure 3-3C]. This in-phasing variability indicates that the two regional hydrological conditions had been governed by the same forcing(s). Previous tropical Atlantic SST and Asian-South American stalagmite $\delta^{18}O$ records show a tight linkage between equatorial hydrological system and ITCZ movement [*Wang et al.*, 2001; *Lea et al.*, 2003; *Wang et al.*, 2007]. The gradient between N- and S-IPWP, with no millennial-timescale anomaly, gradually increased from 0‰ to 0.2‰ through the deglacial periods [Figure 3-3D]. It suggests that a more saline N-IPWP than S-IPWP at the entire record and an increasing salinity difference between N- and S-IPWP over the last G/IG interval.

2.4 Meridional IPWP SST gradient and the southward-shifted ITCZ precipitation boundary

A rapid warming in S-IPWP during the H1 and YD periods, shown in the new compiled SST records [Figure 3-3A], may cause an altered Hadley Cell (HC) circulation, reorientation of the cross equatorial current, and a consequent precipitation reduction in the East Asian Monsoon region. Modern observatory data over the past six decades [Figure 12 of *Feng et al.*, 2013] expresses that an equator-ward shifting of the NH convection branch of HC can be induced by an oceanic warming located at ~10^{o}S This equator-ward shifting of northern branch of HC can cause a southward shift of ITCZ for about 10^{o} [*Feng et al.*, 2013]. This oceanic

process, combined with fast atmospheric bridging [*Chiang and Bitz*, 2005; *Broccoli et al.*, 2006] and confirmed by the marine and cave proxies data [*Wang et al.*, 2001; *Lea et al.*, 2003; *Wang et al.*, 2007], may connect the NH and SH climate systems through a coupled low latitude ocean-atmosphere pathway.

Distinct different precipitation conditions between 10^{o}S in the IPWP during H1 and YD events are illustrated in Figure 3-S3. *Shiau et al.* [2011] proposed an enhanced precipitation during the events in the Coral Sea by using marine sediment thorium isotopic proxy record, which shows a good correlation to the Australian summer monsoon reported by the Lynch's crater records [*Muller et al.*, 2008]. Stalagmite δ^{18}O records from Flores Island are also featured with intense precipitation during YD [*Griffiths et al.*, 2009]. Marine evidences reveal a reduced precipitation/ increased salinity in the northern IPWP region north of 10^{o}S, including South China Sea [*Stenike et al.*, 2006], Sulu Sea [*Rosenthal et al.*, 2003], Philippines Sea [*Stott et al.*, 2002], Java Island [*Mohtadi et al.*, 2012], and Solomon Sea [*This study*] [Figure 3-S3].

On the basis of previous terrestrial and marine hydrological records and our new data, we speculate a sharp precipitation boundary between maritime continents and Australia at about 10^{o}S from Solomon Sea, Arafura Sea, Timor Sea, to the eastern Indian Ocean during the last deglacial period [Figure 3-S3]. The IPWP meridional SST gradient variations and the altered HC circulation may further enhance the precipitation reduction in the Asian monsoon region during the H1 and YD periods.

3. Conclusions

On the basis of our records and previous reports, we found that the meridional IPWP thermal conditions strongly link to interhemispheric high-latitude climates during the last deglaciation: N-IPWP paced by NH and S-IPWP governed by SH. Ice volume corrected $\delta^{18}O_{SW}$ stacked records show an increasing salinity gradient between N- and S-IPWP over the last Termination. We proposed a hypothetical precipitation boundary at about 10^{o}S. Advanced high-resolution model simulations are required to clarify the role of IPWP meridional thermal/hydrological gradient to the altered HC and its relationship with regional and global climate systems over the last deglaciation.

Acknowledgements

MD05-2925 site location was selected by Meng-Yang Lee and collected during the IMAGES PECTEN Cruise, which was conducted by Luc Beaufort and Min-Te Chen. Sediment samples are provided from Taiwan TORI. Chien-Ju Chou, Wan-Lin Hu, and Yu-Ting Hsiao helped to pick foraminifera samples. Yang-Hui Hsu helped to operate climatological database and plotted figures. Thank Delia W. Oppo and Braddock K. Linsley for their generous offering the non-overlapping method MatLab code. This research were funded by Taiwan ROC NSC (98-2811-M-002-129, 99-2611-M-002-005, 100-2116-M-002-009 to CCS, and 95-2611-M-002-019, 96-2611-M-002-019 to KYW), and National Taiwan University (101R7625 to CCS)

References

Anand, A., Elderfield, H., and Conte, M. H., (2003). Calibration of Mg/Ca thermometry in planktonic foraminifera from a sediment trap time series. *Paleoceanography* **18**, 1050, doi:10.1029/2002PA000846.

Bolliet, T., Holbourn, A., Kuhnt, W., Laj, C., Kissel, c., Beaufort, L., Kienast, M., Andersen, N., and Garbe-Schönberg, D., (2011), Mindanao Dome variability over the last 160 kyr: Episodic glacial cooling of the West Pacific Warm Pool. *Paleoceanography* **26**, PA1208, doi: 10.1029/2010PA001966.

Broccoli, A. J., Dahl, K. A., and Stouffer, R. J., (2006), Response of the ITCZ to Northern Hemisphere cooling. *Geophysical Research Letters* **33**, L01702, doi: 10.1029/2005GL024546.

Chiang, J. C. H., and Bitz, C. M., (2005), Influence of high latitude ice cover on the marine Intertropical Convergence Zone. *Climate Dynamics* **25**, 477 – 496.

Cravatte, S., Delcroix, T., Zhang, D., McPhaden, M., and Leloup, J., (2009), Observed freshening and warming of the western Pacific Warm Pool. *Climate Dynamics* **33**, 565 – 589.

de Garidel-Thoron, T., Rosenthal, Y., Bassinot, F., and Beaufort, L., (2005), Stable sea surface temperatures in the western Pacific warm pool over the past 1.75 million years. *Nature* **433**, 294 – 298.

Feng, J., Li, J., and Xie, F., (2013), Long-term variation of the Principal mode of boreal spring Hadley Circulation linked to SST over the Indo-Pacific Warm Pool. *Journal of Climate* **26**, 532-544.

Griffiths, M. L., Drysdale, R. N., Gagan, M. K., Zhao, J.-X., Ayliffe, L. K., Hellstrom, J. C., Hantoro, W. S., Frisia, S., Feng, Y.-X., Cartwright, I., St. Pierre, E., Fischer, M., J., and Suwargadi, B. W., (2009), Increasing Australian-Indonesian monsoon rainfall linked to early Holocene sea-level rise. *Nature Geoscience* **2**, 636 – 639.

Lamy, F., Kaiser, J., Ninnemann, U., Hebbeln, D., Arz, H. W., and Stoner, J., (2004), Antarctic timing of surface water changes off Chile and Patagonian ice sheet response. *Science* **304**, 1959-1962.

Lea, D. W., Pak, D. K., and Spero, H. J., (2000), Climate impact of late Quaternary equatorial Pacific sea surface temperature variations. *Science* **289**, 1719 – 1724.

Lea, D. W., Pak, D. K., Peterson, L. C., and Hughen, K. A., (2003), Synchroneity of tropical high-latitude Atlantic temperatures over the last glacial termination. *Science* **301**, 1361-1364.

Levi, C., Labeyrie, L., Bassinot, F., Guichard, F., Cortijo, E., Waelbroeck, C., Caillon, N., Duprat, J., de Garidel-Thoron, T., and Elderfield, H., (2007), Low-latitude hydrological cycle and rapid climate changes during the last deglaciation. *Geochemistry, Geophysics, Geosystems* **8**, Q05N12, doi: 10.1029/2006GC001514.

Linsley, B. K., Rosenthal, Y., and Oppo, D. W., (2010), Holocene evolution of the Indonesian throughflow and the western Pacific warm Pool. *Nature Geoscience* **3**, 578 – 583.

Mohtadi, M., Oppo, D. W., Steinke, S., Stuut, J.-B. W., De Pol-Holz, R., Hebbeln, D., and Lückge, A., (2011), Glacial to Holocene swings of the Australian-Indonesian monsoon. *Nature Geoscience* **4**, 540 – 544.

Muller, J., Kylander, M., Wüst, R. A. J., Weiss, D., Martinez-Cortizas, A., LeGrande, A. N., Jennerjahn, T., Behling, H., Andreson, W. T., and Jacobson, G., (2008), Possible evidence for wet Heinrich phases in tropical Australia: the Lynch's Crater deposit. *Quaternary Science Reviews* **27**, 468 – 475.

Northern Greenland Ice Core Project Members, (2004), High-resolution record of Northern Hemisphere climate extending into the last interglacial period. *Nature* **431**, 147 – 151.

Oppo, D. W., Rosenthal, Y., and Linsley, B. K., (2009), 2,000-year-long temperature and hydrology reconstructions from the Indo-Pacific warm pool. *Nature* **460**, 1113 – 1116.

Pahnke, K., Zahn, R., Elderfield, H., and Schulz, M., (2003), 340,000-year centennial-scale marine record of Southern Hemisphere climatic oscillation. *Science* **301**, 948-952.

Pena, L. D., Cacho, I., Ferretti, P., and Hall, M. A., (2008), El Niño-Southern Oscillation-like variability during glacial terminations and interlatitudinal teleconnections. *Paleoceanography* **23**, PA3101.

Reynolds, R. W., Rayner, N. A., Smith, T. M., and Stokes, D. C., (2002), An improved in situ and satellite SST analysis for climate. *Journal of Climate* **15**, 1609 – 1625.

Rosenthal, Y., Oppo, D. W., and Linsley, B. K., (2003), The amplitude and phasing of climate change during the last deglaciation in the Sulu Sea, western equatorial Pacific. *Geophysical Research Letters* **30**, 1428, doi: 10.1029/2002GL016612.

Shiau, L.-J., Chen, M.-T., Clemens, S. C., Huh, C.-A., Yamamoto, M., and Yokoyama, Y., (2011), Warm pool hydrological and terrestrial variability near southern Papua New Guinea over the past 50k. *Geophysical Research Letters* **38**, L00F01, doi: 10.1029/2010GL045309.

Steinke, S., Chiu, H.-I., Yu, P.-S., Shen, C.-C., Erlenkeuser, H., Löwemark, L., and Chen, M.-T., (2006), On the influence of sea level and monsoon climate on the southern South China Sea freshwater budget over the past 22,000 years. *Quaternary Science Reviews* **25**, 1475 – 1488.

Stenni, B., Jouzel, J., Masson-Delmotte, V., Röthlisberger, R., Castellano, E., Cattani, O., Falourd, S., Johnsen, S. J., Longinelli, A., Sachs, J. P., Selmo, E., Souchez, R., Steffensen, J. P., Udisti, R., (2003), A late-glacial high-resolution site and source temperature record derived from EPICA Dome C isotope records (East Antarctica). *Earth and Planetary Science Letters* **217**, 183 – 195.

Stott, L., Cannariato, K., Thunell, R., Haug, G. H., Koutavas, A., and Lund, S., (2004), Decline of surface temperature and salinity in the western tropical Pacific Ocean in the Holocene epoch. *Nature* **431**, 56 – 59.

Stott, L., Poulsen, C., Lund, S., and Thunell, R., (2002), Super ENSO and global climate oscillations at millennial time scales. *Science* **297**, 222-226.

Visser, K., Thunell, R., and Stott, L., (2003), Magnitude and timing of temperature change in the Indo-Pacific warm pool during deglaciation. *Nature* **421**, 152 – 155.

Wang, Y. J., Cheng, H., Edwards, R. L., An, Z. S., Wu, J. Y., Shen, C.-C., and Dorale, J. A., (2001), A high-resolution absolute-dated late Pleistocene monsoon record from Hulu Cave, China. *Science* **294**, 2345-2348.

Wang, X., Auler, A. S., Edwards, R. L., Cheng, H., Ito, E., Wang, Y., Kong, X., and Solheid, M., (2007), Millennial-scale precipitation changes in southern Brazil over the past 90,000 years. *Geophysical Research Letters* **34**, L23701, doi:10.1029/2007GL031149.

Weldeab, S., Schneider, R. R., Kölling, M., and Wefer, G., (2005), Holocene African droughts relate eastern equatorial Atlantic cooling. *Geology* **33**, 981-984.

Weldeab, S., Schneider, R. R., and Kölling, M., (2006), Deglacial sea surface temperature and salinity in the western tropical Atlantic in synchrony with high latitude climate instabilities. *Earth and Planetary Science Letters* **241**, 699-706.

Weldeab, S., Lea, D. W., Schneider, R. R., and Andersen, N., (2007), 155,000 years of West African monsoon and ocean thermal evolution. *Science* **316**, 1303-1307.

Williams, A. P, and Funk, C., (2011), A westward extension of the warm pool leads to a westward extension of the Walker circulation, drying eastern Africa. *Climate Dynamics* **37**, 2417 – 2435.

Xu, J., Holbourn, A., Kuhnt, W., Jian, Z., and Kawamura, H., (2008), Changes in ther thermocline structure of the Indonesian outflow during Terminations 1 and Ⅱ. *Earth and Planetary Science Letters* **273**, 152 – 162.

Yan, X.-H., Ho, C.-R., Zheng, Q., and Klemas, V., (1992), Temperature and size variabilities of the western Pacific warm pool. *Science* **258**, 1643-1645.

Ziegler, M., Nürnberg, D., Karas, C., Tiedemann, R., and Lourens, L. J., (2008), Persistent summer expansion of the Atlantic Warm Pool during glacial abrupt events. *Nature Geoscience* **1**, 601 – 605.

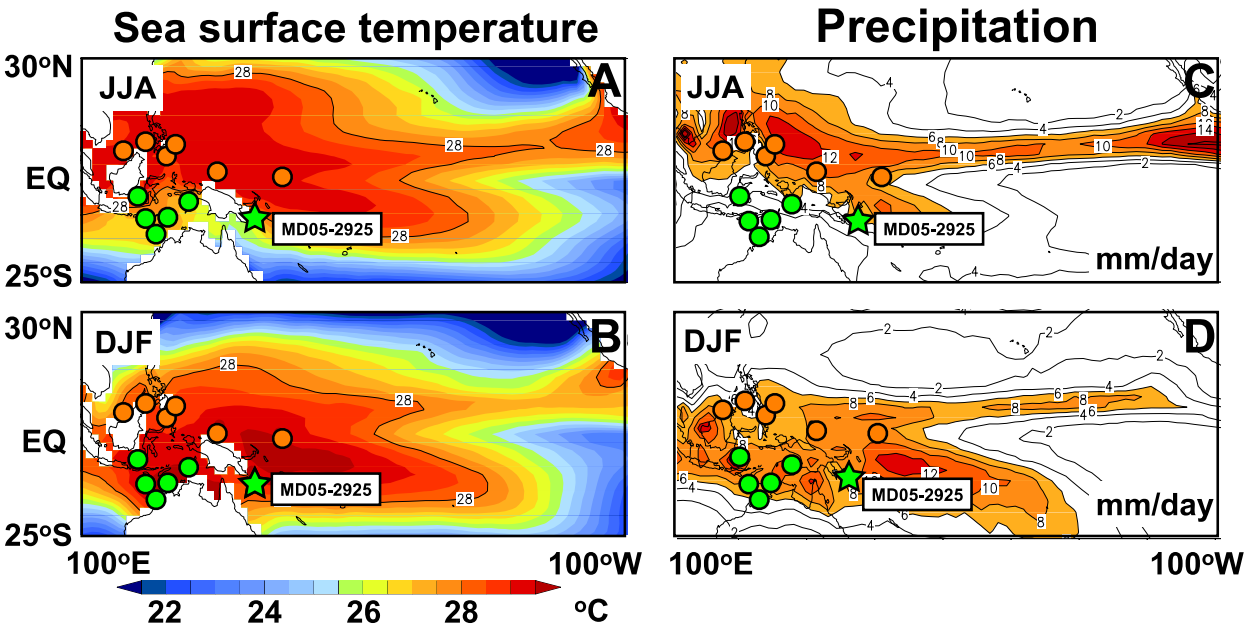

Figure 3-1. Climatological map of the Indo-Pacific Warm Pool (IPWP) sea surface temperature (SST, left) and precipitation (right) during 1950-2004 AD [*Reynolds et al.*, 2002]. Upper panels are from the June-July-August (JJA), and lower panels are from December-January-February (DJF) averages of (A, C) SSTs and (B, D) precipitation distribution maps. SST and precipitation are at 0.5°C and 2 mm/day intervals. Green star is the study site MD05-2925. Orange and green dots are the previous study sites in IPWP region for reconstruction of meridional thermal and precipitation variations during the glacial/interglacial change.

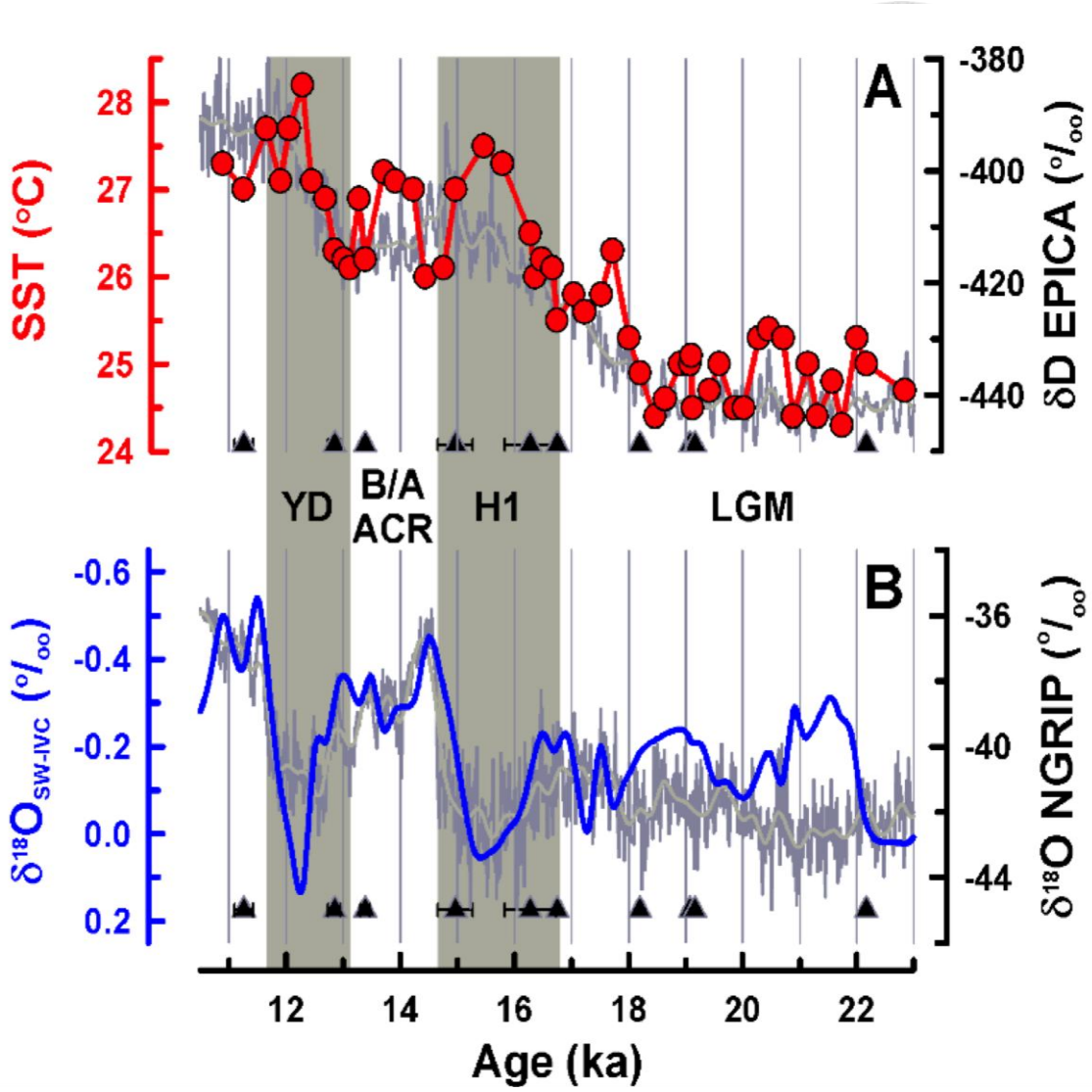

Figure 3-2. Geochemical proxies from the Site MD05-2925. (A) $\delta^{18}O_{SW\text{-}IVC}$ (blue line) and (B) SST (red dots and line) were reconstructed with *G. ruber* Mg/Ca ratios and $\delta^{18}O_C$ [*Anand et al.*, 2003]. Gray line is the Greenland ice core NGRIP [*Northern Greenland Ice Core Project Members*, 2004] oxygen isotope record. Dark gray line denotes the Antarctica EPICA deuterium isotope record [*Stenni et al.*, 2003]. The superimposed dark gray lines are the 200-yr smoothed records. Black triangles are AMS ^{14}C dates [Table 2-1]. Vertical bars denote the H1and YD periods.

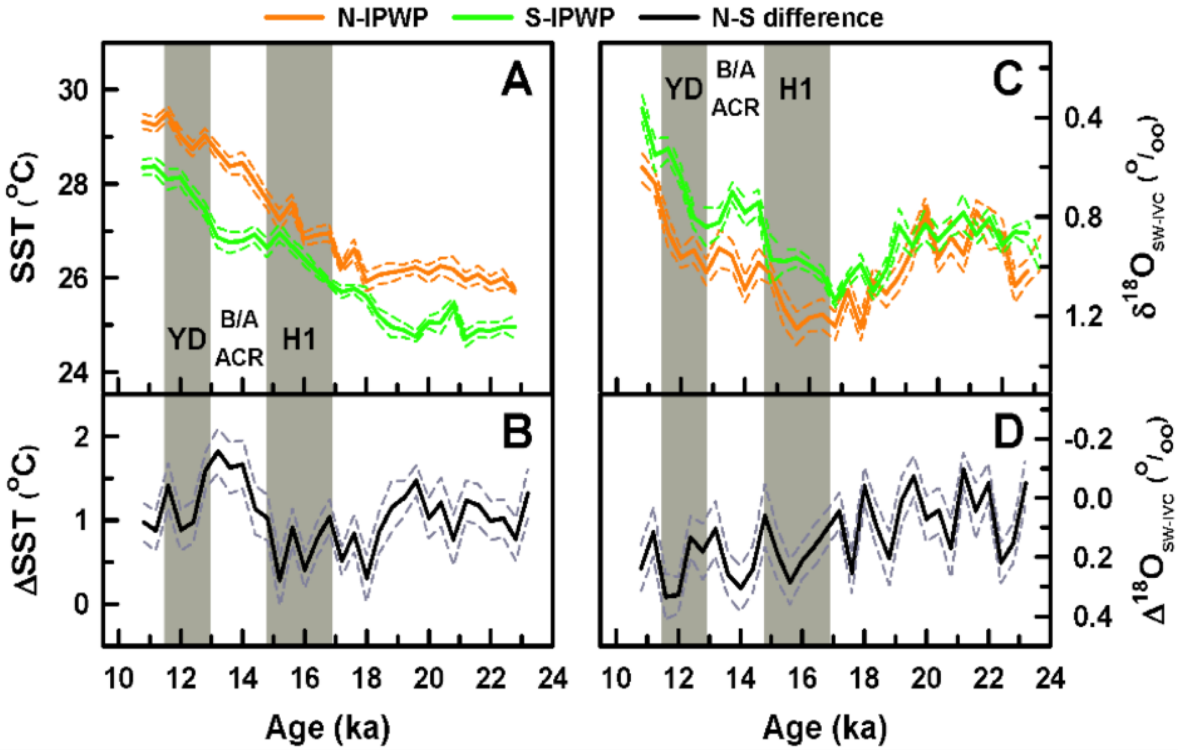

Figure 3-3. Four-hundred-year non-overlapping binned (A) SST and (C) $\delta^{18}O_{SW\text{-}IVC}$ of N- (orange solid lines) and S-IPWP (green solid lines). Lower panel are the differences of (B) SST and (D) $\delta^{18}O_{SW\text{-}IVC}$ between N- and S-IPWP, respectively. The compilations of N- and S-IPWP surface water thermal and hydrological records [see Chapter 2, Table 2-3] were calculated with a non-overlapping binned method [*Linsley et al.*, 2010, see Chapter 2]. All dashed lines represent 1-sigma uncertainty range. Gray bars represent the H1 and YD events.

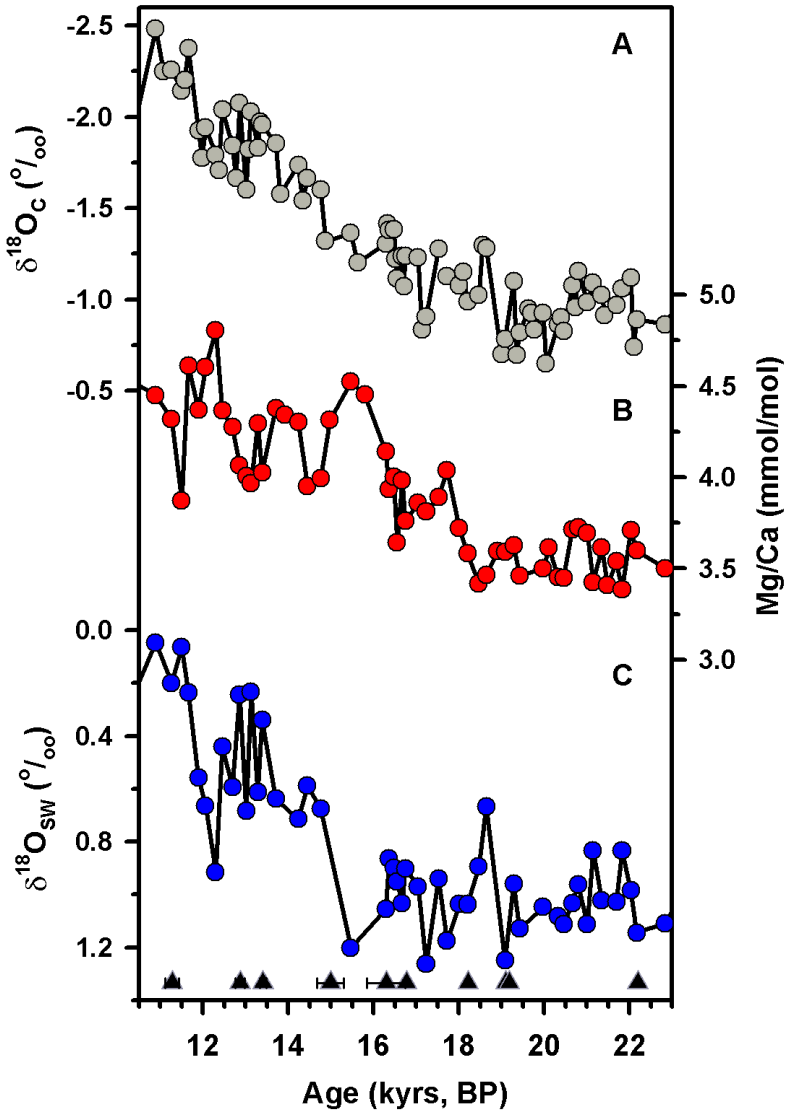

Figure 3-S1. *G. ruber* geochemical proxy records of site MD05-2925, including (A) oxygen isotope ($\delta^{18}O_C$), (B) Mg/Ca ratio, and (C) temperature corrected-only seawater oxygen isotope ($\delta^{18}O_{SW}$). Triangle symbols are corrected radiocarbon dates.

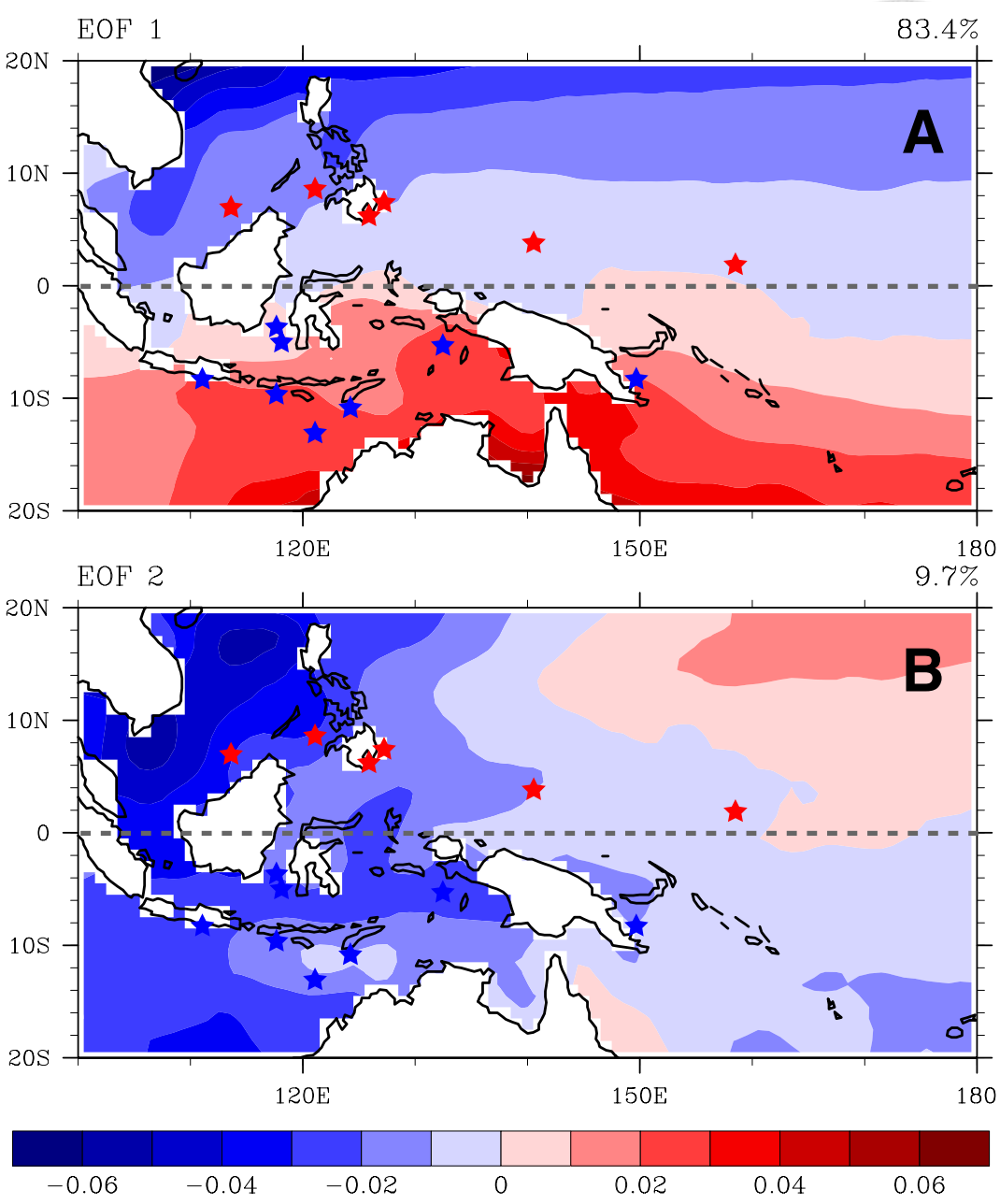

Figure 3-S2. EOF analysis on SST [Dataset from the *Reynolds et al.*, 2002] and selected sites [Table 2-3] used for stacked N- and S-IPWP records. (A) EOF1 explains 83.4% of total variance, which mainly represent the intra-annual seasonality. (B) EOF2 shows a clear zonal change pattern. Red stars represent the selected sites for the N-IPWP group and blue ones for the S-IPWP group.

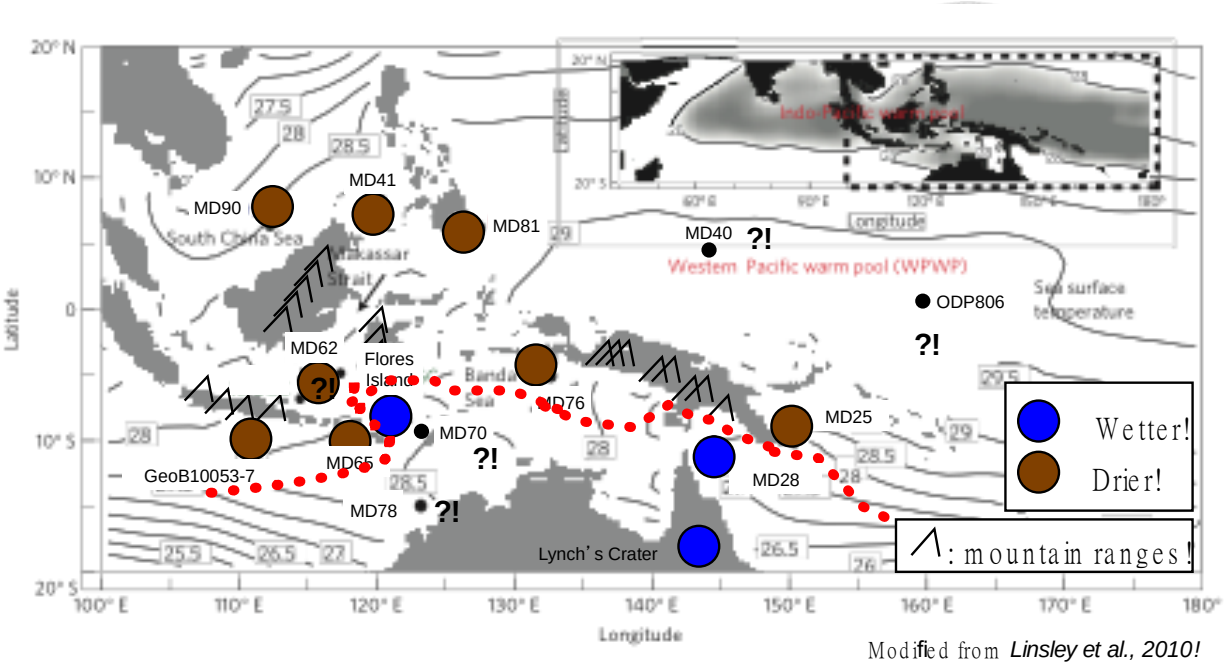

Figure 3-S3. Hypothetical proxy-inferred precipitation boundary during the H1 and/or the YD events (modified from the *Linsley et al.* [2010]). Blue dots represent a relatively wet condition, and brown ones a dry condition. The segment between Java and Flores Islands of this sharp boundary (red dotted line) was proposed by *Mohtadi et al.* [2011], and the one between the Solomon and Coral Seas by this study.

Chapter 4.

Evolution of the Pacific Intertropical Convergence Zone over the past 284,000 years

In manuscript as Yi Liu, **Li Lo**, Zhengguo Shi, Kuo-Yen Wei, Chien-Ju Chou, Yi-Chi Chen, Chung-Che W, Horng-Sheng Mii, Chih-Kai Chuang, Zicheng Peng, Hiroshi Amakawa, George S. Burr & Chuan-Chou Shen. Evolution of the Pacific Intertropical Convergence Zone over the past 284,000 years.

Evolution of the Pacific Intertropical Convergence Zone over the past 284,000 years

Yi Liu[1,2,3#], Li Lo[2#], Zhengguo Shi[3], Kuo-Yen Wei[2], Chien-Ju Chou[2], Yi-Chi Chen[2], Chung-Che Wu[2], Horng-Sheng Mii[4], Chih-Kai Chuang[2], Zicheng Peng[1], Hiroshi Amakawa[2], George S. Burr[2,5] & Chuan-Chou Shen[2*]

1-CAS Key Laboratory of Crust-Mantle Material and Environment, School of Earth and Space Science, University of Science and Technology of China, Hefei 230026, China

2-High-Precision Mass Spectrometry and Environment Change Laboratory (HISPEC), Department of Geosciences, National Taiwan University, Taipei 10617, Taiwan ROC

3-State Key Laboratory of Loess and Quaternary Geology, Institute of Earth Environment, Chinese Academy of Sciences, Xi'an 710075, China

4-Department of Earth Sciences, National Taiwan Normal University, Taipei 11677, Taiwan ROC

5-Department of Physics, University of Arizona, Tucson, Arizona 85721, USA

[#]These authors contributed equally to this work.

*To whom correspondence should be addressed to：

Chuan-Chou Shen: Tel: 886-2-33665878; Fax: 886-2-33651917; email: river@ntu.edu.tw

Submitted to ***Nature Geoscience*** in June 2014

The Intertropical convergence Zone (ITCZ) encompasses the heaviest rain belt on Earth. Continental monsoon records in Chinese and Brazilian stalagmites imply that orbital-scale climate changes are linked to precession-dominated insolation [*Wang et al.*, 2004; *Wang et al.*, 2008]. However, only few direct long-term records, especially in the Pacific [*Tachikawa et al.*, 2011], limit our understanding of long-term natural variability necessary to predict future ITCZ changes. Here we present a tropical precipitation record from the Southern Hemisphere covering the past 284,000 years, inferred from a marine sedimentary sequence collected off the eastern coast of Papua New Guinea. We use rare earth element measurements of planktonic foraminifera as a proxy to reconstruct regional precipitation records and decipher the evolution of the Pacific ITCZ. While precession is expressed in its East Asian counterpart [*Wang et al.*, 2008], our record shows that the Pacific ITCZ migration was influenced significantly by obliquity changes. Transient model simulations suggest that this obliquity forcing could be primarily delivered by a cross-hemispherical thermal/pressure contrast, resulting from the asymmetric continental configuration between Asia and Australia in a coupled East Asian-Australian circulation system.

The Intertropical Convergence Zone (ITCZ) migrates meridionally with the seasonal insolation angle of the sun [*Waliser and Gautier*, 1993] and circles the globe in the tropics, marking the earth's meteorological equator [Figure 4-1a]. The convergence of inter-hemispheric trade winds leads to strong convective clouds, heavy precipitation, and intense latent-heat transfer, altering rainfall patterns worldwide. Owing to its intensive rainfall gradient, a small displacement in the

position of the ITCZ can cause dramatic changes in hydrology and the frequency of extreme weather events—such as droughts, floods, and tropical cyclones [*Waliser and Gautier*, 1993] . The collapse of the Mayan civilization and several Chinese Dynasties has been attributed to persistent droughts associated with ITCZ migrations [*Haug et al.*, 2003; *Yancheva et al.*, 2007]. The current buildup of atmospheric greenhouse gases has the potential to affect the future position of the ITCZ and corresponding climate [*Sachs et al.*, 2009]. An in-depth reconstruction of the position, structure, and migration of the ITCZ is thus critical to our understanding of global climate and sustainable human socioeconomic development.

Lines of indirect evidence from the past 210-220 kyr in Asian and American monsoon records[1,2] suggest that the ITCZ was predominately driven by precessional forcing (~20 kyr). Within the ITCZ territory, short-term terrestrial [*Partin et al.*, 2007; *Griffiths et al.*, 2009; *Ayliffe et al.*, 2013] and marine [*Haug et al.*, 2001; *Mohtadi et al.*, 2011] proxy records were reported. Few 100s-kyr records [*Tachikawa et al.*, 2011] from the meteorological core of the ITCZ, in the low-latitude Pacific, severely hinders us from understanding its natural variability related to orbital forcings in the Quaternary. An understanding of ITCZ responses to orbital forcings has global significance because the region is the largest “heat engine” and moisture source in the world.

Papua New Guinea (PNG), a mountainous terrain located at the southern border of the ITCZ [Figure 4-1; Supplementary Figure 4-S1], delivers a large amount of suspended sediments and solutes to the adjacent oceans as a result of the prodigious precipitation in the region [*Milliman et al.*, 1999; *Nittouer et al.*, 1995].

This transport occurs mostly in the wet season (>90% annual load) when the ITCZ is located over PNG [*Chappell et al.*, 2011]. Archives from nearby marine basins therefore reflect this sediment delivery and provide a direct record of precipitation influenced by the ITCZ position.

Using inductively coupled plasma sector field mass spectrometric (ICP-SF-MS) techniques with 2 ‾ precision of 2-6% [*Shen et al.*, 2011], we have established a 284-kyr record of rare earth elements (REEs) to Ca ratios in the tests of planktonic foraminifer *Globigerinoides ruber*. The foraminiferal tests were sampled from a marine sediment core MD05-2925 (9.3^{o}S, 151.5^{o}E; water depth 1661 m; Figure 4-1; Supplementary Figure 4-S1), collected off the southeastern tip of PNG to reveal the orbital-scale evolution of ITCZ precipitation intensity. Further, new calculations from a previous orbital-accelerated transient experiment using a coupled fast ocean-atmosphere model (FOAM, *Kutzbach et al.*, 2008; *Shi et al.*, 2011) forced by variations in orbital parameters is presented to clarify dynamical ITCZ migration processes in the western Pacific.

Relatively high REE values (e.g., Nd ~30 ‾g/g) are characteristic of solid crustal materials, as compared to dissolved riverine (e.g. ~30 ng/g) or seawater values (<1 pg/g). This fact, in combination with short oceanic residence times (~0.5 kyr, *Tachikawa et al.*, 2003), has led to the study of these elements and isotopes as terrestrial sediment tracers [*Sholkovitz et al.*, 1999; *Burton et al.*, 2000; *Stoll et al.*, 2007] in the ocean. Open-ocean seawater [*Zhang and Nozaki*, 1996] from the Southwest Pacific, planktonic foraminifera [*Haley et al.*, 2005] from the eastern Pacific and coral carbonates [*Wyndham et al.*, 2004] from the Great Barrier Reef

(GBR), all have similar REE patterns, characterized by shale-normalized (SN, *McLennan*, 1989) light (LREE, La-Nd) and middle REE (MREE, Sm-Ho) depletions and heavy REE (HREE, Er-Lu) enrichments (Nd/Yb_{SN} = 0.17-0.28 and Gd/Yb_{SN} = 0.41-0.70; Figure 4-2c, 4-2f, and 4-2g). Marine carbonates show consistent distribution coefficients for all REEs [*Haley et al.*, 2005]. However, PNG coastal coral skeletal REEs from Misima Island [*Fallon et al.*, 2002] show a MREE-enrichment (Gd/Yb_{SN} = 1.3) pattern [Figure 4-2e]. The LREE/HREE ratios also increased by a factor of 3-4 (Nd/Yb_{SN} = 0.87), as compared with GBR coral [*Wyndham et al.*, 2004, Figure 4-2g]. These features are consistent with a terrestrial MREE source (Gd/Yb_{SN} = 2.2) supplied by river runoff [*Sholkovitz et al.*, 1999, Figure 4-2b]. The coral skeletal REE variability is primarily controlled by changes in precipitation [*Fallon et al.*, 2002]. These dissolved REEs represent a PNG "island-weathering signature", and are also recorded in cleaned planktonic foraminiferal tests [Figure 4-2a]. The REE patterns for these foraminiferal carbonates [average Nd/Yb_{SN} = 0.45 ± 0.04, (1 standard deviation of the mean, σ_m); 0.88 ± 0.06 ($1\sigma_m$) for Gd/Yb_{SN}] are distinctively different from open-ocean seawater [*Zhang and Nozaki*, 1996, Figure 4-2c] and shallow-water marine carbonates [*Wyndham et al.*, 2004; *Haley et al.*, 2005, Figure 4-2f, and 4-2g]. These unique enrichments of regional foraminiferal LREEs and MREEs directly reflect regional river runoff. The down-core planktonic foraminiferal REE/Ca sequence can, therefore, be used as a proxy record of past ITCZ-related precipitation over PNG.

All measured *G. ruber* REEs/Ca ratios of core MD05-2925 consistently co-vary with a high correlation coefficient of >0.97 over the past 284 kyr [Supplementary Figure 4-S2]. Here we use Nd/Ca time series [Figure 4-3c] to

represent REE variability and infer regional ITCZ-related precipitation changes. This implication is supported by Nd isotopic data [Supplementary Figure 4-S2, Table 4-S1] and a replicated record from an adjacent marine sedimentary core, ODP 1115B (9.1°1S, 151.5°E; water depth 1149 m) [Supplementary Figure 4-S8].

The MD05-2925 Nd/Ca sequence can be characterized by a sinusoidal curve with low values of 0.2-0.3 ⌈mol/mol and 10s-kyr peaks of 0.4-1.2 ⌈mol/mol. Planktonic foraminifer *G. ruber* Nd/Ca cycles are generally aligned with changes in precession-dominated Southern Hemisphere (SH) summer insolation (SHSI) values [Figure 4-3c and 4-3d]. The agreement indicates that PNG precipitation variations are driven by precessional forcing. Intense PNG precipitation results from the large temperature gradient between land and ocean in response to high SHSI.

Comparison of our Nd/Ca record with contemporaneous stacked Chinese stalagmite $\delta^{18}O$ records [*Wang et al.*, 2001; *Cheng et al.*, 2006; *Wang et al.*, 2008; *Cheng et al.*, 2009] over the past 284 kyr is illustrated in Figure 4-3. The stalagmite $\delta^{18}O$ record has been interpreted as a record of summer monsoon precipitation and Asian summer monsoon (ASM) intensity; with more negative (positive) stalagmite $\delta^{18}O$ values indicating higher (lower) precipitation influenced by stronger (weaker) ASM intensities [*Wang et al.*, 2001; *Cheng et al.*, 2006]. High foraminiferal Nd/Ca-inferred wet periods at PNG broadly match positive stalagmite $\delta^{18}O$-derived dry conditions in mainland China and vice versa [Figure 4-3b and 4-3c]. This interhemispheric precipitation anti-phasing over the entire Asia–Pacific realm can be attributed to latitudinal shifts of the ITCZ and associated rain belts, driven by changes in seasonal insolation, dominated by precession.

In China, cave record-inferred precipitation intensity co-varies with solar radiation [*Wang et al.*, 2008, Figure 4-3a and 4-3b]. However, in PNG there are six incompatible periods of low Nd/Ca-inferred precipitation at about 45, 90, 140, 165, 210, and 250 kyr BP, when the Earth's axial tilt was high [Figure 4-3c and 4-3e]. Modeling results also show consistent suppressed summer precipitation over PNG in the SH tropics at high obliquity periods [Figure 4-4e and 4-4g]. These features indicate that precession is not the only orbital forcing mechanism operating on the ITCZ in the southern low-latitude Pacific. Indeed, spectral power analysis indicates that our foraminiferal Nd/Ca time series is dominated by obliquity periodicity [Supplementary Figure 4-S6a], highlighting the important role of Earth's axial tilt in modulating precipitation in the region of PNG. This finding is also supported by Ti/Ca-inferred terrestrial inputs [Figure 6 of *Tachikawa et al.*, 2011] from a marine sediment core MD05-2920 (2.9^{o}S, 144.5^{o}E, water depth 1843 m).

The obliquity effect on SH tropical Pacific precipitation is most likely associated with its control on the meridional thermal/pressure contrast. Our models suggest that high obliquity is responsible for the establishment of a strong Siberian high cell [Figure 4-4a] and East Asian winter monsoon system [*Shi et al.*, 2011]. Although precessional forcing dominates local land-ocean thermal contrasts and influences the Australian low, the simulated Australian low does not rigidly follow precession. Extreme low pressures are always induced by high obliquity during the past 284 kyr and distinguishably stronger than those induced by precession [Figure 4-4].

Obliquity-induced meridional circulation can affect the intensity of the Australian summer monsoon, the hemispheric counterpart of the Asian winter

monsoon, through a cross-equatorial "pressure-push" process [*An*, 2000, Figure 4-S9]. Specifically at high obliquity, a strong pressure gradient between an intensified Siberian high and Australian low enhances cross-equatorial flow of southerly winds [Figure 4-4a to 3-4c] and reinforces the southward shift of the ITCZ rain belt to the southernmost position. This northward/southward shift of the ITCZ leaves distinct rainfall patterns in different locations. The net effect is to increase precipitation in North Australia [Figure 4-4f], with compensated amounts in PNG at the six periods tagged in Figure 3. The precipitation is, thus, reduced at PNG despite high seasonal insolation [Figure 3 and 4]. Support for such a strong southward migration of the ITCZ by high obliquity also comes from a 100-kyr record at Gregory Lakes (20.3^{o}S, 127.5^{o}E), on the fringe of the desert in semi-arid northwestern Australia [*Fitzsimmons et al.*, 2012; Figure 4-1]. The occurrence of two past high lake stands at 37-50 and 95-105 kyr BP [Figure 4 of *Fitzsimmons et al.*, 2012] matches the high-obliquity window and provides a SH complement to our marine record.

The "pressure-push" forcing [*An*, 2000, Figure 4-S9], strengthened by the capacious Asian landmass, is weak at low-obliquity and the center of the strong convergence rain belt stays in the north, relative to high-obliquity cases. As a result, PNG experiences enormous rainfall during those times in response to high insolation [Figure 4-4d and 4-4e]. At 150 kyr BP, low solar radiation and low obliquity caused a shift of the ITCZ towards the equator. Precipitation declined over PNG and possible drought conditions may have occurred in North Australia, according to our model simulations [Figure 4-4d to 4-4f].

Due to the limited area of the Australian continent, the low pressure near the warm Tibetan Plateau (topographic forcing) in boreal summer is predominately driven by local insolation changes. It results in a precession-controlled ITCZ shift in East Asia, as inferred from Chinese cave records [Figure 4-3]. The northern and southern branches of the ITCZ in the Asian-Pacific realm appear to respond differently to orbital insolation. This interhemispheric asymmetry of ITCZ movements is attributed to different land-sea configurations and topography.

Our planktonic foraminiferal REE record near PNG, and simulated data, reveal that obliquity can shift the position of the ITCZ and operates in tandem with precessional forcing [*Wang et al.*, 2004; *Wang et al.*, 2008]. Given that the obliquity signal is stronger in the Nd/Ca-inferred precipitation record than in the simulation [Supplementary Figure 4-S6], our proposed obliquity-induced "pressure-push" mechanism might be more significant for both PNG and North Australia. Understanding the dynamics of ITCZ migration in the low-latitude Pacific through the Quaternary is essential to deciphering the cryptic nature of past global climate change.

References

An, Z. S., (2000), The history and variability of the East Asian paleomonsoon climate. *Quaternary Science Rev*iew **19,** 171-187.

Ayliffe, L. K., Gagan, M. K., Zhao, J., Dysdale, R. N., Hellstrom, J. C., Hantoro, W. S., Griffiths, M. L., Scott-Gagan, H., St Pierre, E., Cowley, J. A., and Suwargadi, B.W., (2013), Rapid interhemispheric climate links via the Australasian monsoon during the last deglaciation. *Nature Communications* **4,** 2908.

Berger, A. L., (1978), Long-term variations of caloric insolation resulting from the Earth's orbital elements. *Quat*ernary *Reserach* **9,** 139-167.

Burton, K. W., and Vance, D., (2000), Glacial-interglacial variations in the neodymium isotope composition of seawater in the Bay of Bengal recorded by planktonic foraminifera. *Earth* and *Planet*ary *Sci*ence *Lett*ers **176**, 425-441.

Chappell, N. A., Tych, W., Shearman, P., Lokes, B., and Chitoa, J., (2011) in *Sediment Problems and Sediment Management in Asian River Basins* (eds. Walling, D. E.) 92-102 (IAHS Press, Wallingford, 2011)

Cheng, H., Edwards, R. L., Wang, Y., Kong, X., Ming, Y., Kelly, M. J., Wang, X., Dallup, C. D., and Liu, W., (2006), A penultimate glacial monsoon record from Hulu Cave and two phase glacial terminations. *Geology* **34,** 217-220.

Cheng, H., Edwards, R. L., Broecker, W. S., Denton, G. H., Kong, X., Wang, Y., Zhang, R., and Wang X., (2009), Ice Age Terminations. *Science* **326,** 248-252.

Fallon, S. T., White, J. C., and McCulloch. M., (2002), *Porites* corals as recorders of mining and environmental impacts: Misima Island, Papua New Guinea. *Geochimica et Cosmochimica Acta* **66,** 45-62.

Fitzsimmons, K. E., Miller, G. H., Spooner, N. A., and Magee, J. W., (2012), Aridity in the monsoon zone as indicated by desert dune formation in the Gregory Lakes basin, northwestern Australia. *Australian Journal of Earth Sciences* **59,** 469-478.

Griffiths, M. L., Drysdale, R. N., Gagan., M. K., Zhao, J.-x., Ayliffe, L. K., Hellstrom, J. C., Hantoro, W. S., Frisia, S., Feng, Y.-x., Cartwright, I., St. Pierre, E., Fischer, and Suwargadi, B. W., (2009), Increasing Australian–Indonesian monsoon rainfall linked to early Holocene sea-level rise. *Nature Geoscience* **2,** 636-639.

Haley, B. A., Klinkhammer, G. P., and Mix, A. C., (2005), Revisiting the rare earth elements in foraminiferal tests. *Earth* and *Planet*ary *Sci*ence *Lett*ers **239,** 79-97.

Haug. G. H., Günther, D., Peterson, L. C., Sigman, D. M., Hughen, K. A., and Aeschlimann, B., (2003), Climate and the collapse of Maya Civilization. *Science* **299,** 1731-1735.

Haug, G. H., Hughen, K. A., Sigman, D. M., Peterson, L. C., and Röhl, U., (2001), Southward migration of the intertropical convergence zone through the Holocene. *Science* **293,** 1304-1308.

Kutzbach, J. E., Liu, X., Liu, Z., and Chen, G., (2008), Simulation of the evolutionary response of global summer monsoons to orbital forcing over the past 280,000 years. *Climate Dynamics* **30,** 567-579.

McLennan, S. M., (1989), Rare earth elements in sedimentary rocks; influence of provenance and sedimentary processes. *Reviews in Mineralogy and Geochemistry* **21**, 169-200.

Milliman, J. D., Farnsworth, K. L., and Albertin, C. S., (1999), Flux and fate of fluvial sediments leaving large islands in the East Indies. *Journal of Sea Research* **41,** 97-107.

Mohtadi, M., Oppo, D. W., Steinke, S., Stuut, J.-B. W., De Pol-Holz, R., Hebbeln, D., and Lückge, A., (2011), Glacial to Holocene swings of the Australian-Indonesian monsoon. *Nature Geoscience* **4**, 540 – 544.

Nittrouer, C. A., Brunskill, G. J., and Figueiredo, A. G., (1995), Importance of tropical coastal environments. *Geo-Marine Letters* **15**, 121-126.

Partin, J. W., Cobb, K. M., Adkins, J. F., Clark, B., and Fernandez, D. P., (2007), Millennial-scale trends in west Pacific warm pool hydrology since the Last Glacial Maximum. *Nature* **449,** 452-456.

Sachs, J. P., Sachse, D., Smittenberg, R. H., Zhang, Z., Battisti, D. S., and Golubic, S., (2009), Southward movement of the Pacific intertropical convergence zone AD 1400–1850. *Nature Geoscience* **2,** 519-525.

Shen, C.-C., Wu, C.-C., Liu, Y., Yu, J., Chang, C.-C., Lam, D. D., Chou, C.-J., Lo, L., and Wei, K.-Y., (2011), Measurements of natural carbonate rare earth elements in femtogram quantities by inductive coupled plasma sector field mass spectrometry. *Analytical Chemistry* **83,** 6842-6848.

Shi, Z. G., Liu, X. D., Sun, Y. B., An, Z. S., Liu, Z., and Kutzbach, J., (2011), Distinct responses of East Asian summer and winter monsoons to astronomical forcing. *Climate of the Past* **7,** 1363-1370.

Sholkovitz, E. R., Elderfield, H., Szymczak, R., and Casey, K., (1999), Island weathering: river sources of rare earth elements to the Western Pacific Ocean. *Marine Chemistry* **68,** 39-57.

Stoll, H. M., Vance, D., and Arevalos, A. (2007), Records of the Nd isotope composition of seawater from the Bay of Bengal: Implications for the impact of Northern Hemisphere cooling on ITCZ movement. *Earth* and *Planet*ary *Sci*ence *Lett*ers **255**, 213-228.

Tachikawa, K., Athias, V., and Jeandel, C., (2003), Neodymium budget in the modern ocean and paleo-oceanographic implications. *Journal of Geophysical Research* **108,** doi: 10.1029/1999JC000285.

Tachikawa, K., Cartapanis, O., Vidal, L., Beaufort, L., Barlyaeva, T., and Bard, E., (2011), The precession phase of hydrological variability in the Western Pacific Warm Pool during the past 400 ka. *Quaternary Science Rev*iew **30**, 3716-3727.

Waliser, D. E., and Gautier, C. A., (1993), Satellite-derived climatology of the ITCZ. *J*ournal *of Climate* **6,** 2162-2174.

Wang, X. F., Auler, A. S., Edwards, R. L., Cheng, H., Cristall, P. S., Smart, P. L., Richards, d. A., and Shen, C.-C., (2004), Wet periods in northeastern Brazil over the past 210 kyr linked to distant climate anomalies. *Nature* **432,** 740-743.

Wang, Y. J., Cheng, H., Edwards, R. L., An, Z. S., Wu, J. Y., Shen, c.-C., and Dorale, J. A., (2001), A high-resolution absolute-dated late Pleistocene monsoon record from Hulu Cave, China. *Science* **294,** 2345-2348.

Wang, Y. J., Cheng, H., Edwards, R. L., Kong, X., Shao, X., Chen, S., Wu, J., Jiang, x., Wang, X., and Zn, Z., (2008), Millennial- and orbital-scale changes in the East Asian monsoon over the past 224,000 years. *Nature* **451,** 1090-1093.

Wyndham, T., McCulloch, M., Fallon, S., and Alibert, C., (2004), High-resolution coral records of rare earth elements in coastal seawater: biogeochemical cycling and a new environmental proxy. *Geochimica et Cosmochimica Acta*

68, 2067-2680.
Yancheva, G., Nowaczyk, N. R., Mingram, J., Dulski, P., Schettler, G., Negendank, J. F. W., Liu, J., Sigman, d. M., Peterson, L, C., and Haug, G. H., (2007), Influence of the intertropical convergence zone on the East Asian monsoon. *Nature* **445,** 74-77.
Zhang, J., and Nozaki, Y., (1996), Rare earth elements and yttrium in seawater: ICP-MS determinations in the East Caroline, Coral Sea, and South Fiji basins of the western South Pacific Ocean. *Geochimica et Cosmochimica Acta* **60,** 4631-4644.

Acknowledgements

This study used samples offered by the Marine Core Repository and Laboratory, Taiwan Ocean Research Institute (TORI), Taiwan ROC. The location of MD05-2925 site was suggested by M.-Y. Lee (Taipei Municipal University of Education) and collected during the IMAGES PECTEN Cruise, led by L. Beaufort (CEREGE, CNRS/Université Aix-Marseille) and M.-T. Chen (Institute of Applied Geosciences, National Taiwan Ocean University). We thank the scientific party of WEPAMA, MD122/IMAGES VII for coring. A. Chen helped pick foraminiferal specimens. We are thankful for financial support provided by Taiwan ROC NSC (98-2811-M-002-129, 99-2611-M-002-005 and 100-2116-M-002-009, 101-2611-M-002-003 to C.-C.S., and 95-2611-M-002-019 and 96-2611-M-002-019 to K.-Y.W.), National Taiwan University (101R7625 to C.-C.S.), National Key Basic Research Program of China (2013CB956102 to Y.L. and 2013CB955904 to Z.S.), National Science Foundation of China (41003002 to Y.L. and 41290255 and 41105060 to Z.S.). Data of the reported planktonic foraminifer *G. ruber* Nd/Ca record are available in the supplementary materials.

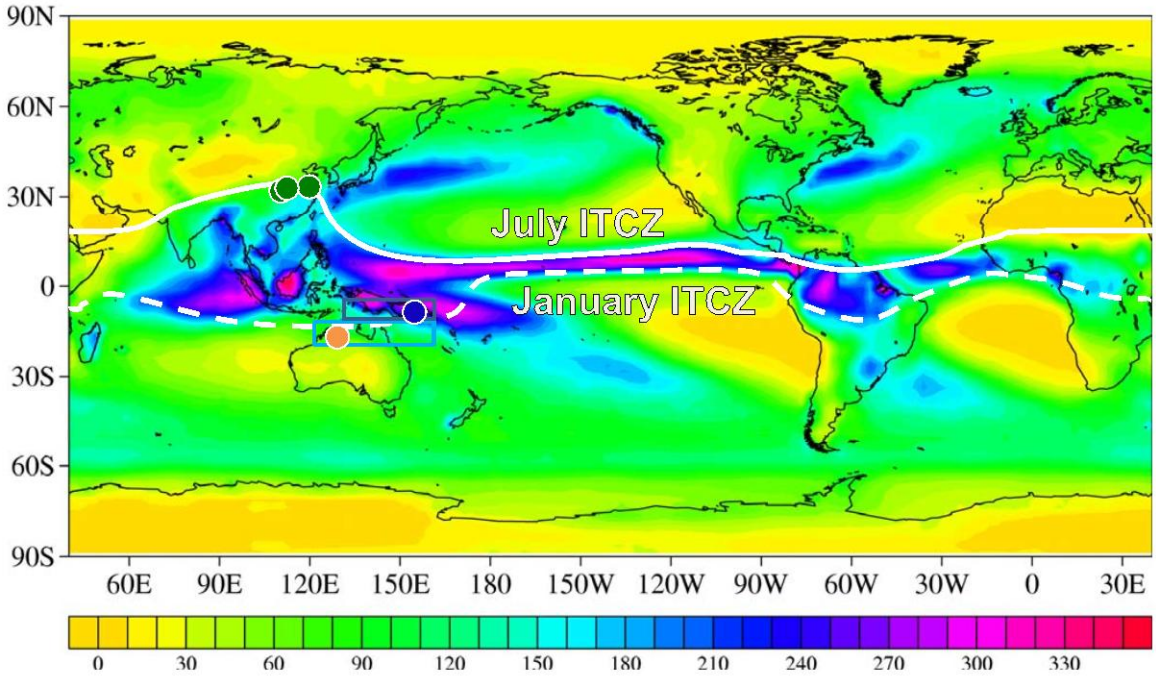

Figure 4-1. Precipitation map and study site. (a) Map of mean annual precipitation (1988-2004; data source: http://jisao.washington.edu/data/gpcp/). Solid and dashed lines represent the mean positions of ITCZ in July and January, respectively. Symbols denote locations of Chinese caves [*Wang et al.*, 2001; *Cheng et al.*, 2006; *Wang et al.*, 2008; *Cheng et al.*, 2009] (green), marine sediment core MD05-2925 in this study (blue), and Gregory Lakes [*Fitzsimmons et al.*, 2012] (brown). Simulated precipitation results in sectors of PNG (5-12°S and 130-160°E, dark blue lines) and North Australia (12-20°S and 120-160°E, cyan lines) are given in Figure 4-4.

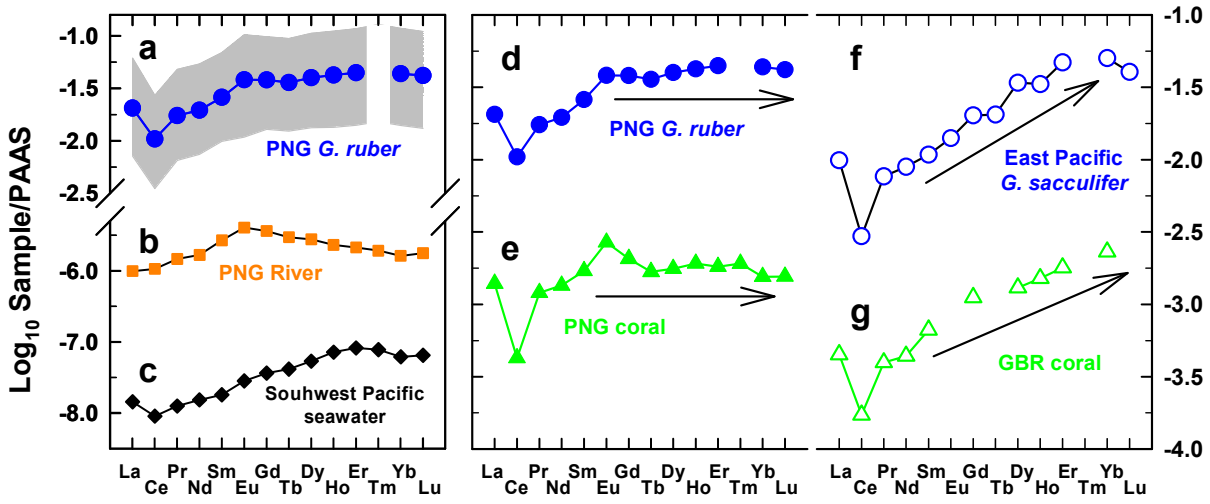

Figure 4-2. Shale normalized [*McLennan*, 1989] REE patterns. (a) Averaged MD05-2925 *G. ruber* data with temporal variability range over the past 284 kyr in this study (gray area). (b) PNG river [*Sholkovitz et al.*, 1999]. (c) Open-ocean surface seawater of the Coral Sea in the Southwest Pacific (depth of 0-200 m from *Zhang and Nozaki*, 1996). Comparison of REE patterns from (d) MD05-2925 *G. ruber* in this study (blue circles), (e) PNG coastal coral [*Fallon et al.*, 2002] (green triangles), (f) East Pacific core-top planktonic foraminifer *G. sacculifer* (site 54MC of *Haley et al.*, 2005) (open circles), and (g) Great Barrier Reef (GBR) coral [*Wyndham et al.*, 2004] (hollow triangles). Arrows depict the trend of the REE patterns.

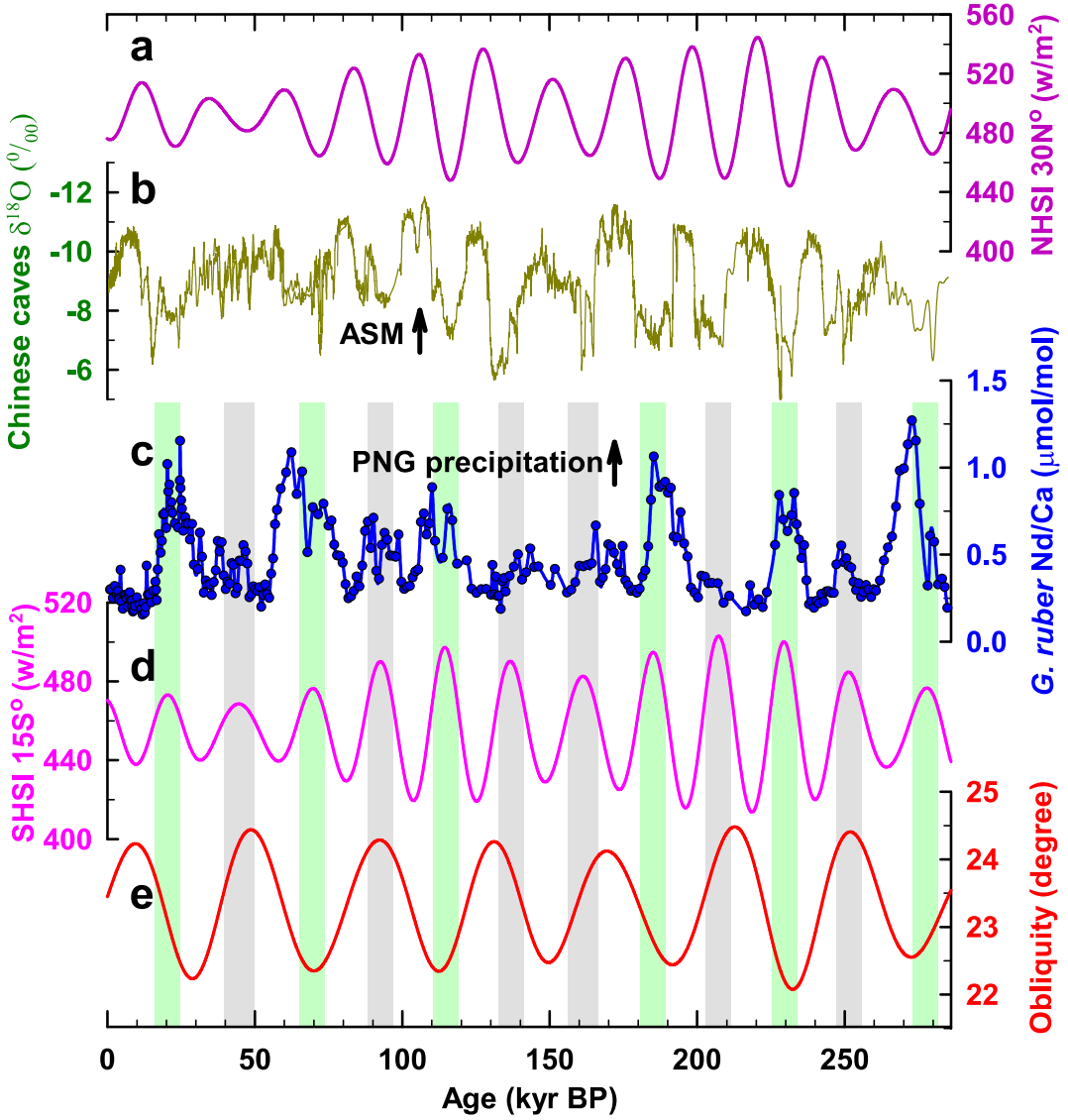

Figure 4-3. Comparison of PNG planktonic foraminifer *G. ruber* Nd/Ca from MD05-2925 with other records over the past 284 kyr. (a) Northern hemisphere summer insolation (NHSI, 15 July) at 30°N [*Berger*, 1978]. (b) Stacked $\delta^{18}O$ of Chinese stalagmites [*Wang et al.*, 2001; *Cheng et al.*, 2006; *Wang et al.*, 2008; *Cheng et al.*, 2009]. (c) MD05-2925 *G. ruber* Nd/Ca (2 ∫ precision: ±2.6%, *Shen et al.*, 2011). (d) Southern hemisphere summer insolation (SHSI, 15 January) at 15°S [*Berger*, 1978]. (e) Earth obliquity [*Berger*, 1978]. Arrows depict an increase of the ASM and the foraminifer-inferred PNG precipitation. PNG precipitation is intensified at six periods with high SHSI (vertical aqua bars), but does not closely reflect high SHSI at six other intervals (gray bars).

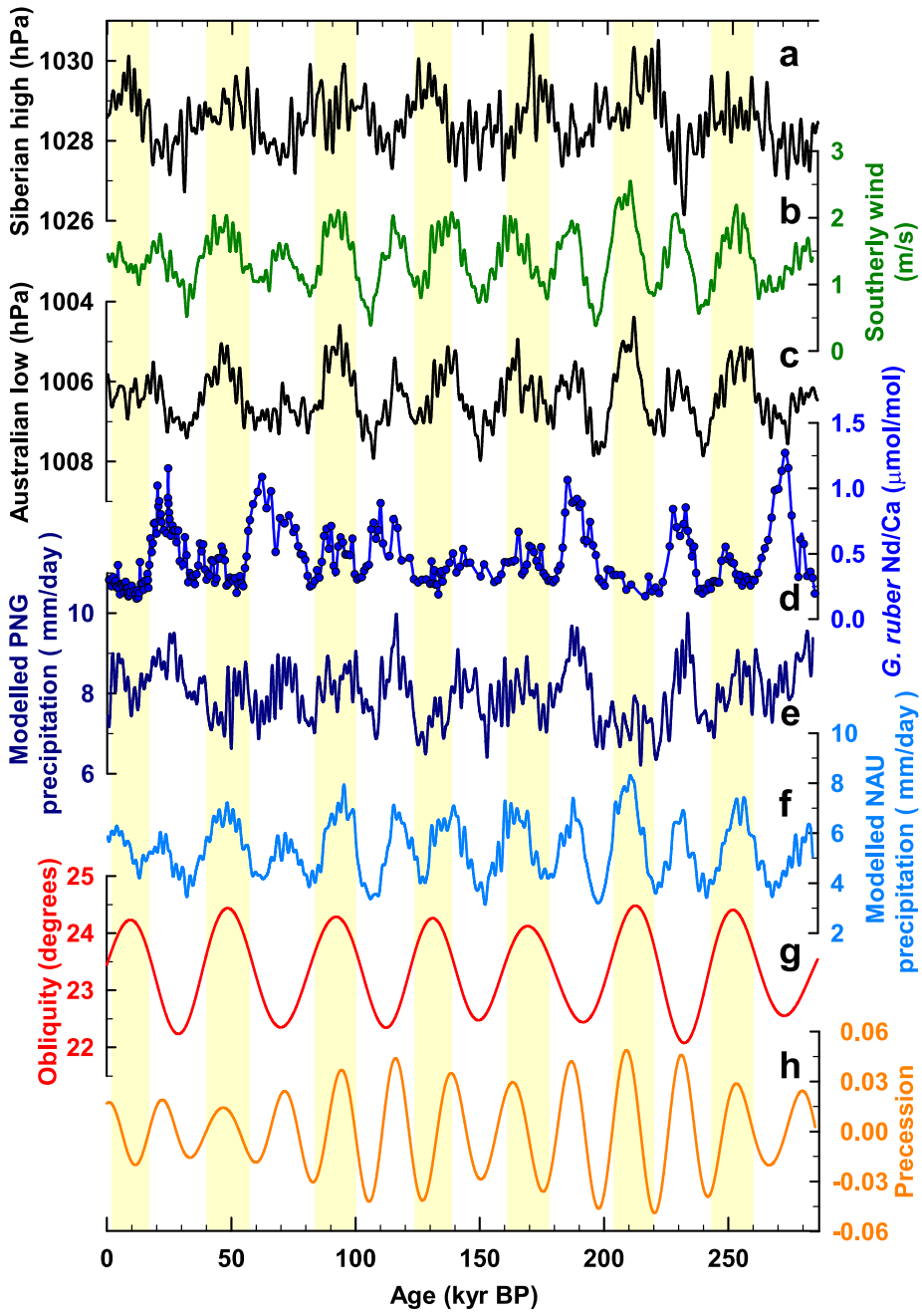

Figure 4-4. Climatological results of the FOAM model simulation in January over the past 284 kyr. (a) Sea level pressure (SLP) for Siberian high (30-70°N and 60-130°E) [*Shi et al.*, 2011]. (b) Cross-equatorial southerly surface wind (0-20°S and 130-160°E). (c) SLP for Australian low (10-35°S and 120-160°E). (e) PNG precipitation (5-12°S and 130-160°E). (f) North Australia (NAU) precipitation (12-20°S and 120-160°E). (d) MD05-2925 *G. ruber* Nd/Ca record, (g) Earth obliquity, and (h) precession [*Berger*, 1978] are given for comparison. Vertical maize bars denote high-obliquity intervals.

Supplementary information of Chapter 4

Evolution of the Pacific Intertropical Convergence Zone over the past 284,000 years

This file includes

Supplementary text

References for supplementary information

Supplementary Table 4-S1

Supplementary Figs 4-S1 to 4-S9

1. Evaluation of different factors on foraminiferal REE contents

Serious influences of metallic oxides on foraminiferal REE contents were reported for the marine sedimentary cores and traps, especially in the Atlantic [*Palmer*, 1985; *Roberts et al.*, 2010; 2012]. An insignificant correlation between Mg/Ca and Fe/Ca data [Figure 4-S3a] indicates the effectiveness of the cleaning techniques. Fe/Ca ratios in our samples (<50 μmol/mol) are much lower than the reported values (>100 μmol/mol) for the diagenetically contaminated foraminiferal test from the EBUS anoxic site [*Haley et al.*, 2005]. Previous studies showed that REE and Fe are positively correlated due to authigenic coatings [*Palmer*, 1985; *Roberts et al.*, 2012; *Tachikawa et al.*, 2013]. An absence of a relationship between Nd/Ca and Fe/Ca [Figure 4-S3b] also suggests that foraminiferal test REE/Ca variation is not attributed to this coating phase. Our and previous studies in the Pacific [*Haley et al.*, 2005; *Pena et al.*, 2013], Indian [*Stoll et al.*, 2005], Mediterranean [*Matinez-Boti et al.*, 2009], and South Atlantic [*Klevenz et al.*, 2008], suggest little influence of metallic oxides on REE contents of chemically-cleaned foraminiferal tests.

The less radiogenic ε_{Nd} values of -1.3~-1.1 of planktonic foraminifer *G. ruber* are different from the surrounding sediment data of 0.1~0.7 [Table 4-S1]. The seawater below 600 m depths show ε_{Nd} values less than -4 near the Solomon Sea [*Grenier et al.*, 2013]. REE concentration and Nd isotope data of planktonic foraminifer tests from plankton tows and sediment traps in the NW Atlantic show 80% of Nd is associated with authigenic metal oxides and organic matter, which form in the water column [*Roberts et al.*, 2012]. In our study area, the planktonic foraminifer Nd isotope data do not reflect those of deep to bottom waters. The

evidence suggests that the foraminiferal test REE source is not from deep/bottom seawater or sediment by post-depositional diagenesis.

If planktonic foraminiferal REE of MD05-2925 were from different surface water masses associated with seasonal ocean circulation, different ε_{Nd} values would be expected on the basis of wide range of +2 to -2 for modern surface water ε_{Nd} values in the equatorial Pacific [*Grenier et al.*, 2013] and would be related to sea level change. Indistinguishable ε_{Nd} values [Figure 4-S2, Table 4-S1] at two different ages of 49.5-50.1 kyr BP with low foraminiferal Nd levels of 0.30-0.32 ⌈mol/mol and 58.8-60.6 kyr BP with high foraminiferal Nd contents of 0.88-0.97 ⌈mol/mol suggest a single predominant source. There is no significant different between REE patterns for periods with low and high foraminiferal REE contents over the entire MD05-2925 record [Figure 4-S4]. Only 10-20% variation of shale-normalized (SN, *McLennan*, 1989) Nd/Yb (Nd/Yb_{SN}) and Gd/Yb_{SN} ratios shows stable light REE/heavy REE (LREE/HREE) and middle REE/HREE (MREE/HREE) ratios over the past 284 kyrs [Figure 4-S5]. This also supports the existence of one dominant source for planktonic foraminiferal REE. The missing of 100 kyr-periodicity of MD05-2925 *G. ruber* REE/Ca record [Figures. 4-S2, 4-S6a] does not favor sea level-dependent ocean circulation process.

The Australian continent is the largest aeolian dust source in this region. However, the aeolian dust is not expected to be transported to our study site [*Jickells et al.*, 2005]. Dust deposition from the remote East Asian continent is also negligible [*Jickells et al.*, 2005]. Moreover, the shale-normalized flat REE pattern of aeolian dust [*Gabrielli et al.*, 2010] is distinctively different from the planktonic foraminiferal

pattern.

Could boundary exchange [*Lacan and Jeandel*, 2001], a mechanism involving the release of dissolved REEs to seawater from particulates in the marine shelf setting, result in planktonic foraminifer *G. ruber* REE variability? The absence of a 100-kyr glacial-interglacial sea-level cycle [Figure 4-S2, 4-S6a] does not support this mechanism. The onset of a decreasing Nd/Ca trend at 20 kyr BP preceded sea level rise by 2 kyrs during the last glaciation [Figure 4-S7]. This trend ended at 17 kyr BP, 3 kyrs earlier than the cessation of ice melting [Figure 4-S7]. This asynchroneity also indicates boundary exchange is not a major factor.

An in-phase correlation between Nd/Ca and Mn/Ca variations is observed in Figure 4-S5. This relationship could conceivably imply redox-induced micron-scale precipitation of $MnCO_3$ [*Roberts et al.*, 2012]. However, no clear correlation (R^2 = 0.069) between records of Mn/Ca and Ce anomalies [$Ce^* = (Ce_{SN} \times Nd_{SN})/(Pr_{SN} \times Pr_{SN})$], a proxy of redox conditions [*Elderfield*, 1988; *German and Elderfield*, 1990], suggests that such a reaction is not manifest in our records [Figure 4-S5]. Planktonic foraminiferal Mn/Ca ratios have been considered as a tracer for dissolved terrestrial input [*Klinkhammer et al.*, 2009]. In-phase variations of Mn/Ca and REE/Ca are here attributed to a common terrestrial source from PNG [*Sholkovitz et al.*, 1999].

2. Replicated foraminiferal REE/Ca records

To demonstrate the fidelity of MD05-2925 REE records [Figure 4-S2], we performed a replication test on planktonic foraminifer *G. ruber* REE/Ca time series in the sedimentary core, ODP 1115B (9.1°S, 151.5°E; water depth 1149 m), from an

adjacent site within the same climatic zone, 19 km north of the MD05-2925 site. For each 5-cm interval of the upper 486 cm of this core, 20-30 foraminiferal tests of down-core planktonic foraminifer *G. ruber* (white, *s.s.* 250-300 μm) were picked. After chemical cleaning process, oxygen stable isotopes and trace elements [**see Chapter 2**] were analyzed. *G. ruber* REE/Ca variations in ODP 1115B are coherent with the MD05-2925 record [Figure 4-S8]. This synchroneity of two REE/Ca sequences demonstrates the robustness of our methodology.

References for supplementary information

An, Z. S., (2000), The history and variability of the East Asian paleomonsoon climate. *Quaternary Science Rev*iew **19,** 171-187.

Elderfield, H., Whitfield, M., Burton, J. D., Bacon, M. P., and Liss, P. S, (1988), The oceanic chemistry of rare earth elements. *Philosophical Transactions of the Royal Society A*. **325**, 105-126.

Fitzsimmons, K. E., Miller, G. H., Spooner, N. A., and Magee, J. W., (2012), Aridity in the monsoon zone as indicated by desert dune formation in the Gregory Lakes basin, northwestern Australia. *Australian Journal of Earth Sciences* **59,** 469-478.

Gabrielli, P., Planchon, F., Barbante, C., Boutron, C. F., Petit, J. R., Bulat, S., Hong, S., Cozzi, G., and Cescon, P., (2010), Ultra-low rare earth element content in accreted ice from sub-glacial Lake Vostok, Antarctica. *Geochimica et Cosmochimica Acta* **73**, 5959-5974 (2010).

German, C. R., and Elderfield, H., (1990), Application of the Ce anomaly as a paleoredox indicator: The ground rules. *Paleoceanography* **5**, 823-833.

Grenier, M., Jeandel, C., Lacan, F., Vance, D., Venchiarutti, C., Cross, A., and Cravate, S., (2013), From the subtropics to the central equatorial Pacific Ocean: Neodymium isotopic composition and rare earth element concentration variations. *Journal of Geophysics Research* **118**, 1-27.

Haley, B. A., Klinkhammer, G. P., and Mix, A. C., (2005), Revisiting the rare earth elements in foraminiferal tests. *Earth* and *Planet*ary *Sci*ence *Lett*ers **239,** 79-97.

Jickells, T. D., An, A. S., Andersen, K. K., Baker, A. R., Bergametti, G., Brooks, N., Cao, J. J., Boyd, P. W., Duce, R. A., Hunter, K. A., Kawahata, H., Kubilay, N., IaRoche, J., Liss, P. S., Mahowald, N., Prospero, J. M., Ridgwell, A. J., Tegen, I., and Torres, R., (2005), Global iron connections between desert dust, ocean biogeochemistry, and climate. *Science* **308,** 67-71.

Klevenz, V., Vance, D., Schmidt, D. N., and Mezger, K., (2008), Neodymium isotopes in benthic foraminfera: Core-top systematics and a down-core record from the Neogene south Atlantic. *Earth* and *Planet*ary *Sci*ence *Lett*ers **265,** 571-587.

Klinkhammer, G. P., Mix, A. C., and Haley, B. A., (2009), Increased dissolved terrestrial input to the coastal ocean during the last deglaciation. *Geochemistry Geophysics Geosystems* **10,** Q03009, doi: 10.1029/2008GC002219.

Lacan, F., and Jeandel, C., (2001), Tracing Papua New Guinea imprint on the central Equatorial Pacific Ocean using neodymium isotopic compositions and Rare Earth Element patterns. *Earth and Planetary Science Letters* **186,** 497-512.

Lisiecki, L. E., and Raymo, M. E., (2005), A Pliocene-Pleistocene stack of 57 globally distributed benthic $\delta^{18}O$ records. *Paleoceanography* **20**, PA1003.

Martinez-Boti, M. A., Vance, D., and Mortyn, P. G., (2009), Nd/Ca ratios in plankton-towed and core top foraminifera: Confirmation of the water column acquisition of Nd. *Geochemistry Geophysics Geosystems* **10**, Q08018, doi: 10.1029/2009GC002701.

McLennan, S. M., (1989), Rare earth elements in sedimentary rocks; influence of provenance and sedimentary processes. *Reviews in Mineralogy and Geochemistry* **21**, 169-200.

Palmer, M., (1985), Rare earth elements in foraminiferal tests, *Earth* and *Planet*ary *Sci*ence *Lett*ers **73**, 285-298 .

Pena, L. D., Goldstein, S. L., Hemming, S. R., Jones, K. M., Calvo, E., Pelejero, C., and Cacho, I., (2013), Rapid changes in meridional advection of Southern Ocean intermediate waters to the tropical Pacific during the last 30 kyr. *Earth* and *Planet*ary *Sci*ence *Lett*ers **368,** 20-32 .

Roberts, N. L., Piotrowski, A. M., McManus, J. F., and Keigwin, L. D., (2010), Synchronous deglacial overturning and water mass source changes. *Science* **327**, 75-78.

Roberts, N. L., Piotrowski, A. M., Elderfield, H., Eglinton, T. I., and Lomas, M. W., (2012), Rare earth element association with foraminifera. *Geochimica et Cosmochimica Acta* **94,** 57-71.

Schulz, M., and Mudelsee, M., (2002), REDFIT: estimating red-noise spectra directly from unevenly spaced paleoclimatic time series. *Computers and Geosciences* ***2*8**, 421-426.

Shi, Z. G., Liu, x. D., Sun, Y. B., An, Z. S., Liu, Z., and Kutzbach, J., (2011), Distinct responses of East Asian summer and winter monsoons to astronomical forcing. *Climate of the Past* **7,** 1363-1370 (2011).

Sholkovitz, E. R., Elderfield, H., Szymczak, R., and Casey, K., (1999), Island weathering: river sources of rare earth elements to the Western Pacific Ocean. *Marine Chemistry* **68,** 39-57.

Stoll, H. M., Vance, D., and Arevalos, A., (2005), Records of the Nd isotope composition of seawater from the Bay of Bengal: Implications for the impact of Northern Hemisphere cooling on ITCZ movement. *Earth* and *Planet*ary *Sci*ence *Lett*ers **255,** 213-228.

Tachikawa, K., Toyofuku, T., Basile-Doelsch, I., and Delhaye, T., (2013), Microscale neodynium distribution in sedimentary planktonic foraminiferal tests and associated mineral phases. *Geochimica et Cosmochimica Acta* **100,** 11-23.

Table 4-S1. Planktonic foraminifer and sediment Nd isotopic composition of core MD05-2925

Sample	Depth (cm)	Age (kyr BP)	Number of tests	$^{143}Nd/^{144}Nd$*	ε_{Nd}*
Foraminifer					
G. ruber	472-477	49.5-50.1	580	0.512584 ± 0.000016	-1.06 ± 0.32
G. ruber	537-542	58.8-60.6	250	0.512571 ± 0.000012	-1.30 ± 0.24
Sediment	472-473	49.5	-	0.512673 ± 0.000017	0.68 ± 0.32
	477-478	50.1	-	0.512642 ± 0.000020	0.08 ± 0.39
	537-538	58.8	-	0.512673 ± 0.000016	0.68 ± 0.31
	542-543	60.6	-	0.512655 ± 0.000013	0.34 ± 0.25

* Errors are 2 ∫ of the mean.

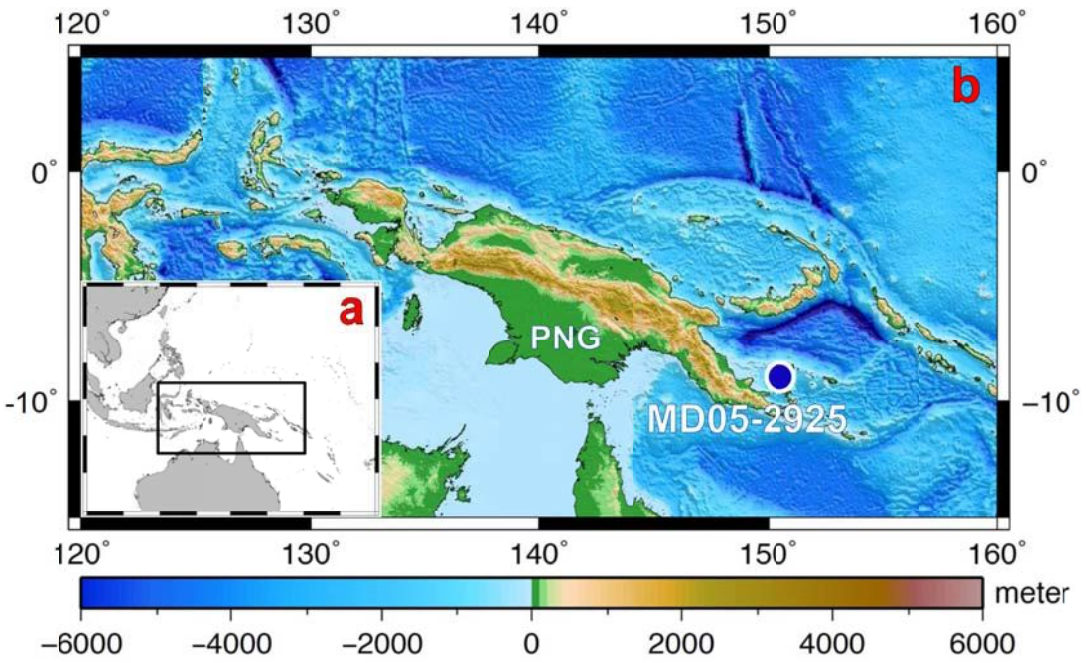

Figure 4-S1. Maps of (a) the western Pacific, and (b) topography of Papua New Guinea (PNG) and surrounding ocean basins. Blue symbol denotes the marine sediment core MD05-2925

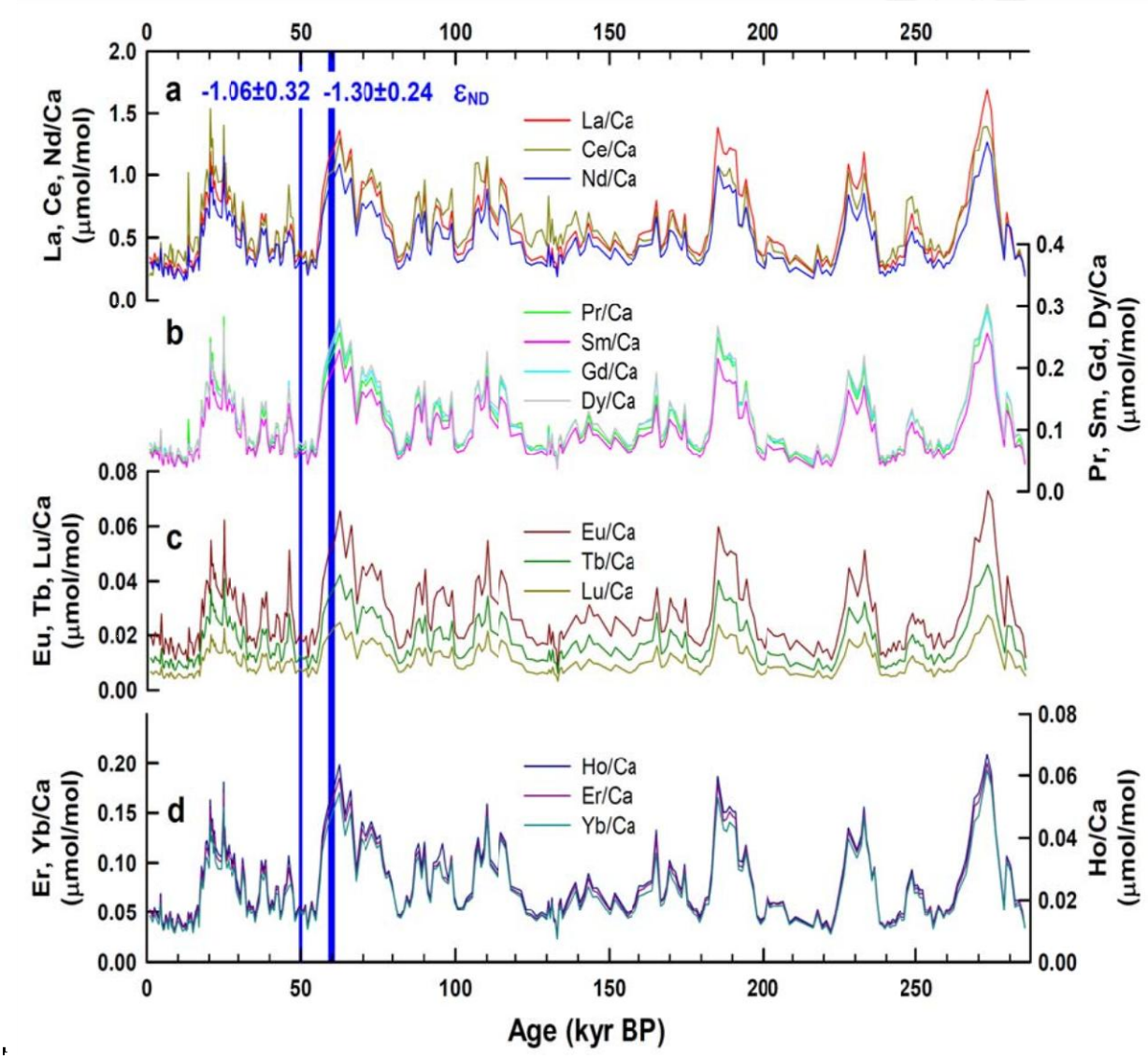

Figure 4-S2. Time series of REE/Ca of planktonic foraminifera *G. ruber*. (a) La/Ca, Ce/Ca and Nd/Ca. (b) Pr/Ca, Sm/Ca, Gd/Ca and Dy/Ca. (c) Eu/Ca ,Tb/Ca and Lu/Ca. (d) Ho/Ca, Er/Ca and Yb/Ca. ε_{Nd} values at ages of 49.5-50.1 and 58.8-60.6 kyr BP are given in panel (a).

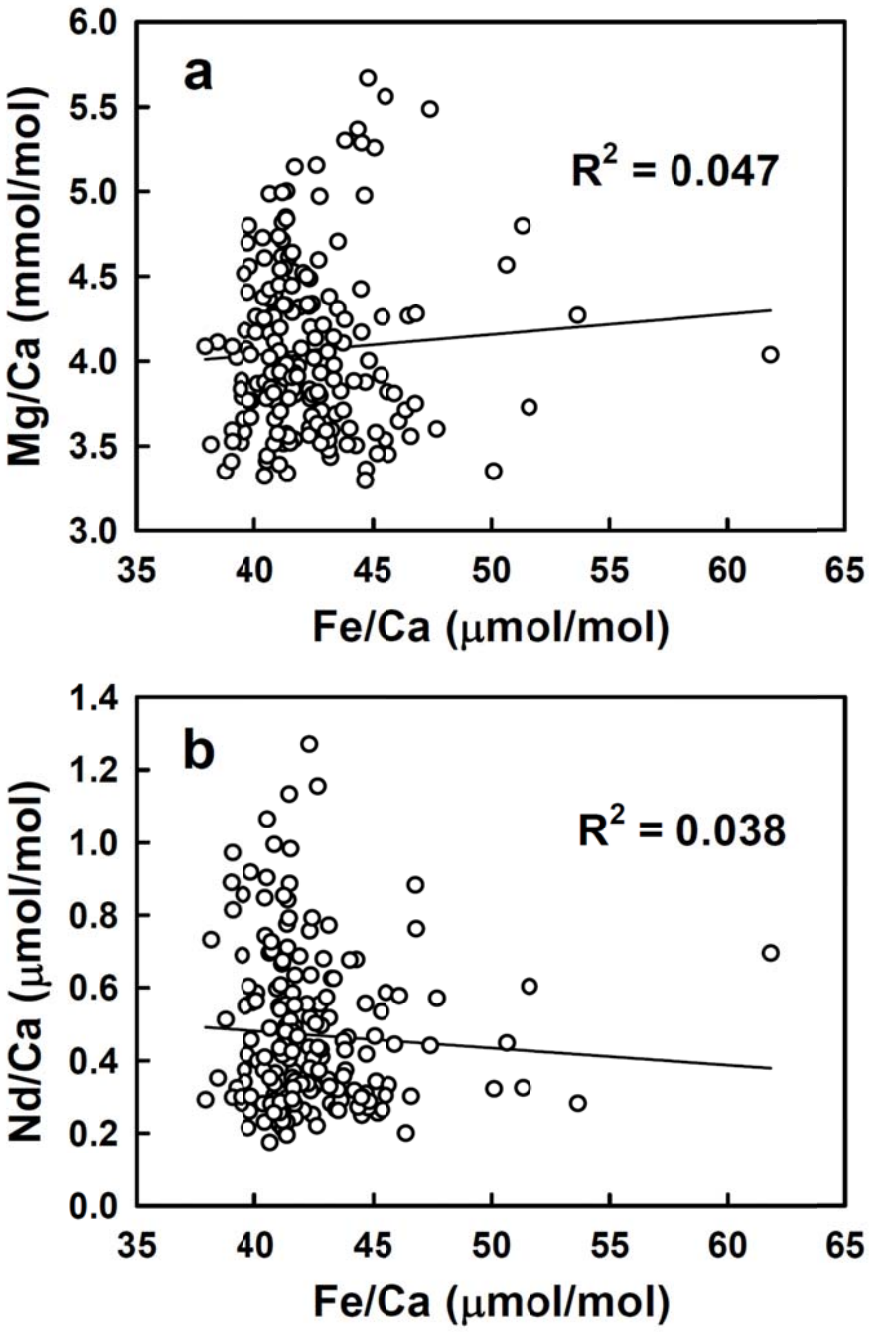

Figure 4-S3. Plots of MD05-2925 *G. ruber* (a) Mg/Ca vs. Fe/Ca and (b) Nd/Ca vs. Fe/Ca.

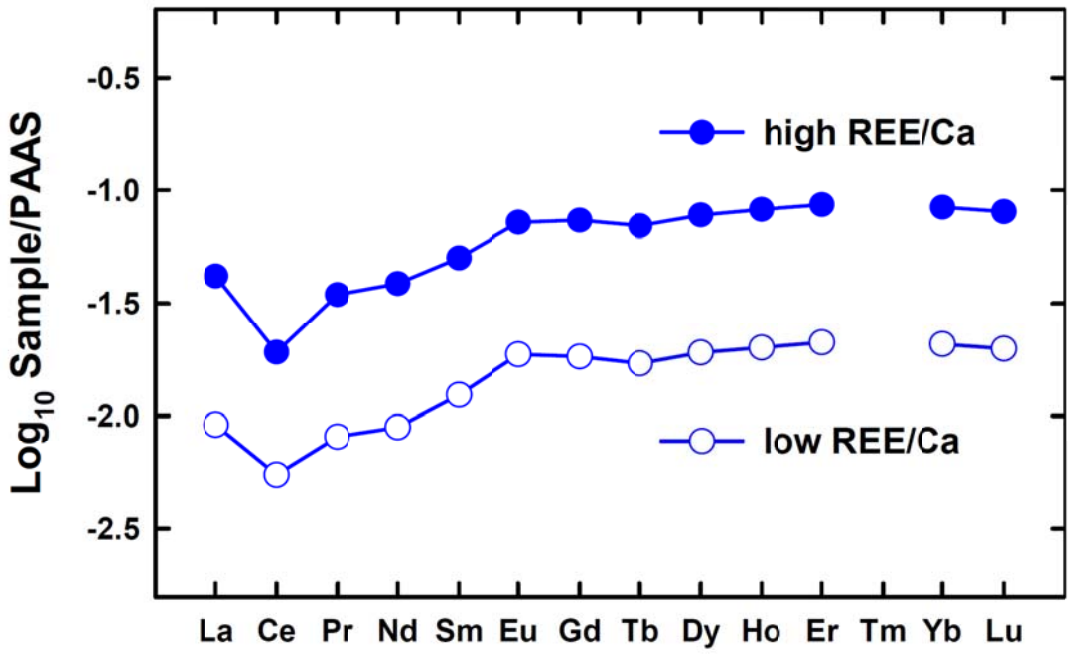

Figure 4-S4. Shale normalized [*McLennan*, 1989] REE patterns. Averaged MD05-2925 *G. ruber* data with low REE/Ca ratios (Nd/Ca <0.25 ⌈mol/mol; open circles) and high REE/Ca ratios (Nd/Ca >0.75 ⌈mol/mol; solid circles).

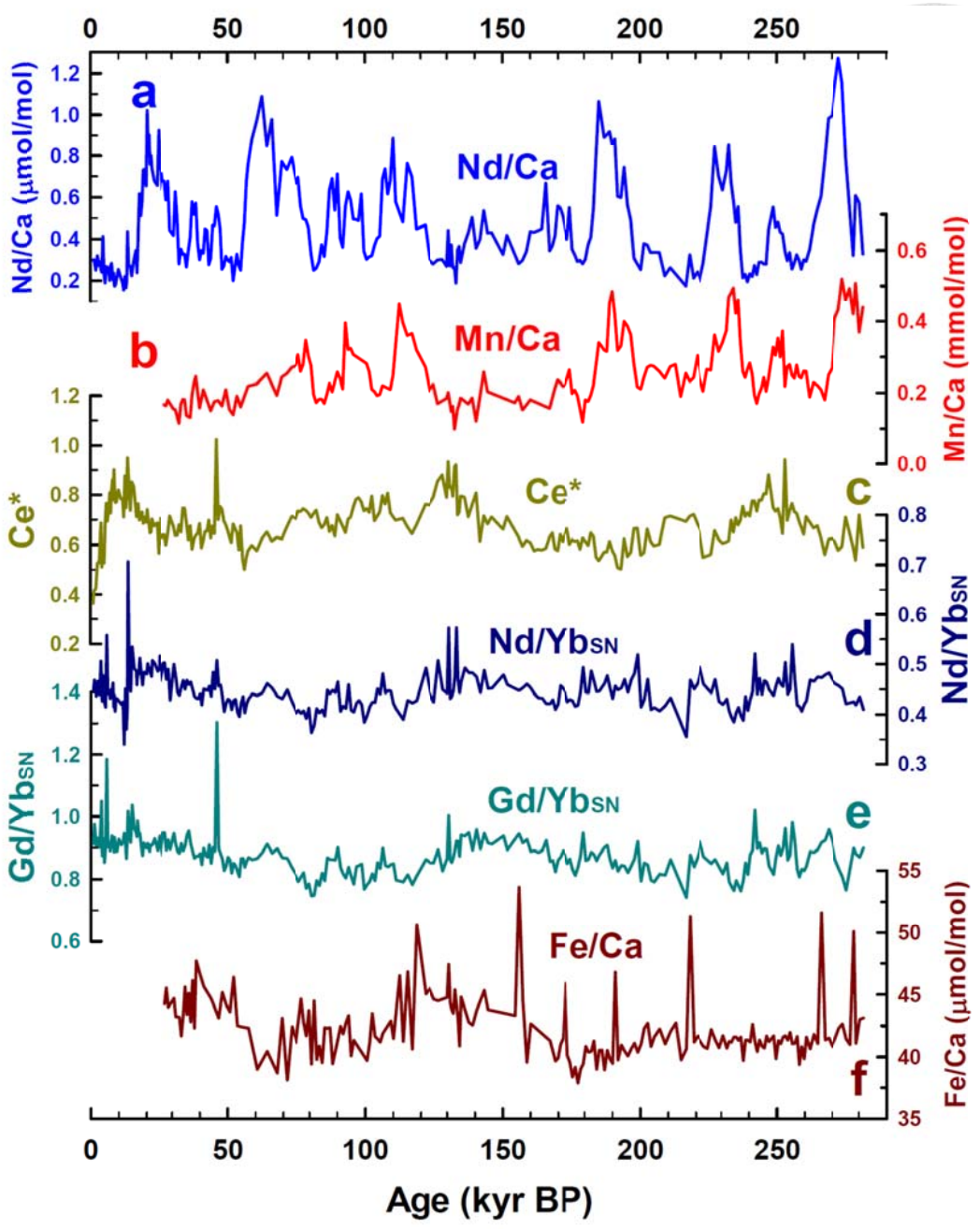

Figure 4-S5. Time series of Trace elemental patterns of MD05-2925 *G. ruber*. (a) Nd/Ca. (b) Mn/Ca. (c) Ce* [Ce* = $(Ce_{SN} \times Nd_{SN})/(Pr_{SN} \times Pr_{SN})$]. (d) Nd/Yb_{SN}. (e) Gd/Yb_{SN}. (f) Fe/Ca.

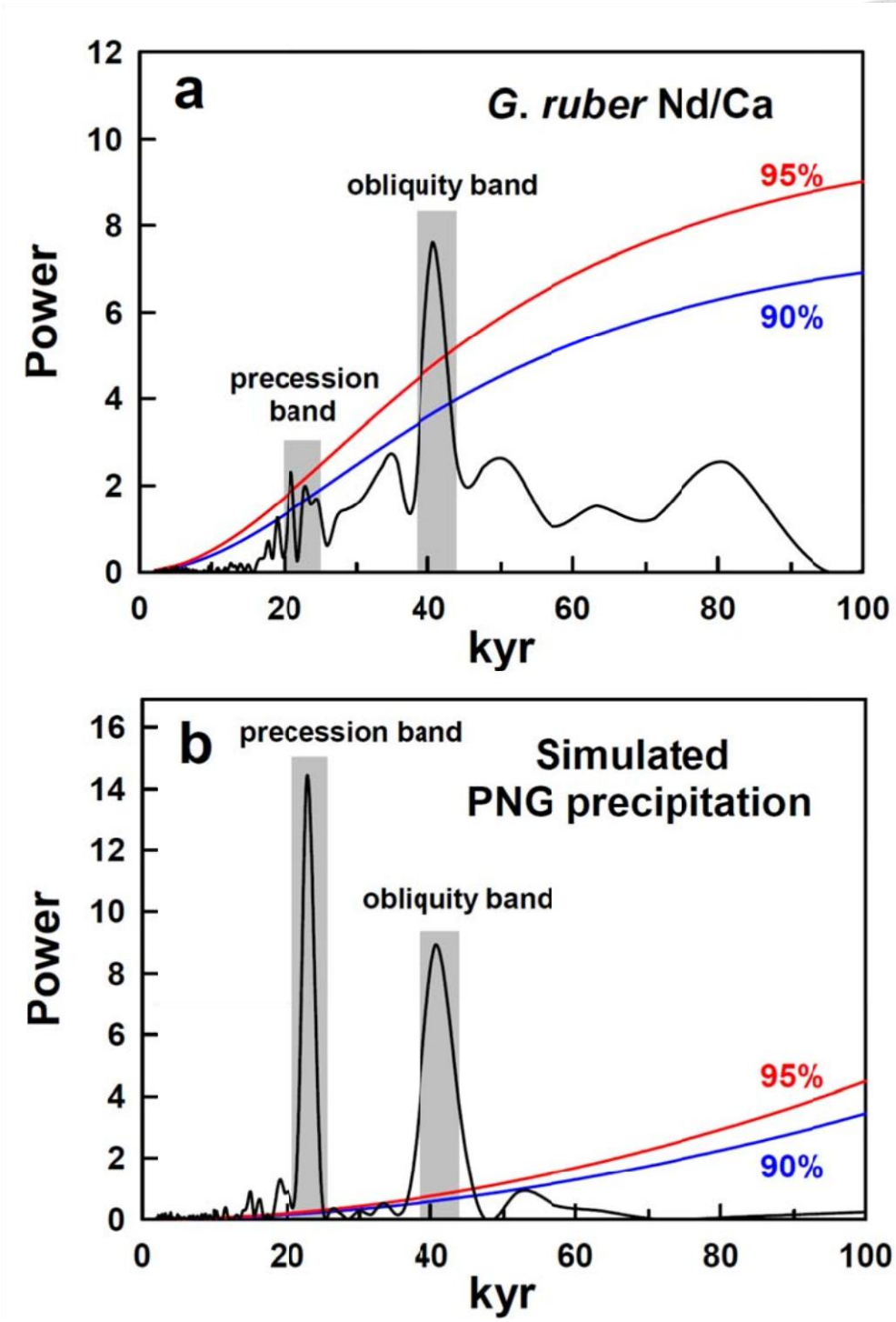

Figure 4-S6. Spectral power analysis results. (a) MD 05-2925 planktonic foraminifer *G. ruber* Nd/Ca record. (b) Simulated PNG precipitation (5-12°S and 130-160°E) over the past 284 kyr. We used REDFIT v 3.8 [*Schulz and Mudelsee*, 2002] to perform spectral analyses. Red and blue lines respectively denote 95% and 90% significance levels of coherence. Vertical bars are the significant precession and obliquity bands.

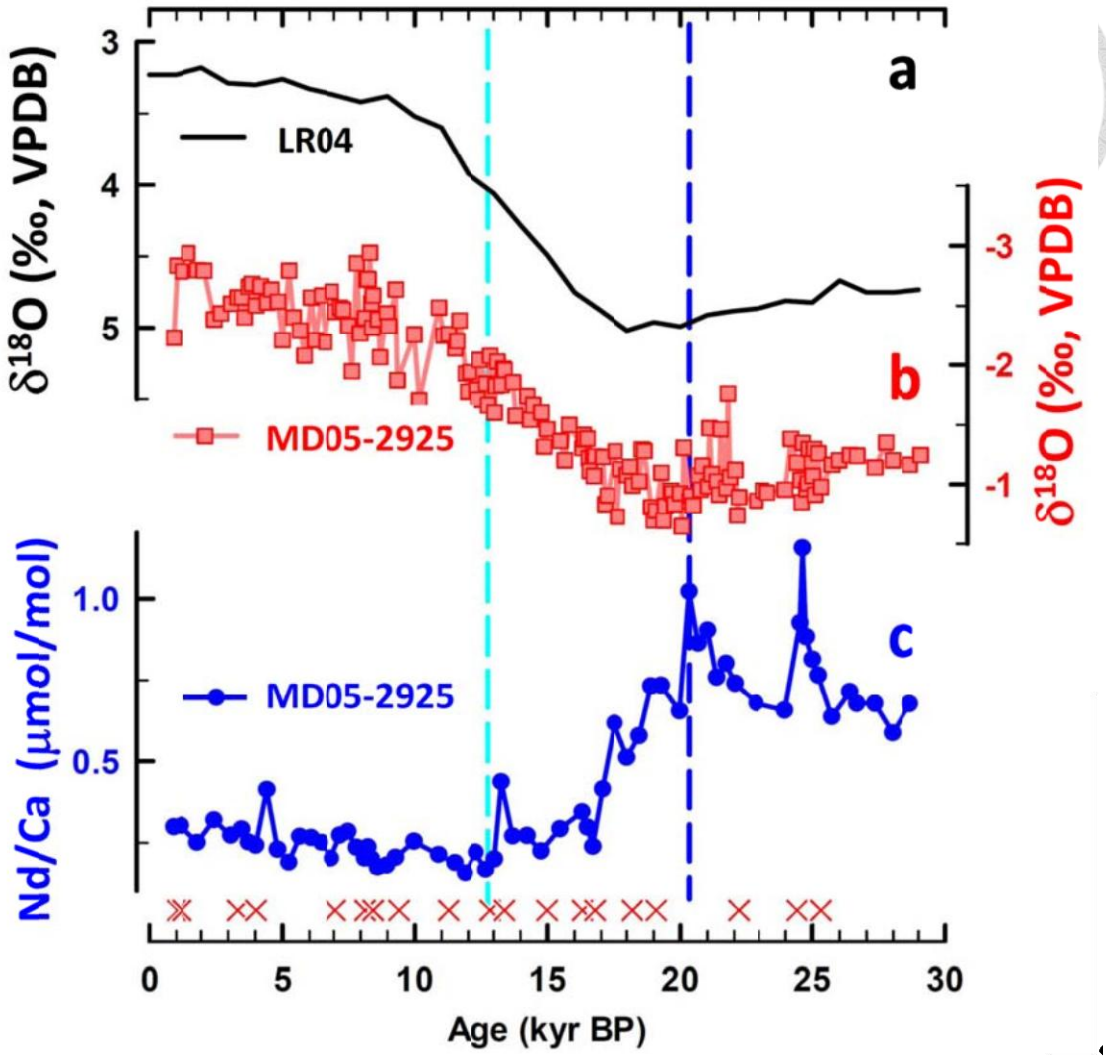

Figure 4-S7. Comparison between (a) benthic $\delta^{18}O$ LR04 [*Lisecki and Raymo*, 2005], and (b) $\delta^{18}O$ and (c) Nd/Ca of *G. ruber* from MD05-2925 over the past 30 kyrs. Cross symbols denote calibrated AMS ^{14}C dates. Blue (cyan) dashed line indicates the onset (ending) of decreasing Nd/Ca trend since 30 kyr BP.

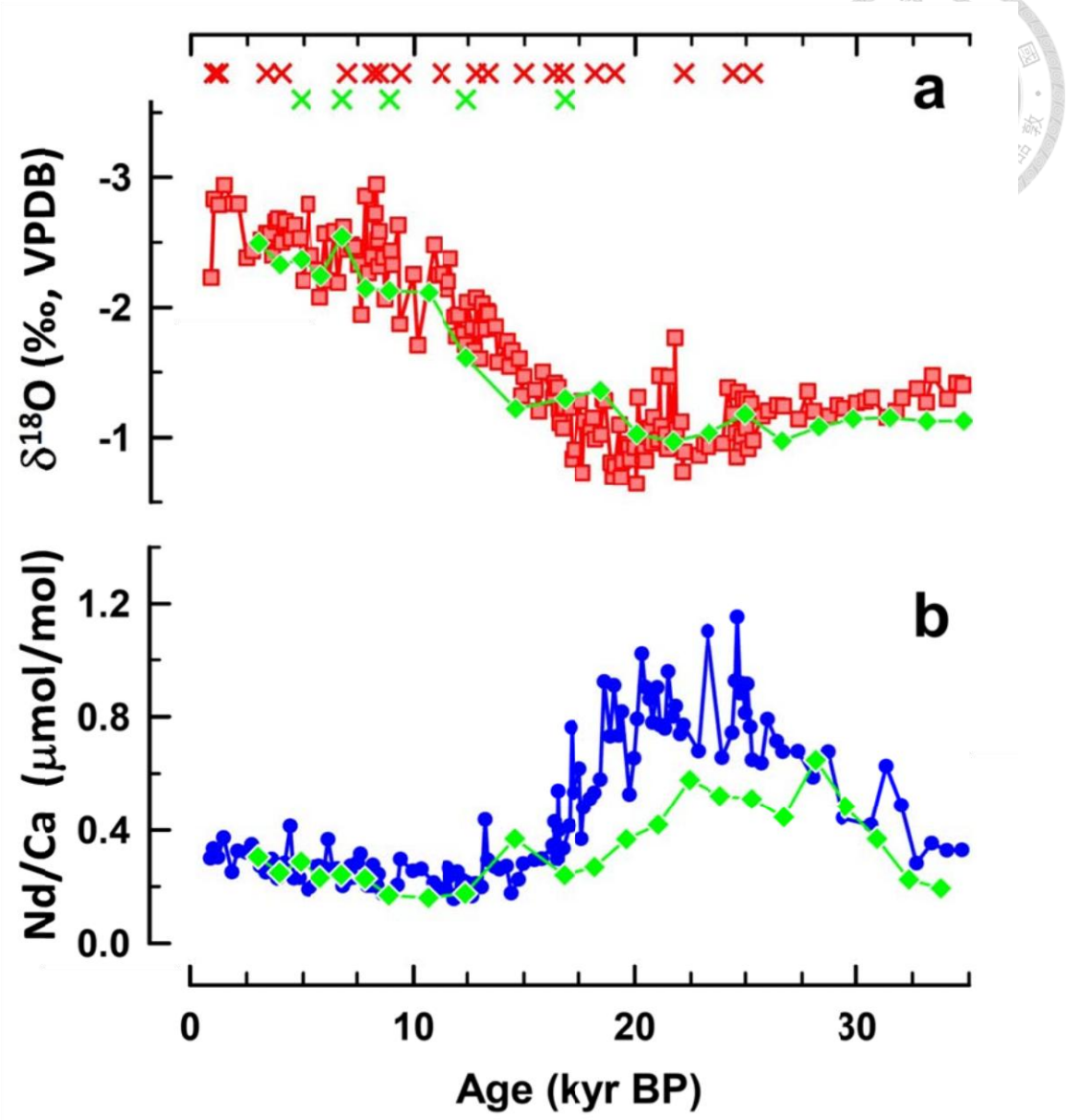

Figure 4-S8. Time series of foraminiferal $\delta^{18}O$ and Nd/Ca for MD05-2925 and ODP 1115B over the past 34 kyrs. (a) Planktonic foraminifer *G. ruber* $\delta^{18}O$ records of MD05-2925 (red) and ODP 1115B (green). Calibrated AMS ^{14}C dates are color-coded by core. Chronology of ODP 1115B was established using the ^{14}C dates and age control points at 57.8, 75.0, 112.0, 130.0, 135.0, and 167 kyr BP by matching the *G. ruber* $\delta^{18}O$ record with MD05-2925 sequence [Figure 4-S2]. (b) Co-variation of planktonic foraminifer *G. ruber* Nd/Ca records between MD05-2925 (blue) and ODP 1115B (green).

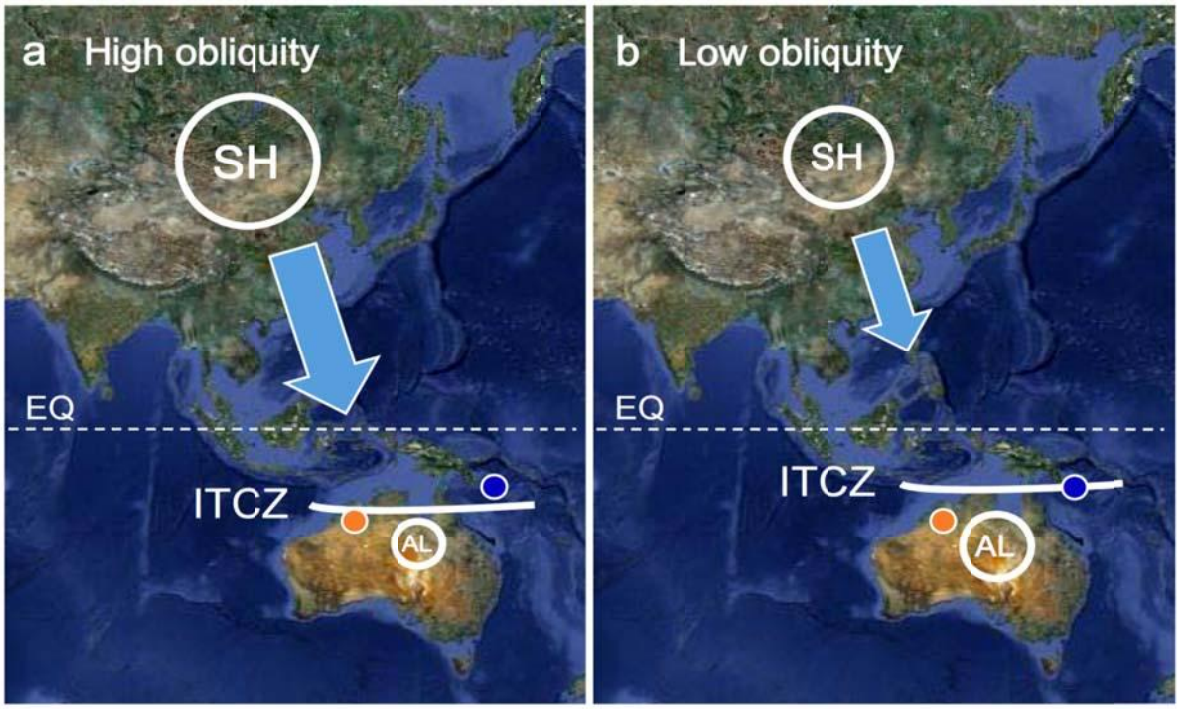

Figure 4-S9. Cartoons illustrating our proposed pressure-push [*An*, 2000; *Shi et al.*, 2011] mechanism driving the southern branch of the ITCZ in the Asia-Pacific realm on orbital scale during high Southern Hemisphere summer insolation.

SH: Siberian high; **AL:** Australian low; **Light blue arrow:** surface wind intensity; **Solid white line**, position of ITCZ; **Blue cycle:** marine sediment core MD05-2925 site; **Brown cycle**, Gregory Lakes [*Fitzsimmons et al.*, 2012].

(a) High obliquity. A strong pressure gradient between intensified SH and AL enhances cross-equatorial flow reinforces the southward shift of the ITCZ rain belt to the southernmost position. The net effect is to increase precipitation in North Australia, with compensated amounts in PNG.

(b) Low obliquity. The cross-equatorial "pressure-push" forcing is weak at low-obliquity and the center of strong convergence rain belt stays in the north, relative to high-obliquity cases. As a result, PNG experiences enormous rainfall while North Australia receives less rainfall.

Chapter 5.

Non-linear response of South-IPWP SST to greenhouse gases radio-forcing changes during the past 360,000 years

In manuscript as Li Lo, Sheng-Pu Chang, Kuo-Yen Wei, Shih-Yu Lee*, Chuan-Chou Shen*, Tsong-Hua Ou, Yi-Chi Chen, Chih-Kai Chuang, Horng-Sheng Mii, George S. Burr, Min-Te Chen, Ying-Hung Tung, Meng-Chieh Tsai. Non-linear response of S-IPWP SST to greenhouse gases radio-forcing during the past 360,000 years

Non-linear response of South-IPWP SST to greenhouse gases forcing changes during the past 360,000 years

Li Lo[1], Sheng-Pu Chang[1], Kuo-Yen Wei[1], Shih-Yu Lee[2,*], Chuan-Chou Shen[1,*], Tsong-Hua Ou[3], Yi-Chi Chen[1], Chih-Kai Chuang[1], Horng-Sheng Mii[4], George S. Burr[5], Min-Te Chen[6], Ying-Hung Tung[1], Meng-Chieh Tsai[1]

1. High-Precision Mass Spectrometry and Environment Change Laboratory (HISPEC), Department of Geosciences, National Taiwan University, Taipei 10617, Taiwan, R.O.C.

2. Research Center for Environmental Changes, Academia Sinica, Taipei 11529, Taiwan, R.O.C.

3. Institute of Applied Mechanics, National Taiwan University, Taipei 10617, Taiwan, R. O.C.

4. Department of Earth Sciences, National Taiwan Normal University, Taipei 11677, Taiwan, R.O.C.

5. NSF-Arizona Accelerator Mass Spectrometry Laboratory, University of Arizona, Tucson, AZ 85721, USA.

6. Institute of Applied Geosciences, National Taiwan Ocean University, Keelung 20224, Taiwan, R.O.C.

*To whom correspondence should be addressed to:
Shih-Yu Lee: Tel: 886-2-27871925; Fax: 886-2-27871924; email: shihyu@gate.sinica.edu.tw

Chuan-Chou Shen: Tel: 886-2-33665878; Fax: 886-2-33651917; email: river@ntu.edu.tw

To be submitted to *Nature*

(Impact factor: 38.597)

March. 2014

Tropical Pacific temperature plays a pivotal role in heat and moisture

budget in the Earth's climate systems. Its response to greenhouse radiative forcing (RF) is a key question in global warming research. Here we present the past 360 thousand years sea surface temperature (SST) record from the South Indo-Pacific Warm Pool (S-IPWP) to demonstrate the non-linear response behavior to greenhouse gases concentration over the past four glacial/interglacial cycles. The SSTs rose drastically with sensitivity changed significantly (0.5 to 1.4 $^{o}C/Wm^{-2}$) when equivalent CO_2 ($pCO_{2equ.}$) exceeded a threshold value at 220 ± 10 ppmv. We speculate that the southern equatorial Pacific has responded as a non-linear amplifier to both the Sub-Antarctic Mode Water/Antarctic Intermediate Water (SAMW/AAIW) formation and greenhouse gas concentrations to deliver the Earth's climate from a deglaciation to a full interglacial condition once the atmospheric CO_2 concentration passes the critical thresholds. The non-linear relationship between southern equatorial Pacific SST and greenhouse gas concentration is a key feature shown by the past tropical climate changes related to the Southern Hemisphere. Such non-linearity and its mechanism should be bear in mind when we try to look into the future warming projections.

Rapid rise of anthropogenic CO_2 emission in the past six decades has posted a threat to human sustainability. A doubled CO_2 (560 ppmv) concentration of pre-industrial value was projected to occur in Years 2050-2100 and may cause global mean temperature warming for 2.0-4.5^{o}C by the end of 21st century, which may accompany with large-scale ice sheet melt, rainfall belt shift, and sea level rise [*IPCC*, 2007]. To identify the interactions among various forcing agents and feedback processes in the projected warming scenario is crucial for policy decision, and social security. Tropical Pacific Ocean is the most important water vapor and moisture

supplier to the middle and high latitudes. Understanding sea surface temperature (SST) response to radiative forcing (RF) changes is crucial to make future predictions. Modern climate theory, however, could only assume constant sensitivity of the tropical ocean temperate to the greenhouse gases concentrations without comprehensive observation for climate transitions from low to high greenhouse gas concentrations. Thus, studies of the past tropical Pacific SST could provide valuable information during the past global fast warming periods, *e.g.* glacial-interglacial (G/IG) transitions [*Lea et al.*, 2000; *de Garidel-Thoron et al.*, 2005].

The sensitivity of tropical Pacific Ocean sea surface temperature to greenhouse gase radiative forcing (mainly contribute by CO_2) changes during the past four to five G/IG cycles have been previously addressed by *Lea*, [2004] and *Dyez and Ravelo*, [2012]. They performed linear regression analyses to estimate SST responses to changes in pCO_2. Based on the regression coefficients obtained from the paleoclimate records, they project a 33-36^{o}C tropical Pacific SST for the future doubling CO_2 scenario. Alternatively, the CO_2 radiative effect on SST may not be linear and the climate may switch non-linearly as suggested by other studies [*e.g.*, *Paillard*, 2001; *Peacock et al.*, 2006; *Carlson and Winsor*, 2012]. Linear versus non-linear regression differences would not only affect the accuracy of the prediction to the future climate evolution but also challenge our knowledge of the interactions between climate components within the system. To obtain better understanding of the tropical Pacific response to pCO_2 changes, we need high-resolution SST records to address fast changes during the fast G/IG transitions and spatial recovery to identify possible climate teleconnections.

In this study, we reconstructed a high resolution SST (200- to 900-yrs resolution) record from the Solomon Sea, on the South Indo-Pacific Warm Pool (S-IPWP), of the past four G/IG cycles during the past 360 thousand years (360 ka), and examined the non-linearity between the tropical Pacific SST and RF. We proposed that the SST is in fact nonlinear to RF and after a major threshold level at 220 ± 10 ppmv, which S-IPWP SST linearly increases ~1.9 ± 0.4^{o}C (by the sensitivity changes from 0.5 to 1.4 ^{o}C/Wm^{-2}, when $pCO_2 \geq 220 \pm 10$ ppmv). We also discuss a potential mechanism to explain this non-linearity of S-IPWP SST changes are the results of the combination of Southern Ocean sea ice induced intermediate/mode water formations and the changes of greenhouse gase concentrations.

We reconstruct ΔSST (Eq. 1) and ΔRF_{GHG} (greenhouse gases, GHG, Eq. 2) by referencing measured SST from marine sediment core and EPICA ice core greenhouse gases concentrations to present day value.

$$\Delta SST = \Delta SST_i - \Delta SST_0 \qquad \text{(Eq. 1)}$$

ΔSST defined as the temperature differences between the past (ΔSST_i) and modern annual average temperature (ΔSST_0, ~28 ^{o}C, *Locarnini et al.*, 2010). ΔRF_{GHG} defined as [*Ramaswamy et al.*, 2001] the differences between the certain past CO_2 level ($[CO_2]$) and the pre industrial greenhouse gases level ($[CO_2]_0$ = 280 ppmv). It is worthy to notice that the CH_4 only contribute <5%, and the negative feedback from N_2O is negligible to RF [Figure 5-2]. The equations to determine ΔRF_{GHG} are listed below:

$$\Delta RF_{GHG} \approx \Delta RF_{CO2} = 4.841 \ln([CO_2]/[CO_2]_0) + 0.0906 (\sqrt{[CO_2]} - \sqrt{[CO_2]_0}) \qquad \text{(Eq. 2,)}$$

The correlation of Solomon Sea ΔSST to ΔRF_{GHG} shows striking non-linear climate sensitivity that is different from the linear sensitivity reported by previous studies [*Lea*, 2004; *Dyez and Ravelo*, 2012]. We adapt the commonly used non-overlapping binned method [*Oppo et al.*, 2009; *Linsley et al.*, 2010] to identify the relationship between ΔSST and equivalent pCO_2 (pCO_{2equ}, *Lea*, 2004; *Dyez and Ravelo*. 2012, supplementary information) by every 10 ppmv CO_2 step from 170-290 ppmv and then to average responded ΔSST changes [Figure 5-3]. The standard deviation of means of ΔSST have also been calculated [Figure 5-2, 5-S4]. Significant transition between 210 – 230 ppmv revealed the threshold change. Thus we identified threshold 220 ± 10, ppmv as the sensitivity change threshold. ΔSST varies from -2.4 to 0.4^{o}C response pCO_{2equ} from 210 to 270 ppmv (sensitivity is ~1.4 $^{o}C/Wm^{-2}$). Linearly increasing ΔSST after 220 ppmv threshold show high sensitivity than previous reported [*Lea*, 2004, *Dyez and Ravelo*, 2012, supplementary information for discussion]. We also calculated the ΔSST to ΔRF_{GHG} response during the time periods. We separated the time series into four periods: (1) 0-70, (2) 71-160, (3) 161-270, and (4) 271-360 kyrs, which represent different G/IG cycles, to test is there any differences of response during the different periods [Figure 5-S6]. The result shows there is no significant different response between the last four G/IG transitions.

To identify whether this non-linear climate sensitivity is robust, we also reexamined previous SST studies by the planktonic foraminiferal Mg/Ca ratios in the Pacific Ocean [ODP 806 and TR163-19, *Lea et al.*, 2000; MD97-2140, *de Garidel-Thoron et al.*, 2005; ODP 1240, *Pena et al.*, 2008; ODP 871, *Dyez and Ravelo*, 2012, supplementary information]. MD05-2925, TR163-19, and ODP 1240 are clearly showed the non-linear relationship to the ΔRF_{GHG} during the past three to four G/IG

cycles [Figure 5-4]. These comparisons further revealed that the Southern Hemisphere (SH) records (MD05-2925, this study) or SH-related eastern equatorial Pacific (EEP) upwelling sites (ODP 1240, and TR163-19) have higher sensitivity (1.2 to 1.4 $^{o}C/Wm^{-2}$) to the ΔRF_{GHG}. With 1- or 4-kyrs resolution resampling in time domain, the compiled record from the EEP also show the non-linearity with a major threshold around the same range of pCO_{2equ} from Soloman Sea. However, those in the Northern Hemisphere sites (ODP 806, MD97-2140, and ODP 871) showed clearly linear trends (sensitivity is ~0.8 $^{o}C/Wm^{-2}$, supplementary information), and the controlling factor(s) is/are still unknown. The compilation tropical Pacific sites results support our interpretation to the non-linear response of ΔSST to ΔRF_{GHG} to the regional scale in the south Pacific or affected by the Southern Hemispheric high latitude sites by the EEP upwelling system. A similar trend between Antarctic temperature changes with Solomon SST was found in this study during the past 360 thousand years (R^2 = 0.63 or 0.67, if the marine isotope stage, MIS 7.4 to 7.2 is omitted, supplementary information, and Figure 5-S3). The correlation implies a persistent teleconnection between Solomon Sea and Antarctica regions [Figure 5-S2, 5-S5]. These results point out the links of S-WPWP and EEP regions to the Southern Ocean modulation.

The key process to cause this non-linear SST response may be both the sea ice coverage in the Southern Ocean and CO_2 radiative forcing during the last four G/IG cycles. Sea-ice coverage in the Southern Ocean controls the major atmospheric-oceanic exchange of CO_2 on the G/IG timescales by introducing flip-flop behavior of the formation of Sub-Antarctic mode water (SAMW) and Antarctic intermediate water (AAIW) [*Jaccards et al.*, 2013]. Fast linkages between SAMW/AAIW to South Pacific Tropical Water (SPTW, Figure 5-1), and then to the equatorial Pacific region

have been reported by the subtropical gyre and resurface processes (e.g. upwelling and mixing, *Hartin et al.*, 2011; *Pena et al.*, 2013; *Qu et al.*, 2013]. These "oceanic tunneling" point out tight links of S-IPWP and EEP regions to the Southern Ocean modulation. Followed by the gradual melting of sea ice in the Sub-Antarctic Zone during the termination periods, the positive latent and sensible heating may have trigger sudden retrieval of Southern Ocean sea ice and results in warming and better ventilated SAMW [*Sigman et al.*, 2010]. The 220 ± 10 ppmv pCO_2 may be the corresponding pCO_2 level where the runaway melting occurred. To take last termination as an example, 220 ± 10 ppmv pCO_2 were just occurred during the major Heinrich event 1, where the meridional circulation was crashed [*McManus et al.*, 2004] and the Southern Ocean warmed and better ventilated (major deep sea carbon reservoir releasing, *Anderson et al.*, 2009; *Skinner et al.*, 2010). Geochemical proxies from the benthic foraminiferal $\delta^{13}C$ and surface temperature in the SW-Pacific have been reported to indicate a major SAMW/AAIW re-producted/better ventilated period [*Pahnke et al.*, 2003; *Pahnke et al.*, 2005]. Sea ice retreated induced warming SAMW/AAIW and fast pCO_2 releasing during the termination periods may be the reason for the non-linear response of S-IPWP SST to atmospheric pCO_2.

The implications of the non-linear response of S-IPWP system may be the non-linear amplifier to the glacial termination through the energy and atmospheric circulation. Once the pCO_{2equ} exceeded 220 ppmv, the S-IPWP SSTs increase by ~2^{o}C linearly. The warm SST and increase latent heating in turn may be a positive feedback contributing to the high latitude ice sheet collapse [*Clark et al.*, 2007]. Rapid warming in the south and east equatorial Pacific may be further weakening the south branch of Hadley circulation and then strengthen the SH westerlies. Thus,

further enhanced SO upwelling would released more CO_2 [*Lee et al.*, 2011]. Certain threshold involves south subtropical Pacific to Antarctica physical oceanography and biogeochemical process has also been reported by *Jaccard et al.* [2013] during the past one million years G/IG oscillations. To connect the South and North Hemisphere climatic system through S-IPWP SST during the past four G/IG cycles may lead us to a more dynamic view of how tropical climate system play a role in the fast transition Earth's climate.

In this study we pointed the non-linearity of tropical SST to the greenhouse gase radiative forcing, however, the even more complicated situation we may face for the future prediction. First, we identified the non-linearity of the South and East equatorial Pacific SST changes, there is no simple interpretation of how there is regional differences within the tropical Pacific Ocean. Second, would the sensitivity changes through time? During the early Brunhes period (400-780 ka), the average interglacial period pCO_2 levels were (15-20 ppmv) lower than the late Brunhes period (0-400 ka). The tropical SSTs, however, showed the similar interglacial SST range over the equatorial Pacific Ocean [*Liu and Hebert*, 2004; *de Garidel-Thoron et al.*, 2005; *Medina-Elizalde and Lea*, 2008]. Would this imply the sensitivity had been yielded through the middle-Brunhes period, or only it is because the buffer of the sensitivity changes? Third, would there has another threshold in the higher pCO_2 world? The tropical climate sensitivity would keep persistent, yield, or even higher when we cross another threshold? To understand the complexity of tropical ocean thermal response to greenhouse gases RF changes and consequential high latitude teleconnections, we need to higher resolution SST records from different hemispheres, more accurate greenhouses gases concentration reconstruction or direct evidence from

ice core back to previous high pCO_2 world, and new physical modeling to point the linkages between tropical and both high latitude climate systems in millennial to orbital timescales.

Acknowledgement

Authors would like to thanks the chief scientist Luc Beafufort of 2005 (PECTEN) cruise supported by the (IMAGES) group.

References

Anderson, R. F., Ali, S., Bradtmiller, L. I., Nielsen, S. H. H., Fleisher, M. Q., Anderson, B. E., Burckle, L. H., (2009), Wind-driven upwelling in the Southern Ocean and the deglacial rise in atmospheric CO_2. *Science* **323**, 1443-1448.

Carlson, A. E., and Winsor, K., (2012), Northern Hemisphere ice-sheet responses to past climate warming. *Nature Geoscience* **5**, 607-613.

Clark, P. U., Hostetler, S. W., Pisias, N. G., Schmittner, A., and Meissner, K., J., (2007), Mechanism for a ~7-kyr climate and sea-level oscillation during marine isotope stage 3, in *Ocean Circulation: Mechanisms and Impacts*, A. Schmittner, J. Chiang, S. Hemming, Eds. Geophysical Monograph 173, American Geophysical Union, Washington, DC, pp. 209–246.

Dyez, K. A., and Ravelo, A. C., (2012), Late Pleistocene tropical Pacific temperature sensitivity to radiative greenhouse gas forcing. *Geology* **41**, 23-26.

Hartin, C. A., Fine, R. A., Sloyan, B. M., Talley, L. D., Cherekin, T. K., Happell, J., (2011), Formation rates of Subantarctic mode water and Antarctic intermediate water within the South Pacific. *Deep-Sea Research Part 1* **158**, 524-534.

IPCC AR4 report. Contribution of Working Groups I, II and III to the Fourth Assessment Report of the Intergovernmental Panel on Climate Change. Core Writing Team, Pachauri, R.K. and Reisinger, A. (Eds.). IPCC, Geneva, Switzerland. pp. 104 (2007).

Jaccard, S. L., Hayes, C. T., Martinez-Garcia, A., Hodell, D. A., Anderson, R. F., Sigman, D. M., and Haug, G. H., (2013), Two modes of change in Southern Ocean productivity over the past million years. *Science* **339**, 1419-1423.

Lea, D. W., Pak, D. K., and Spero, H. J., (2000), Climate impact of late Quaternary equatorial Pacific sea surface temperature variations. *Science* **289**, 1719 – 1724.

Lea, D. W., (2004), The 100,000-yr cycle in tropical SST, greenhouse forcing, and climate sensitivity. *Journal of Climate* **17**, 2170-2179.

Lee, S.-Y., Chiang, J. C. H., Matsumoto, K., and Tokos, K. S., (2011), Southern Ocean wind response to North Atlantic cooling and the rise in atmospheric CO_2: Modeling perspective and paleoceanographic implications. *Paleoceanography* **26**, PA1214.

Linsley, B. K., Rosenthal, Y., and Oppo, D. W., (2010), Holocene evolution of the Indonesian throughflow and the western Pacific warm Pool. *Nature Geoscience* **3**, 578 – 583.

Liu, Z., and Herbert, T. D., (2004), High-latitude influence on the eastern equatorial Pacific climate in the early Pleistocene epoch. *Nature* **427**, 720-723.

Lüthi, D., Le Floch, M., Bernhard, B., Blunier, T., Barnola, J.-M., Siegenthaler, U., Raynaud, D., Jouzel, J., Fischer, H., Kawamura, K., and Stocker, T. F., (2008), High-resolution carbon dioxide concentration record 650,000-800,000 years before present. *Nature* **453**, 379-382.

McManus, J. F., Francois, R., Gherardi, J.-M., Keigwin, L. D., and Brown-Leger, S., (2004), Collapse and rapid resumption of Atlantic meridional circulation linked to deglacial climate changes. *Nature* **428**, 834-837.

Medina-Elizalde, M., and Lea, D. W., (2005), The mid-Pleistocene transition in the tropical Pacific. *Science* **310**, 1009-1012 .

Oppo, D. W., Rosenthal, Y., and Linsley, B. K., (2009), 2,000-year-long temperature and hydrology reconstructions from the Indo-Pacific warm pool. *Nature* **460**, 1113 – 1116.

Paillard, D., (2001), Glacial cycles: toward a new paradigm. *Review of Geophysics* **39**, 325-346.

Pahnke, K. Zahn, R., Elderfield, H., Schulz, M., (2003), 340,000-year centennial-scale marine record of Southern Hemisphere climatic oscillation. *Science* **301**, 948-952.

Pahnke, K., and Zahn, R., (2005), Southern Hemisphere water mass conversion linked with North Atlantic climate variability. *Science* **307**, 1741-1746.

Peacock, S., Lane, E., Restrepo, J. M., (2006), A possible sequence of events from the generalized glacial-interglacial cycle. *Global Biogeochemical Cycles* **20**, GB2010.

Pena, L. D., Cacho, I., Ferretti, P., and Hall, M. A., (2008), El Niño-Southern Oscillation-like variability during glacial terminations and interlatitudinal teleconnections. *Paleoceanography* **23**, PA3101.

Pena, L. D., Goldstein, S. L., Hemming, S. R., Jones, K. M., Calvo, E., Pelejero, C., and Cacho, I., (2013), Rapid changes in meridional advection of Southern Ocean intermediate waters to the tropical Pacific during the last 30 kyr. *Earth* and *Planet*ary *Sci*ence *Lett*ers **368,** 20-32 .

Qu, T., Gao, S., and Fine, R. A., (2013), Subduction of South Pacific tropical water and its equatorward past way shown by a simulated passive tracer. *Journal of Physical Oceanography* **43**, 1551-1656.

Ramaswamy, V., Boucher, O., Haigh, J., Hauglustaine, D., Haywood, J., Myhre, G., Nakajima, T., Shi, G., Solomon, S., and Betts, R., (2001), Radiative forcing of climate change in, *Climate Change 2001: The Scientific Basis*, Houghton, J. T., *et al.* eds., Cambridge University Press, 319-416.

Sigman, D. M., Hain, M. P., and Haug, G. H., (2010), The polar ocean and glacial cycles in atmospheric CO_2 concentration. *Nature* **466**, 47-55.

Skinner, L. C., Fallo, S., Waelbroeck, C., Michel, and Barker, S., (2010), Ventilation of the deep Southern Ocean and deglacial CO_2 rise. *Science* **328**, 1147-1151.

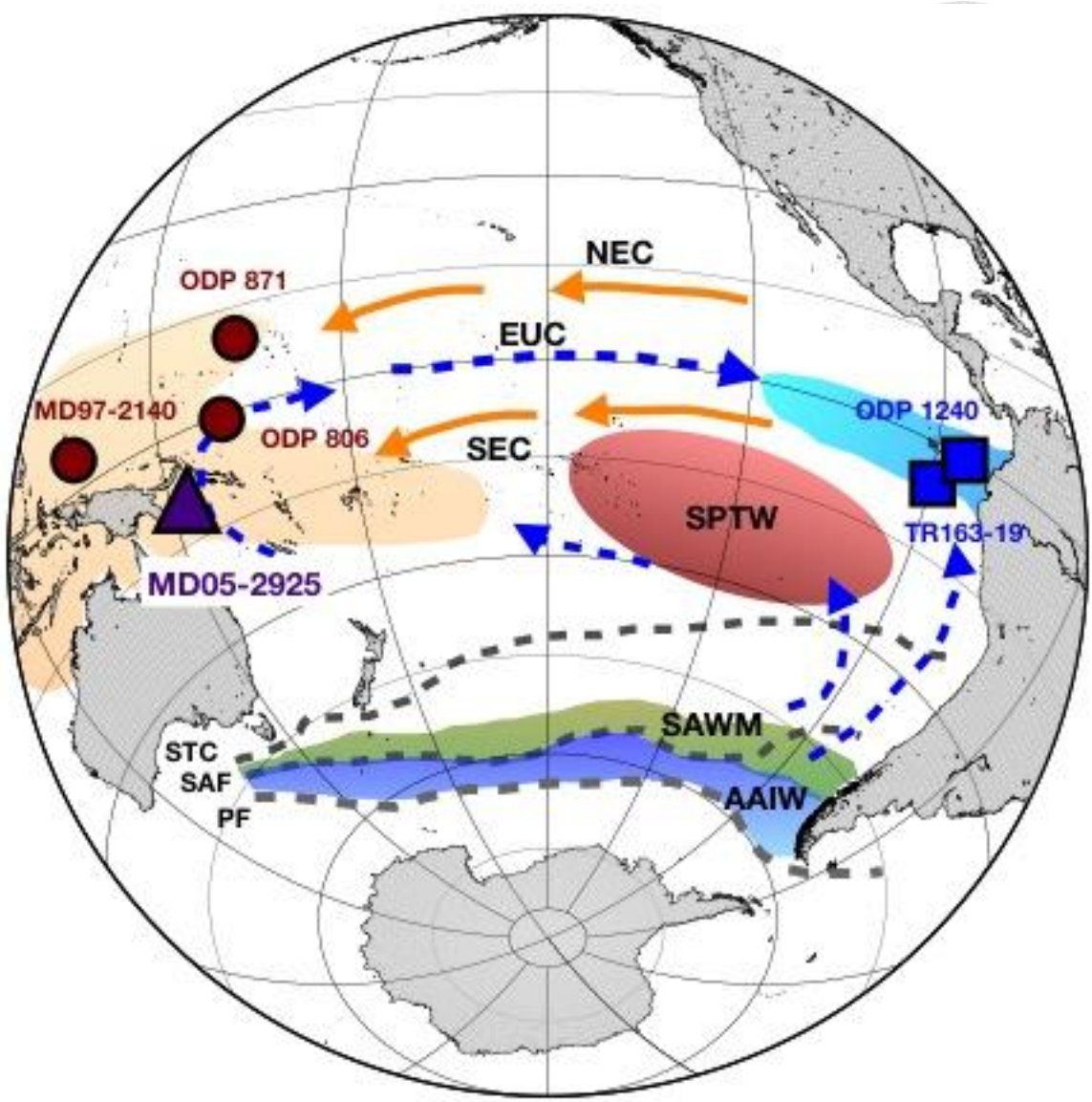

Figure 5-1. Schematic circulation, water masses distribution, and site location map. Purple triangle represents site MD05-2925 (9.3^{o}S, 151.5^{o}E) in this study, and red circles and blue squares are selected sites in the equatorial Pacific. Gray dashed lines show the Polar Front (PF), Subanatarctic Front (SAF), and Subtropical convergence zone (STC), respectively. Blue and green shadings indicate the formation region of Subanatarctic Mode Water (SAMW), and Antarctic Intermediate Water (AAIW), respectively. Dark red, orange, and blue shadings represent South Pacific Tropical Water (SPTW), Western Pacific Warm Pool (WPWP), and Eastern Equatorial Pacific (EEP) cold tongue regions, respectively. Blue dashed arrays represent the undercurrent pathways, (Equatorial Under Current, EUC, and orange solid ones represent surface current systems, South Equatorial Current (SEC) and North Equatorial Current (NEC). SAMW/AAIW transport Southern hemisphere (SH) high latitude to the SPTW, and then spread out the South Pacific Ocean through the EUC and EEP wind-driven upwelling [*Pena et al.*, 2013] system and resurfacing process through water masses mixing [*Qu et al.*, 2013] within decades.

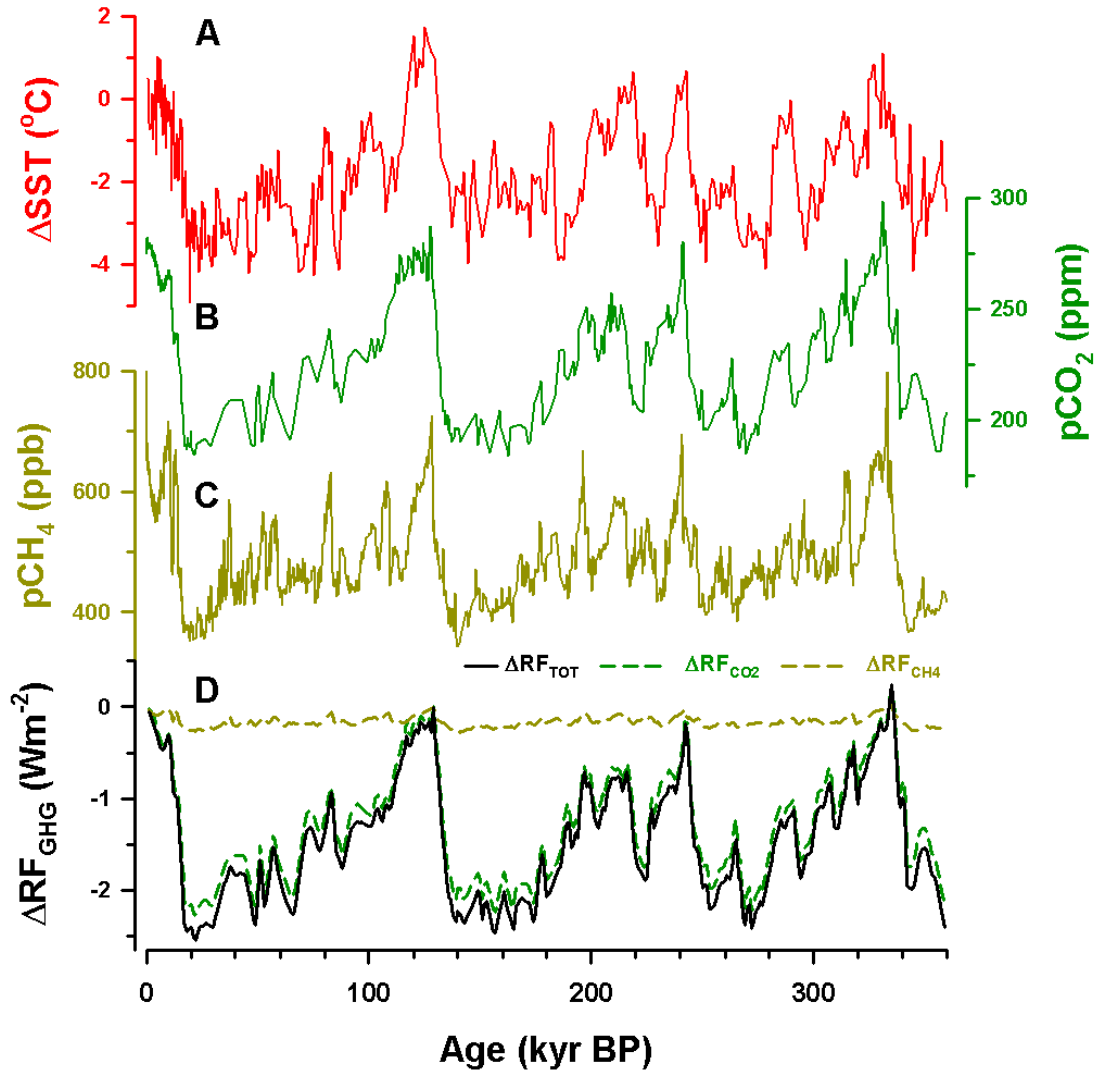

Figure 5-2. Site MD05-2925 planktonic foraminiferal, *Globigerinoides ruber*, geochemical proxies data. (A) Mg/Ca-inferred SST, (B) atmospheric pCO_2 [*Lüthl et al.*, 2008], (C) CH_4 , and (D) calculated ΔRF_{GHG}. The green and yellow dashed lines represent the ΔRF_{GHG} induced by atmospheric CO_2 and CH_4, respectively. Black line is the total ΔRF_{GHG}.

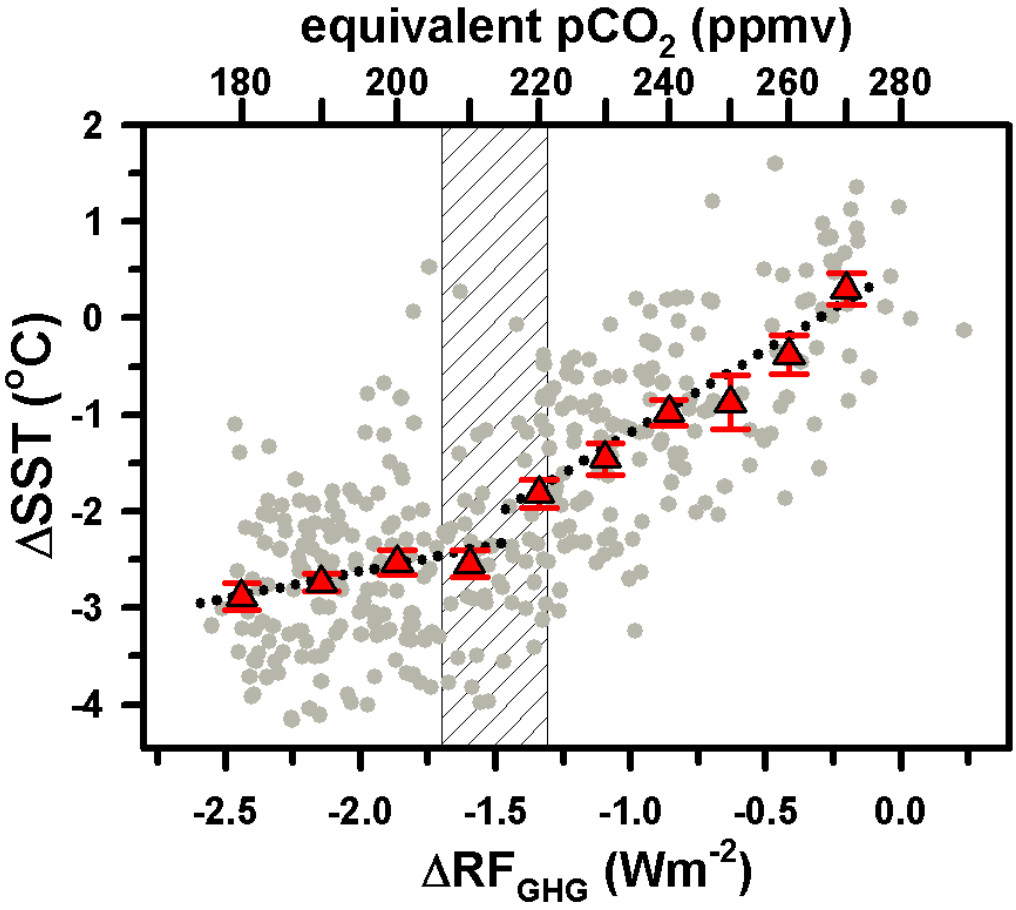

Figure 5-3. Non-linear climate sensitivity. Past Solomon SST changes (ΔSST) to changes in greenhouse gas radiative forcing (ΔRF_{GHG}). Both ΔRF_{GHG} and ΔSST dataset has been interpolated to 1-kyr interval. Standard deviation of mean for every 10 ppmv equivalent pCO_2 has been calculated by non-overlapping binned method (red triangles, *Oppo et al.*, 2009; *Linsley et al.*, 2010). The dark bar represents the significant difference threshold for the non-linear SST changes around 220 ± 10 ppmv.

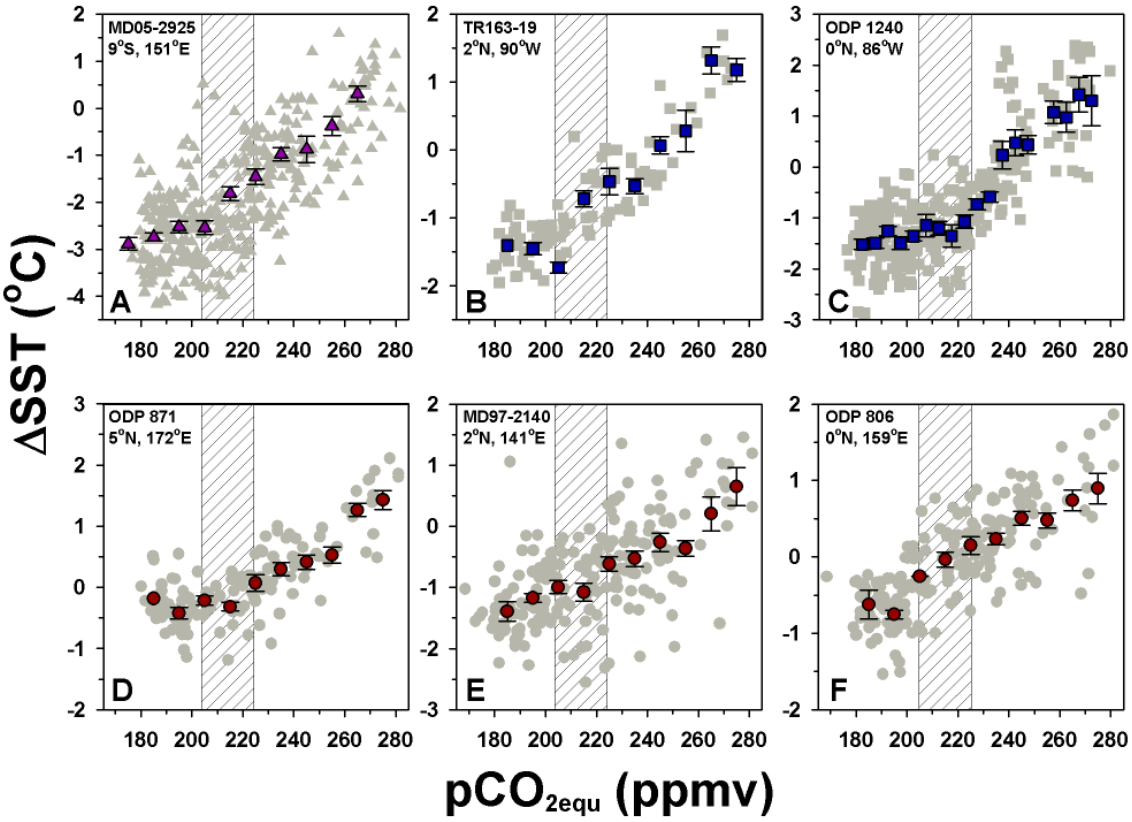

Figure 5-4. Tropical Pacific SST sensitivity. The SST sensitivity of (A) Solomon Sea (MD05-2925, purple triangles, this study), (B, C) eastern equatorial Pacific (TR163-19, and ODP 1240, blue squares, *Lea et al.*, 2000; *Pena et al.*, 2008, respectively), and (D-F) western Pacific (ODP 871, MD97-2140, and ODP 806, dark red circles, *Dyez and Ravelo*, 2012, *de Garidel-Thoron et al.*, 2005; and *Lea et al.*, 2000, respectively). Only the MD05-2925 and ODP 1240 SST were resampled into 1-kyr resolution, the others were resampled into 4-kyr resolution. Gray circles, squares, and triangles represent the raw dataset for each site.

Supplementary Information for Chapter 5

Non-linear response of South-IPWP SST to greenhouse gases forcing changes during the past 360,000 years

This file includes:

Supplementary text

References in supplemental information

Supplementary Table 5-S1

Supplementary Figure 5-S1 to 5-S5

1. Solomon Sea Mg/Ca-inferred sea surface temperature (SST) variations during the past 360 kyrs

Average Solomon Sea *G. ruber* Mg/Ca ratios varies from the glacial ~3.5 to interglacial 4.5-5.0 mmol/mol, respectively. We adapted *Anand et al.* [2003] all species composite equation $Mg/Ca = 0.38 \times e^{(0.09 \times SST)}$. Depth-induced dissolution correction factors from previous studies [*Lea et al.*, 2000; *Dekens et al.*, 2002; *Dyez and Ravelo*, 2012] would cause abnormal SST during the interglacial period (>32^{o}C). Our cleaning method has controlled all the reagents pH values ~9, and detailed possible containment of high-Mg materials from authigenic Mn-Fe oxide or clay minerals (Mn/Ca, Fe/Ca, and Al/Ca ratios, *Lea et al.*, 2005), reagents and containers. Clean, transparent, and delicate preserved *G. ruber* could be observed through the study sediment sequence. We argue that there is no additional dissolution correction is needed on the MD05-2925 Mg/Ca ratios, although further preservation index may be needed for further confirmation to our suggestion.

Solomon Sea SST showed larger glacial/interglacial (G/IG) variations (~4^{o}C) during the past four G/IG cycles. Glacial carbonate preservation is generally better in the Pacific Ocean basin [*Farrell and Prell*, 1989], thus we excluded these variations caused by the degree of preservation. The nature of this region is located in the southern margin of the WPWP region, the seasonal southern margin of WPWP (≥28^{o}C SST) could be shifted latitudinally for ~15^{o} (5^{o} – 20^{o}S). Strong obliquity pacing was observed in Solomon Sea SST through the time series analysis by Arand package software [*Howell*, 2001, Figure 5-S1].

2. MIS 7 problem

For the data compatibility concern, we employed the "Spleo-age" timescales for the ΔT and pCO_2 from the EPICA Dome C records [*Barker et al.*, 2011], and then resampled MD05-2925 SST and EPICA records into 1-kyr time resolution from 1-361 ka.

Barker et al. [2011] used the rate of Antarctica temperature change to identify millennial timescales oscillations, and then further revised Antarctic ice core age model to the East Asian spleothem U-Th absolute age scale. For the EPICA ice core, we adapted both EDC3 [*Parrenin et al.*, 2007] and "Spleo-age" model [*Barker et al.*, 2011] for comparisons. Phase relationships between MD05-2925 SST to ΔT and pCO_2 by EDC3 age model are + (MD05-2925 SST lead) 1.6 ± 0.9 and 3.0 ± 1.2 kyrs on the precession band, and 2.5 ± 1.3 and 4.7 ± 2.5 kyrs on the obliquity band, respectively. For the "Spelo-age" scale there are no significant lead or lag relationship either on the precession or obliquity bands [Table 5-S1].

However, both age models show significant SST leading (~5-kyrs or ~2-kyrs for the EDC3 and Spelo-age scale, respectively, Figure S4) during the MIS 7.4-7.0 (195-212 ka). The rest of the time span, MD05-2925 SST shows well correlation with ΔT (R^2 = 0.63, and R^2 = 0.67, if the MIS 7.4-7.0 period was omitted, Figure 5-S3). Several possibilities could account for this age inconsistent: (1) Age model of LR04 isotope compilation. The LR04 record has been proved to be a good representative to the global ice volume change for the last five million years, and the method of its astronomical tuning process has been proved to be reliable. (2) The need of ice core age model calibration. Further high-resolution measurement and age control by ice flow model should account for 2-3 kyrs inconsistent between these two records.

We assumed the fast response during the other three terminations should be similar. Thus, we prefer to adapt Spleo-age scale for the following discussion. The phase analysis between Solomon SST to ΔT and pCO_2 is not significant under the 1-kyr resampling.

We also calculated the ΔSST with ΔRF_{GHG} relationship under two different age scales, and no significant differences between these two age models. Thus the adaptation of Spleo-age scale only affect the lead-lag relationship, but not the non-linear response of ΔSST to ΔRF_{GHG}.

Further study around MIS 7.4-7.0 is still need to be emphasis because that almost all the MIS 7 is in the "intermediate stage" which defined by *Peacock et al.* [2006]. Dual terminations (Termination 3 and 3A, *Cheng et al.*, 2009) may imply fast glacial inception during the MIS 7.4 and fast melting during the MIS 7.3-7.0. Processes of these boundary condition adjustments during this stage are worthy to further study.

3. ΔSSTs responses during the different time periods

To test ΔSST response during different time periods, we separated the time series into four periods: (1) 0-70, (2) 71-160, (3) 161-270, and (4) 271-360 kyrs, which represent G/IG cycles [Figure 5-S5]. This comparison light up some insight to understand the major difference between this study and previous studies [*Lea*, 2004; *Dyez and Ravelo*, 2012]. The lower the resolution, the less the dataset could capture the rapid transition between G-IG (terminations), and glacial inception. If the climate sensitivity was calculated by the averaged certain periods, the smoothed dataset might

not be able to represent to full picture of sensitivity variations. If the glacial and interglacial periods were averaged and plotted against ΔRF_{GHG}, it is obvious that the two domain data will bias the regression method preference.

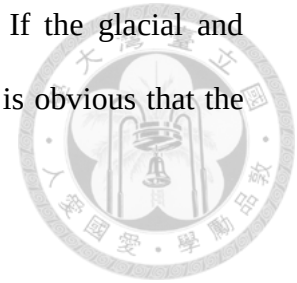

4. Average response tropical WPWP ΔSST to ΔRF_{GHG}

As the Mg/Ca ratio-inferred SSTs could represent more annual mean SST in the tropical Pacific, we summarized the updated *G. ruber* Mg/Ca ratio records which at least included three G/IG cycles, and then calculated their ΔSST to ΔRF_{GHG} relationships to check the robustness of our interpretation. ODP 806 (0.3°N, 159.4°E, water depth 2520 m, *Lea et al.*, 2000), MD97-2140 (2.0°N, 141.7°E, water depth 2547 m, *de Garidel-Thoron et al.*, 2005), ODP 871 (5.6°N, 172.3°E, water depth 1255 m, *Dyez and Ravelo*, 2012), TR163-19 (2.3°N, 91°W, water depth 2348 m, *Lea et al.*, 2000), and ODP 1240 (0.0°N, 86.5°E, water depth 2921 m, *Pena et al.*, 2008) have been collected. It is worth notice that all of theses cores are from the north of the equator, although TR163-19 and ODP 1240 have been identified to be influenced by the east equatorial Pacific cold tongue, which may be influenced by the Southern Hemisphere remote forcing. ODP 806 and TR163-19 Mg/Ca have been newly calibrated by the dissolution correction equation proposed by *Dyez and Ravelo* [2012]. We compared these two methods and found no significant differences of out interpretation (Figure 4). Due to the effect of time resolution, we resampled ODP 806, ODP 871, TR163-19, and MD97-2140 into 4-kyr, and ODP 1240 into 1-kyr time resolution and then compared to the same time resampled Antarctica ΔT and pCO_2 records to calculated ΔRF_{GHG}. We first replicate the methods that previously *Lea* [2004] and *Dyez and Revelo* [2012] have been done. The sensitivities were calculated under the EDC3 Antarctic ice core age model [*Parrenin et al.*, 2007]. The average

sensitivities were similar with previous they reported (1.0-1.2 $^{o}C/Wm^{-2}$). Here in this study we re-calculated all the dataset by the "Spleo-age" of Antarctic ice core age model [*Barker et al.*, 2011]. The sensitivities from ODP 806, 871, and TR163-19 were slightly lower to ~0.8 $^{o}C/Wm^{-2}$ from the total linear regression results. Our major aims in this study are to focus on the comparison of the pattern of sensitivities changes and the identification of major threshold.

For the further support of non-linearity SST changes of S-WPWP, *Tachikawa et al.* [2014] also report close relationship between the Bismack Sea surface temperatures from Site MD05-2920 (2.9^{o}S, 144.5^{o}E, water depth 1843 m) and Antarctic ΔT during the past 400,000 years. The Antarctic ΔT is nonlinearly correlated with ΔRF_{GHG}.

References in supplemental information

Anand, P., Elderfield, H., and Conte, M. H., (2003), Calibration of Mg/Ca thermometry in planktonic foraminifera from a sediment trap time series. *Paleoceanography* **18**, PA1050. doi:10.1029/2002PA000846

Barker S., Knorr, G., Edwards, R. L., Parrenin, F., Putnam, A. E., Skinner, L. C., Wolff, E., and Ziegler, M., (2011), 800,000 Years of Abrupt Climate Variability. *Science* **334**, 347-351. doi: 10.1126/science.1203580

Cheng, H., Edwards, R. L., Broecker, W. S., Denton, G. H., Kong, X., Wang, Y., Zhang, R., and Wang X., (2009), Ice Age Terminations. *Science* **326,** 248-252.

de Garidel-Thoron, T., Rosenthal, Y., Bassinot, F., and Beaufort, L., (2005), Stable sea surface temperatures in the western Pacific warm pool over the past 1.75 million years. *Nature* **433**, 294-298. doi: 10.1038/nature03189

Dekens, P. S., Lea, D. W., Pak, D. K., and Spero, H. J., (2002), Core top calibration of Mg/Ca in tropical foraminifera: Refining paleotemperature estimation. *Geochemistry, Geophysics, Geosystems* **3**, GC0002000. doi: 10.1029/2001GC000200

Dyez, K. A., and Ravelo, A. C., (2012), Late Pleistocene tropical Pacific temperature sensitivity to radiative greenhouse gas forcing. *Geology* **41**, 23-26. doi: 10.1130/G33425.1

Farrell, J.W., and Prell, W. L., (1989), Climatic change and calcium carbonate preservation: An 800,000-year bathymetric reconstruction from the central equatorial Pacific. *Paleoceanography* **4**, 447-466. doi:10.1029/PA004i004900447

Howell, P., (2001), ARAND time series and spectral analysis package for the Macintosh, Brown University. IGBP PAGES/World Data Center for Paleoclimatology Data Contribution Series #2001-031. NOAA/NGDC Paleoclimatology Program, Boulder, Colorado, USA..

Jouzel, J., Masson-Delmotte, V., Cattani, O., Dreyfus, G., Falourd, S., Hoffmann, G., Minster, B., Nouet, J., Barnola, J. M., Cahppellaz, J., Fischer, H., Gallet, J. C., Johnson, S., Leuenberger, M., Loulergue, L., Luethi, D., Oerter, H., Parrenin, F., Raisbeck, G., Raynaud, D., Schilt, A., Schwander, J., Selmo, E., Souchez, R., Spahni, R., Stauffer, B., Steffensen, J. P., Stenni, B., Stocjer, T. F., Tison, J. L., Werner, M., and Wolff, E. W., (2007), Orbital and millennial Antarctic climate variability over the past 800,000 years. *Science* **317**, 793-796.

Laskar, J., Robutel, P., Joutel, F., Gastineau, M., Correia, A. C. M., and Levrard, B., (2004), A long term numerical solution for the insolation quantities of the Earth. *Astronomy and Astrophysics.* **428**, 261-285. doi: 10. 1051/0004-6361:20041335

Lea, D. W., Pak, D. K., and Spero, H. J., (2000), Climate impact of late Quaternary equatorial Pacific sea surface temperature variations. *Science* **289**, 1719 – 1724.

Lea, D. W., (2004), The 100,000-yr cycle in tropical SST, greenhouse forcing, and climate sensitivity. *Journal of Climate* **17**, 2170-2179.

Lea, D. W., Pak, D. K., and Paradis, G., (2005), Influence of volcanic shards on foraminiferal Mg/Ca in a core from the Galápagos region. *Geochemistry, Geophysics, Geosystems* **6**, Q11P04. doi:10.1029/2005GC000970

Linsley, B. K., Rosenthal, Y., and Oppo, D. W., (2010), Holocene evolution of the

Indonesian throughflow and the western Pacific warm Pool. *Nature Geoscience* **3**, 578 – 583.

Lisiecki, L. E., and Raymo, M. E. A Pliocene-Pleistocene stack of 57 globally distributed benthic $\delta^{18}O$ records. *Paleoceanography* **20**, PA1003 (2005). doi:10.1029/2004PA001071

Lüthi, D., Le Floch, M., Bernhard, B., Blunier, T., Barnola, J.-M., Siegenthaler, U., Raynaud, D., Jouzel, J., Fischer, H., Kawamura, K., and Stocker, T. F., (2008), High-resolution carbon dioxide concentration record 650,000-800,000 years before present. *Nature* **453**, 379-382.

Oppo, D. W., Rosenthal, Y., and Linsley, B. K., (2009), 2,000-year-long temperature and hydrology reconstructions from the Indo-Pacific warm pool. *Nature* **460**, 1113 – 1116.

Parrenin, F., Barnola, J.-M., Beer, J., Blunier, T., Castellano, E., Chappellaz, J., Drefus, G., Fischer, H., Fujita, S., Jouzel, J., Kawamura, K., Lemieux-Dudon, B., Loulergue, L., Masson-Delmotte, V., Narcisi, B., Petit, J.-R., Raisbeck, G., Raynaud, D., Duth, U., Schwander, J., Severi, M., Spahni, R., Steffensen, J. P., Svensson, A., Udisti, R., Waelbroeck, C., and Wolff, E., (2007), The EDC3 chronology for the EPICA Dome C ice core. *Climate of the Past* **3**, 485-497.

Peacock, S., Lane, E., Restrepo, J. M., (2006), A possible sequence of events from the generalized glacial-interglacial cycle. *Global Biogeochemical Cycles* **20**, GB2010.

Pena, L. D., Cacho, I., Ferretti, P., and Hall, M. A., (2008), El Niño–Southern Oscillation–like variability during glacial terminations and interlatitudinal teleconnections. *Paleoceanography* **25**, PA3101. doi:10.1029/2008PA001620

Tachikawa, K., Timmermann, A., Vidal, L., Sonzogni, C., Timm, O. E., (2014), CO_2 radiative forcing and Intertropical Convergence Zone influences on western Pacific warm pool climate over the past 400 ka. *Quaternary Science Reviews* **86**, 24-34.

Table 5-S1. Phase relationships among astronomical parameters, ice volume, SST, ΔT, and pCO_2.

	MD05-2925 SST			
	Precession		**Obliquity**	
Astronomical parameters[a]	-2.2 ± 0.7*		-3.3 ± 1.1*	
Ice volume (LR04)[b]	2.8 ± 1.1		4.2 ± 1.4	
	Spleo-age[c]	**EDC3[d]**	**Spleo-age**	**EDC3**
ΔT[e]	1.3 ± 1.8	1.6 ± 0.9	1.3 ± 1.5	2.5 ± 1.3
pCO_2[f]	3.5 ± 1.8	3.0 ± 1.2	3.7 ± 2.6	4.7 ± 2.5

*. Negative values represent MD05-2925 SST lag, and positive ones represent MD05-2925 lead. The unit is thousand years (kyrs).

[a]. *Laskar et al.*, [2004]

[b]. *Lisiecki and Raymo*, [2005]

[c]. *Barker et al.*, [2011]

[d]. *Parrenin et al.*, [2007]

[e]. *Jouzel et al.*, [2007]

[f]. *Lüthl et al.*, [2008]

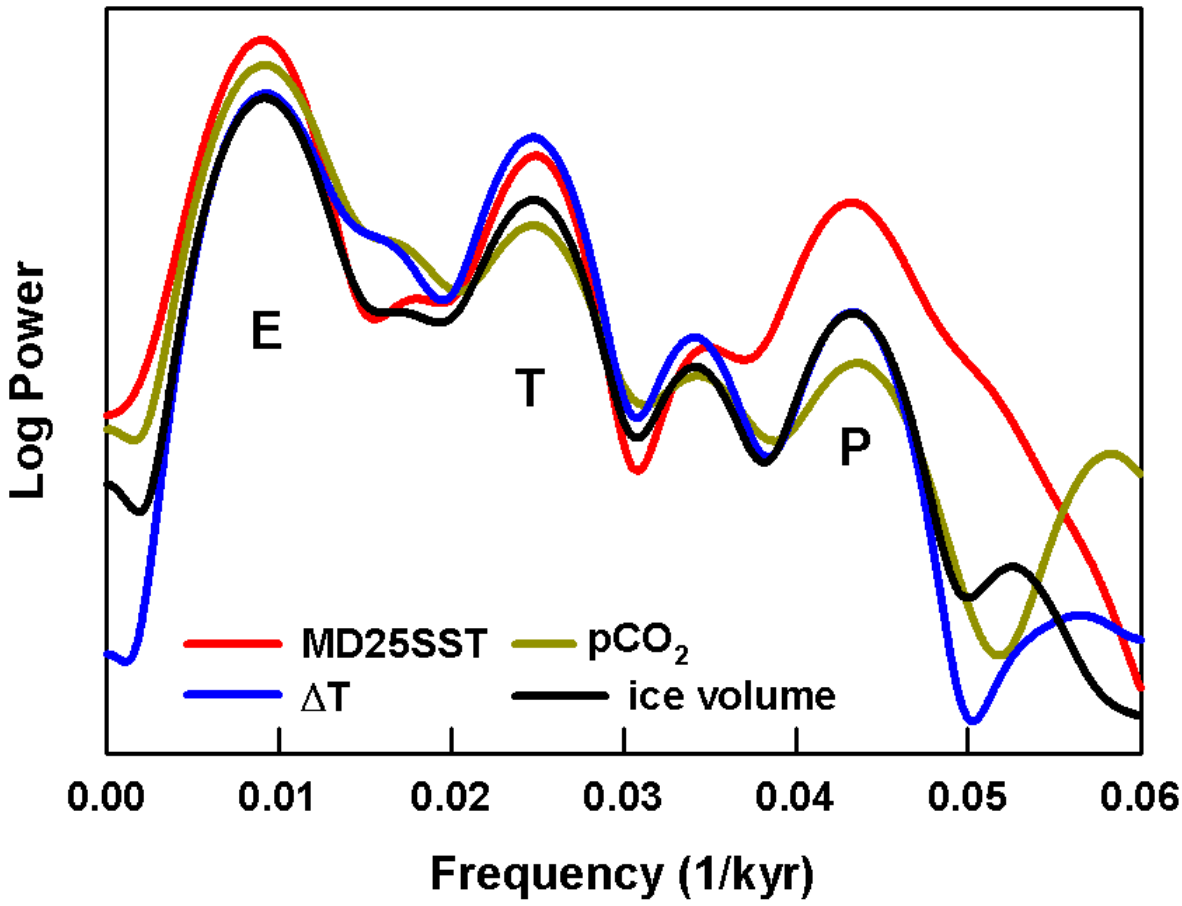

Figure 5-S1. The spectral analyses results of MD05-2925 (red), LR04 composite represent global ice volume (black), Antarctic temperature (blue, *Jouzel et al.*, 2007), and atmosphere CO_2 (yellow, *Lüthl et al.*, 2008) during the past 360 ka. Each of the records were resampled into 1-kyr resolution and analyzed by Arand software [*Howell*, 2001].

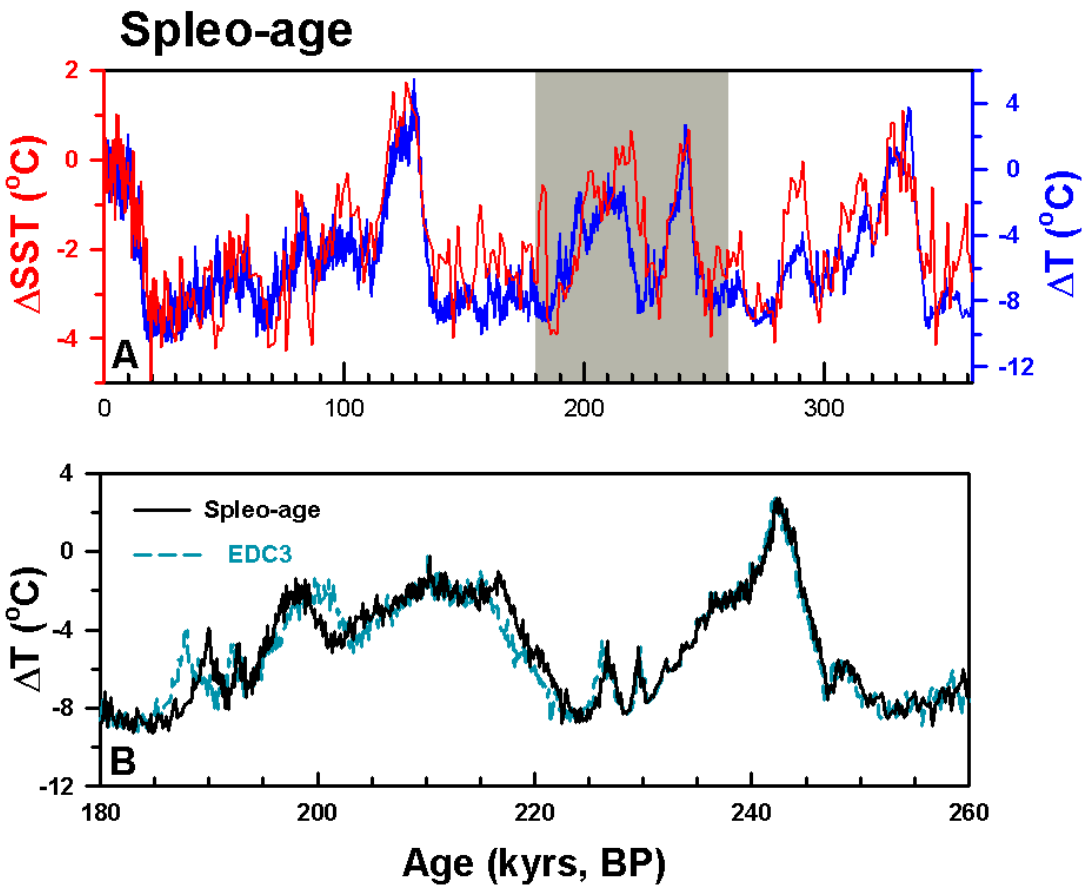

Figure 5-S2. Correlation of Solomon SST and Antarctic ΔT. (A) MD05-2925 SST changes (ΔSST, red, this study) versus Antarctic temperature changes in Spleo-age scale (ΔT, blue, *Jouzel et al.*, 2007; black, *Barker et al.*, 2011). The gray bar area is represent MIS 7 period in (B). The comparison between Spleo-age scale [*Barker et al.*, 2011] and EDC3 age [*Parrenin et al.*, 2007].

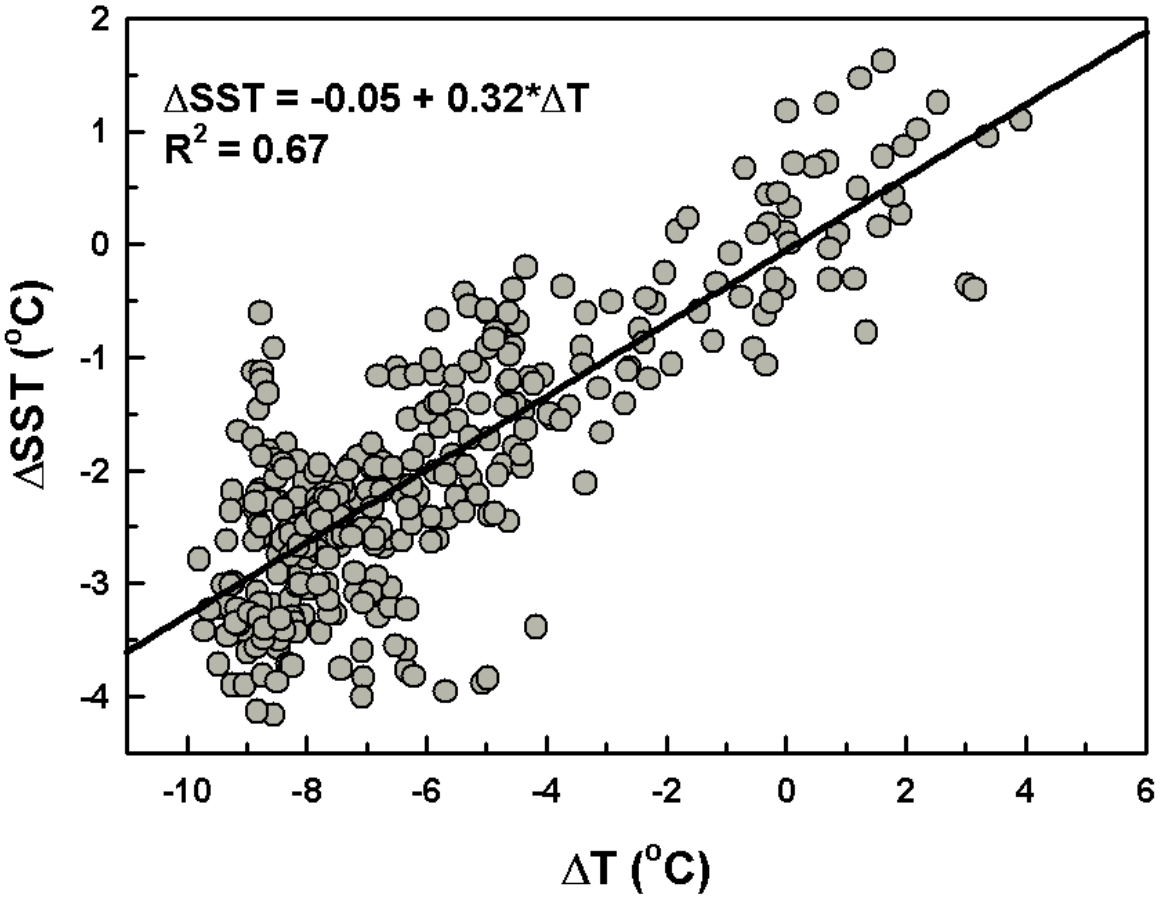

Figure 5-S3. Correlation coefficient between Solomon SST and Antarctic ΔT. The ΔSST and ΔT were resampled into 1-kyr resolution, and the problematic period during the MIS 7 (195-212 ka) was omitted.

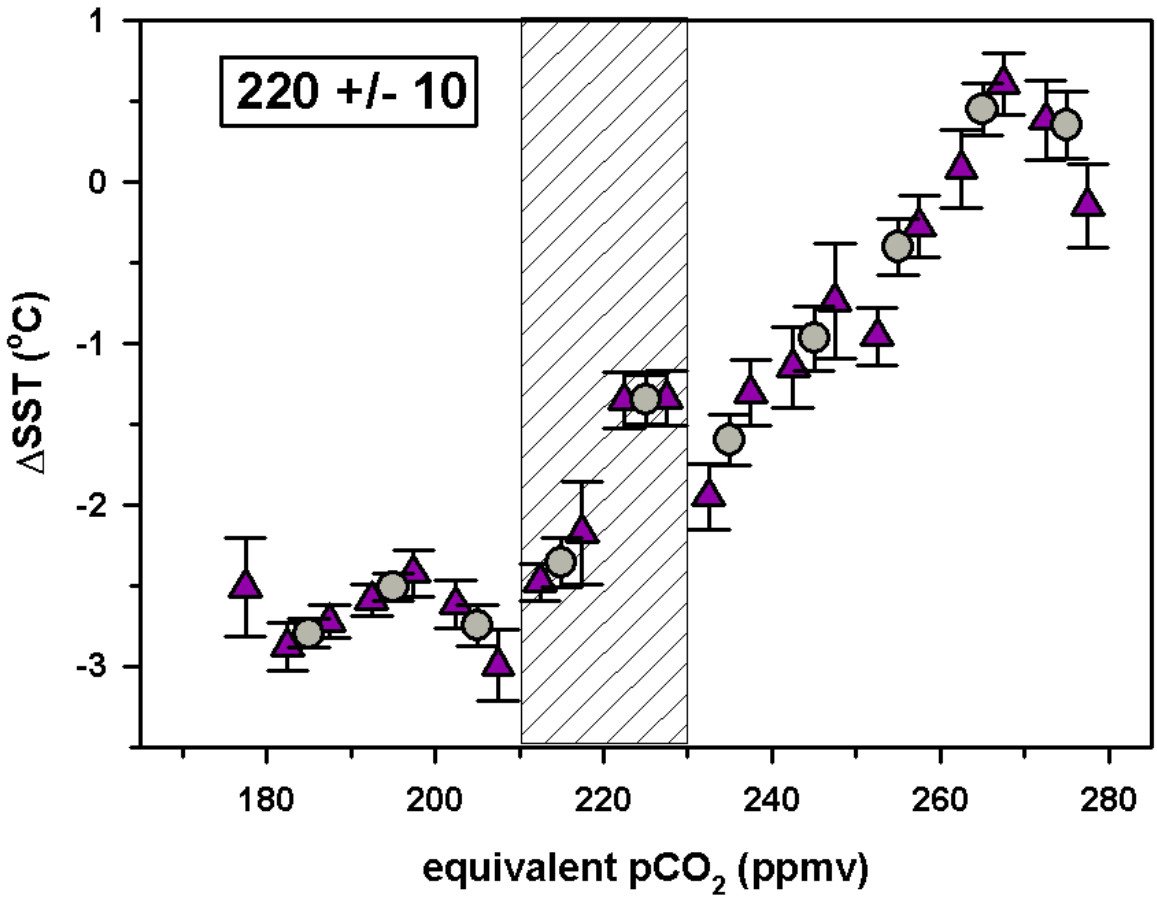

Figure 5-S4. Solomon SST sensitivity and thresholds identification. The non-overlapping binned method [*Oppo et al.*, 2009; *Linsley et al.*, 2010] was applied to calculate ΔSST changes and standard deviation of mean by the 5 (purple triangles) and 10 (gray circles) ppmv equivalent CO_2 (CO_{2equ}) step. The threshold was identified by the significant differences between the standard deviation of means.

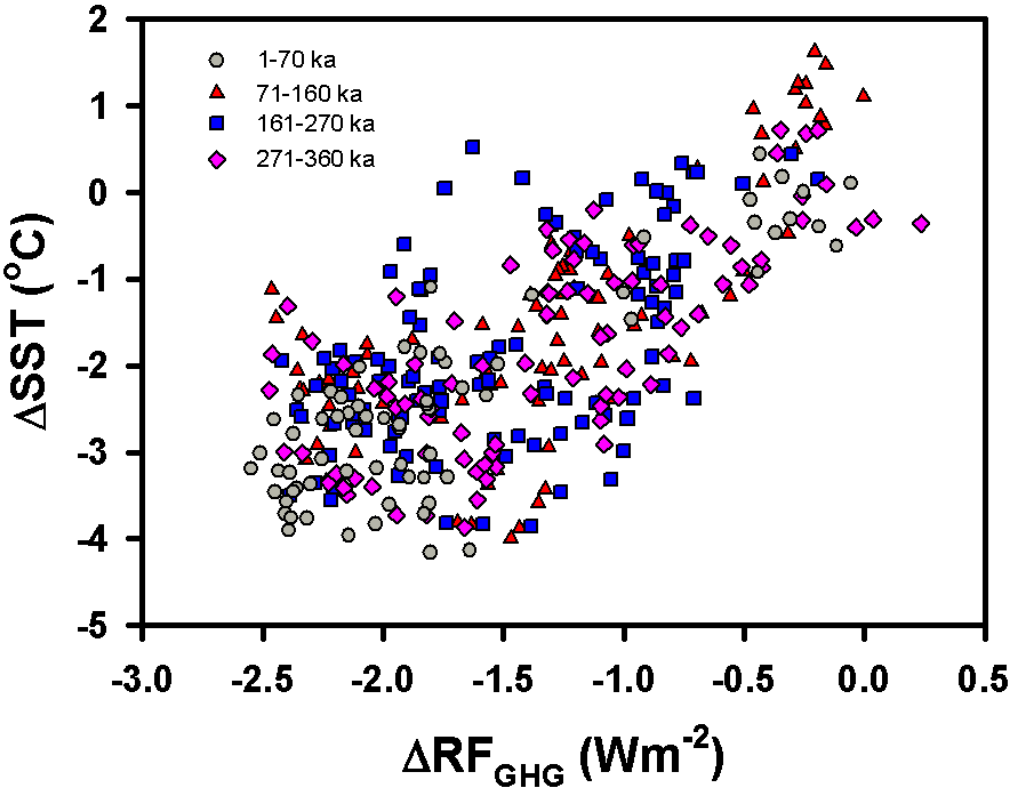

Figure S5. Solomon SST sensitivity variations during the past 360 kyrs. 0-70 (gray circles), 71-160 (red triangles), 161-270 (blue squares), and 271-360 (pink diamonds) ka Solomon SST sensitivity changes.

Data Tables

Table A. *Globigerinoides ruber* oxygen and carbon isotope, (‰, VPDB)

Age kyr BP	Depth (cm)	$\delta^{18}O$	$\delta^{13}C$	Age kyr BP	Depth (cm)	$\delta^{18}O$	$\delta^{13}C$
0.89	0	-2.23	0.61	8.44	102	-2.58	0.16
1.02	2	-2.83	1.20	8.64	105	-2.38	0.60
1.22	5	-2.79	1.29	8.70	106	-2.07	0.83
1.47	7	-2.94	0.90	8.96	110	-2.43	0.63
1.85	10	-2.80	0.97	9.02	111	-2.33	0.93
2.10	12	-2.80	1.17	9.28	115	-2.63	0.72
2.47	15	-2.38	0.94	9.35	116	-1.87	0.82
2.72	17	-2.44	1.01	9.97	120	-2.26	0.76
3.10	20	-2.52	0.91	10.15	121	-1.71	0.91
3.35	22	-2.57	1.59	10.89	125	-2.48	0.60
3.50	25	-2.57	1.16	11.07	126	-2.25	0.69
3.60	27	-2.40	1.17	11.26	127	-2.26	0.63
3.76	30	-2.66	1.31	11.50	130	-2.14	0.59
3.86	32	-2.68	1.14	11.58	131	-2.20	0.50
4.01	35	-2.50	0.77	11.66	132	-2.38	0.30
4.18	37	-2.66	1.07	11.90	135	-1.93	0.71
4.42	40	-2.53	1.02	11.98	136	-1.78	0.87
4.58	42	-2.63	1.24	12.06	137	-1.94	0.75
4.83	45	-2.53	0.73	12.30	140	-1.79	1.05
4.99	47	-2.21	1.03	12.38	141	-1.71	0.52
5.23	50	-2.79	1.13	12.46	142	-2.04	0.77
5.40	52	-2.40	1.26	12.69	145	-1.84	0.63
5.64	55	-2.29	0.86	12.77	146	-1.66	1.05
5.81	57	-2.08	0.78	12.85	147	-2.08	0.82
6.05	60	-2.57	0.86	13.02	150	-1.60	0.77
6.21	62	-2.21	1.42	13.07	151	-1.82	0.89
6.46	65	-2.58	1.00	13.12	152	-2.03	0.05
6.62	67	-2.19	0.63	13.28	155	-1.83	0.14
6.86	70	-2.62	0.85	13.34	156	-1.97	0.67
7.03	72	-2.45	0.84	13.39	157	-1.96	0.32
7.21	75	-2.48	0.85	13.71	160	-1.85	1.00
7.34	77	-2.46	0.44	13.81	161	-1.58	0.99
7.53	80	-2.33	1.34	14.24	165	-1.74	0.39
7.65	82	-1.95	0.41	14.34	166	-1.54	0.98
7.84	85	-2.86	0.82	14.45	167	-1.66	0.52
7.96	87	-2.27	0.98	14.76	170	-1.60	0.43
8.15	90	-2.39	1.05	14.87	171	-1.32	0.81
8.20	92	-2.72	0.62	14.97	172	-1.47	0.62
8.27	95	-2.72	0.94	15.46	175	-1.36	0.47
8.32	97	-2.94	0.08	15.63	176	-1.20	0.86
8.39	100	-2.52	0.72	15.79	177	-1.50	0.66
8.42	101	-2.31	0.88	16.28	180	-1.31	0.78

Age kyr BP	Depth (cm)	$\delta^{18}O$	$\delta^{13}C$	Age kyr BP	Depth (cm)	$\delta^{18}O$	$\delta^{13}C$
16.32	181	-1.42	0.41	21.48	252	-1.47	0.70
16.36	182	-1.38	0.77	21.69	255	-0.97	0.93
16.48	185	-1.38	0.75	21.76	256	-1.76	1.11
16.51	186	-1.22	0.60	21.82	257	-1.06	0.38
16.55	187	-1.11	0.63	22.03	260	-1.12	0.49
16.67	190	-1.24	0.46	22.10	261	-0.74	1.21
16.71	191	-1.07	0.55	22.17	262	-0.89	0.86
16.75	192	-1.24	0.65	22.84	265	-0.86	1.09
17.04	195	-1.23	0.71	23.06	266	-0.95	1.18
17.13	196	-0.84	0.92	23.29	267	-0.93	0.84
17.23	197	-0.91	0.97	23.96	270	-0.96	1.23
17.52	200	-1.28	0.50	24.19	271	-1.38	0.64
17.62	201	-0.73	0.89	24.41	272	-1.18	0.58
17.72	202	-1.13	0.88	24.54	275	-1.04	0.49
18.01	205	-1.08	0.77	24.59	276	-0.85	0.81
18.10	206	-1.15	0.51	24.63	277	-1.35	1.00
18.20	207	-0.99	0.52	24.77	280	-0.96	1.01
18.47	210	-1.02	1.04	24.81	281	-1.01	1.15
18.55	211	-1.30	0.69	24.86	282	-1.30	1.04
18.64	212	-1.28	0.94	24.99	285	-1.07	0.81
18.91	215	-0.81	0.69	25.04	286	-1.30	0.34
18.99	216	-0.70	0.64	25.08	287	-0.91	1.32
19.08	217	-0.78	0.42	25.21	290	-1.26	0.76
19.29	220	-1.10	0.92	25.30	292	-0.98	0.72
19.36	221	-0.70	0.68	25.73	295	-1.16	1.06
19.43	222	-0.82	0.80	26.02	297	-1.20	0.82
19.63	225	-0.95	0.94	26.45	300	-1.25	0.50
19.70	226	-0.92	0.82	26.74	302	-1.24	0.51
19.77	227	-0.83	0.90	27.45	307	-1.14	0.56
19.97	230	-0.92	0.94	27.88	310	-1.35	0.84
20.04	231	-0.65	0.58	28.17	312	-1.20	1.10
20.11	232	-1.31	0.66	28.89	317	-1.16	0.97
20.32	235	-0.86	0.59	29.32	320	-1.25	0.86
20.39	236	-0.90	0.77	29.60	322	-1.22	0.81
20.45	237	-0.83	1.02	30.32	327	-1.27	0.83
20.66	240	-1.08	0.54	30.75	330	-1.28	0.58
20.73	241	-0.96	0.57	31.04	332	-1.30	0.84
20.80	242	-1.16	1.14	31.75	337	-1.15	0.86
21.00	245	-0.98	0.68	32.18	340	-1.20	0.84
21.07	246	-1.47	0.51	32.47	342	-1.30	1.06
21.14	247	-1.09	0.88	33.19	347	-1.38	0.72
21.34	250	-1.02	0.75	33.62	350	-1.27	0.70
21.41	251	-0.91	0.31	33.90	352	-1.48	0.95

Age kyr BP	Depth (cm)	$\delta^{18}O$	$\delta^{13}C$	Age kyr BP	Depth (cm)	$\delta^{18}O$	$\delta^{13}C$
34.62	357	-1.30	1.12	56.12	507	-1.54	0.71
35.05	360	-1.42	1.14	56.55	510	-1.60	0.50
35.34	362	-1.40	0.90	56.83	512	-1.63	0.49
36.05	367	-1.33	0.84	57.55	517	-1.33	0.29
36.48	370	-1.47	0.48	57.98	520	-1.31	0.47
36.77	372	-1.26	0.66	58.27	522	-1.17	0.53
37.49	377	-1.28	1.17	58.98	527	-1.52	1.19
37.92	380	-1.29	0.74	59.41	530	-1.13	0.95
38.20	382	-1.36	0.78	59.70	532	-1.37	0.64
38.92	387	-1.17	0.89	60.42	537	-1.20	1.22
39.35	390	-1.26	1.01	60.85	540	-1.04	0.84
39.64	392	-1.36	0.79	61.13	542	-1.10	0.99
40.35	397	-1.35	0.89	61.85	547	-1.55	0.54
40.78	400	-1.35	0.54	62.28	550	-1.15	0.89
41.07	402	-1.39	0.98	62.57	552	-1.26	1.06
41.79	407	-1.56	0.96	63.71	560	-1.39	0.96
42.22	410	-1.36	1.17	64.00	562	-1.34	0.87
42.50	412	-1.48	0.95	66.75	567	-1.66	1.07
43.22	417	-1.30	0.99	68.40	570	-1.59	0.89
43.65	420	-1.53	0.96	69.50	572	-1.66	0.85
43.94	422	-1.57	1.12	72.25	577	-1.92	0.87
44.65	427	-1.55	0.66	73.90	580	-1.85	0.84
45.08	430	-1.51	0.73	75.00	582	-1.99	1.00
45.37	432	-1.50	0.97	75.98	587	-1.89	1.39
46.09	437	-1.23	0.79	76.95	592	-2.11	1.04
46.52	440	-1.34	1.01	77.93	597	-1.99	1.31
46.80	442	-1.28	0.98	78.51	600	-1.85	1.26
47.52	447	-1.38	1.03	78.91	602	-1.98	1.05
48.23	452	-1.37	1.22	79.88	607	-2.11	1.00
48.95	457	-1.51	0.91	80.47	610	-1.92	0.98
49.67	462	-1.57	0.97	80.86	612	-1.76	1.44
50.38	467	-1.48	0.94	81.83	617	-2.07	0.95
50.81	470	-1.69	0.72	82.42	620	-2.04	1.12
51.10	472	-1.67	0.60	82.81	622	-2.07	0.92
51.82	477	-1.48	0.58	83.79	627	-2.08	1.10
52.25	480	-1.63	0.59	84.37	630	-2.14	0.82
52.53	482	-1.57	0.82	84.76	632	-2.03	1.07
53.25	487	-1.60	0.78	85.74	637	-2.02	1.08
53.68	490	-1.71	0.79	86.33	640	-2.13	0.88
53.97	492	-1.58	0.95	86.72	642	-2.15	1.24
54.68	497	-1.63	0.94	87.69	647	-1.98	0.94
55.11	500	-1.54	0.43	88.28	650	-1.78	0.96
55.40	502	-1.58	0.54	88.67	652	-1.64	1.05

Age kyr BP	Depth (cm)	$\delta^{18}O$	$\delta^{13}C$	Age kyr BP	Depth (cm)	$\delta^{18}O$	$\delta^{13}C$
89.64	657	-1.77	1.36	120.05	800	-2.37	0.89
90.23	660	-1.86	0.96	120.54	802	-2.39	0.65
90.62	662	-1.72	1.22	121.77	807	-2.47	0.80
91.60	667	-1.75	0.85	122.51	810	-2.65	0.87
92.18	670	-1.96	0.94	123.00	812	-2.80	0.79
92.57	672	-1.79	0.92	124.06	817	-2.63	0.21
93.55	677	-1.81	1.23	124.69	820	-2.65	0.78
94.14	680	-2.15	1.13	125.11	822	-2.52	0.69
94.53	682	-1.90	0.80	126.17	827	-2.46	0.82
95.50	687	-2.06	0.78	126.80	830	-2.55	0.61
96.09	690	-1.94	0.92	127.22	832	-2.55	0.53
96.48	692	-1.93	1.29	128.28	837	-2.31	0.50
97.46	697	-1.97	0.90	128.91	840	-2.43	0.52
98.04	700	-1.92	0.86	129.33	842	-2.19	0.61
98.43	702	-1.91	1.00	130.39	847	-2.33	0.45
99.41	707	-2.16	1.12	131.02	850	-2.44	0.55
99.99	710	-2.17	0.59	131.44	852	-1.92	0.58
100.38	712	-2.09	0.63	132.50	857	-1.46	0.25
101.36	717	-1.99	1.03	133.13	860	-1.35	0.47
101.95	720	-2.16	0.63	133.56	862	-1.41	0.26
102.34	722	-2.11	1.00	134.61	867	-0.99	0.39
103.31	727	-2.11	0.78	135.24	870	-1.08	0.83
103.90	730	-2.07	0.73	135.67	872	-0.90	0.19
104.29	732	-2.05	0.84	136.72	877	-1.14	0.23
105.27	737	-2.18	0.67	137.78	882	-1.20	0.04
105.85	740	-2.14	0.60	138.83	887	-1.36	0.20
106.24	742	-2.19	0.92	139.47	890	-0.81	0.31
107.22	747	-1.96	0.70	139.89	892	-0.94	0.23
107.80	750	-2.21	0.85	140.94	897	-1.11	0.29
108.25	752	-2.05	0.96	142.00	902	-0.99	0.54
109.48	757	-2.24	0.48	143.39	907	-0.86	0.80
110.21	760	-2.08	0.88	144.22	910	-1.58	0.04
110.70	762	-2.06	0.80	144.78	912	-1.38	0.70
111.93	767	-1.91	0.78	146.17	917	-1.44	0.45
112.67	770	-2.00	0.76	149.78	930	-0.99	0.53
113.16	772	-1.85	0.95	150.33	932	-1.13	0.33
114.39	777	-1.95	0.86	151.72	937	-1.05	0.94
115.13	780	-1.95	0.86	154.50	947	-1.16	0.34
115.62	782	-2.10	0.75	155.89	952	-1.08	0.33
116.85	787	-2.11	0.40	157.28	957	-1.15	0.65
117.59	790	-2.32	0.66	158.11	960	-1.03	0.74
118.08	792	-2.31	0.84	158.67	962	-1.00	0.30
119.31	797	-2.22	0.52	160.06	967	-1.04	0.58

Age kyr BP	Depth (cm)	$\delta^{18}O$	$\delta^{13}C$	Age kyr BP	Depth (cm)	$\delta^{18}O$	$\delta^{13}C$
161.44	972	-0.90	0.62	208.50	1182	-2.01	1.11
162.83	977	-0.99	0.76	209.88	1187	-2.03	0.65
164.22	982	-1.16	0.45	211.25	1192	-2.18	0.77
165.61	987	-1.25	0.46	212.63	1197	-2.05	0.62
166.44	990	-1.27	0.12	214.00	1202	-2.01	0.98
167.00	992	-1.35	0.71	215.38	1207	-2.02	0.61
167.96	997	-1.05	0.35	216.75	1212	-1.91	0.60
168.92	1002	-1.02	0.38	218.13	1217	-1.72	0.19
169.88	1007	-1.32	0.34	219.50	1222	-1.61	0.55
170.85	1012	-1.11	0.83	220.88	1227	-1.69	0.39
171.81	1017	-1.55	0.31	222.25	1232	-1.46	0.40
172.77	1022	-1.32	0.45	223.63	1237	-1.36	0.49
173.73	1027	-1.78	0.91	225.00	1242	-1.57	0.48
174.69	1032	-1.40	0.54	226.05	1247	-1.31	0.65
175.65	1037	-1.84	0.53	227.10	1252	-1.58	0.30
176.62	1042	-1.46	1.01	228.15	1257	-1.61	0.34
177.58	1047	-1.66	0.50	229.20	1262	-1.40	0.71
178.54	1052	-1.46	0.43	230.25	1267	-1.48	0.88
179.50	1057	-1.71	0.09	231.30	1272	-2.01	0.93
180.46	1062	-1.38	0.68	232.35	1277	-1.94	0.92
181.42	1067	-1.54	0.48	233.40	1282	-1.99	0.84
182.38	1072	-1.60	0.53	234.45	1287	-2.05	0.70
183.35	1077	-1.32	0.56	235.50	1292	-2.02	0.41
184.31	1082	-1.23	0.24	236.55	1297	-2.15	0.98
185.27	1087	-1.32	0.21	237.60	1302	-2.20	0.59
186.23	1092	-1.17	0.27	238.65	1307	-2.33	0.59
187.19	1097	-1.46	0.49	239.70	1312	-2.25	0.74
188.15	1102	-1.72	0.55	240.75	1317	-1.75	0.40
189.12	1107	-1.60	1.11	241.80	1322	-1.56	0.22
190.08	1112	-1.74	0.77	242.85	1327	-1.53	0.37
191.04	1117	-1.84	1.10	243.90	1332	-1.36	0.46
192.00	1122	-1.77	0.87	244.95	1337	-1.40	0.04
193.38	1127	-1.70	0.79	246.00	1342	-1.31	0.19
194.75	1132	-1.92	0.98	246.81	1347	-1.24	0.48
196.13	1137	-2.05	1.10	247.62	1352	-1.33	0.01
197.50	1142	-1.92	1.29	249.24	1362	-1.05	0.43
198.88	1147	-2.28	1.19	250.06	1367	-1.37	-0.04
200.25	1152	-2.13	0.86	250.87	1372	-1.21	0.28
201.63	1157	-2.06	0.71	251.68	1377	-0.99	0.22
203.00	1162	-1.78	0.48	252.49	1382	-1.21	0.71
204.38	1167	-1.74	0.35	253.30	1387	-1.16	0.21
205.75	1172	-1.88	0.81	254.11	1392	-1.19	0.51
207.13	1177	-1.95	0.76	254.92	1397	-1.30	0.13

Age kyr BP	Depth (cm)	$\delta^{18}O$	$\delta^{13}C$	Age kyr BP	Depth (cm)	$\delta^{18}O$	$\delta^{13}C$
255.73	1402	-1.43	0.04	301.35	1615	-2.06	0.66
256.54	1407	-1.44	0.06	302.51	1620	-1.76	0.86
257.36	1412	-1.40	-0.14	303.68	1625	-1.90	1.08
258.17	1417	-1.30	0.53	304.85	1630	-1.95	1.00
258.98	1422	-1.54	0.10	306.02	1635	-1.86	1.23
259.79	1427	-1.33	0.39	307.19	1640	-2.03	0.66
260.60	1432	-1.42	-0.16	308.36	1645	-1.77	1.05
262.30	1437	-1.56	0.31	309.99	1652	-2.21	0.59
264.00	1442	-1.19	0.42	311.16	1657	-2.03	0.71
265.70	1447	-1.31	0.06	312.33	1662	-2.29	0.71
267.40	1452	-1.25	0.82	313.50	1667	-2.20	0.65
269.10	1457	-1.09	0.43	314.66	1672	-2.04	0.77
270.80	1462	-1.16	0.74	315.83	1677	-2.11	0.57
272.50	1467	-1.21	0.69	317.00	1682	-1.70	0.86
274.20	1472	-1.47	0.60	318.08	1687	-1.85	0.42
275.90	1477	-1.33	0.94	319.15	1692	-2.00	0.90
277.60	1482	-1.33	0.35	320.23	1697	-1.98	0.99
279.30	1487	-1.60	0.73	321.31	1702	-2.20	0.13
281.00	1492	-1.51	0.53	322.38	1707	-2.31	0.49
281.66	1497	-1.82	0.81	323.46	1712	-2.41	1.06
282.06	1500	-1.82	1.02	324.54	1717	-2.65	0.92
282.72	1505	-1.55	0.95	325.62	1722	-2.40	1.07
283.39	1510	-2.03	0.77	326.69	1727	-2.43	0.51
284.05	1515	-2.00	0.79	327.77	1732	-2.51	0.77
284.71	1520	-2.06	0.87	328.85	1737	-2.42	0.56
285.37	1525	-2.11	0.67	329.92	1742	-2.41	0.50
286.04	1530	-2.16	0.65	331.00	1747	-2.24	0.38
286.70	1535	-1.96	0.87	332.08	1752	-2.49	0.15
287.36	1540	-2.07	0.58	333.15	1757	-2.22	0.46
288.02	1545	-2.05	0.79	334.23	1762	-2.17	0.42
288.69	1550	-1.60	0.89	335.31	1767	-2.22	-0.14
289.35	1555	-1.78	0.82	336.38	1772	-1.62	0.02
290.01	1560	-1.67	1.20	337.46	1777	-1.51	-0.10
290.67	1565	-1.70	0.93	339.62	1787	-1.17	0.23
291.34	1570	-1.66	0.97	340.69	1792	-1.04	0.34
292.00	1575	-1.68	0.69	341.77	1797	-1.17	-0.04
293.17	1580	-1.69	0.82	342.85	1802	-0.73	0.72
294.34	1585	-1.63	0.66	343.92	1807	-1.13	0.41
295.50	1590	-1.54	0.89	345.00	1812	-1.02	0.15
296.67	1595	-1.47	0.74	346.26	1817	-1.11	0.45
297.84	1600	-1.50	0.60	347.52	1822	-0.82	0.47
299.01	1605	-1.81	0.96	350.04	1832	-1.08	0.51
300.18	1610	-1.88	0.83	351.30	1837	-1.13	0.50

Age kyr BP	Depth (cm)	$\delta^{18}O$	$\delta^{13}C$
352.56	1842	-1.15	0.68
353.81	1847	-1.19	0.54
355.07	1852	-1.24	0.71
356.33	1857	-1.33	0.33
357.59	1862	-1.07	0.73
358.73	1867	-1.27	0.60
359.35	1872	-1.16	1.01
359.98	1877	-1.43	0.73
360.60	1882	-1.58	1.06

Table B. *G. ruber* Mg/Ca (mmol/mol) and inferred SST

Age kyr BP	Depth (cm)	Mg/Ca	SST (°C)	Age kyr BP	Depth (cm)	Mg/Ca	SST (°C)
0.89	0	4.94	28.49	8.77	107	4.75	28.06
1.02	2	4.88	28.37	8.96	110	4.24	26.81
1.22	5	4.48	27.41	9.09	112	4.53	27.53
1.47	7	4.41	27.25	9.28	115	4.62	27.77
2.10	12	4.46	27.37	9.41	117	4.49	27.43
2.47	15	4.54	27.57	9.97	120	4.69	27.93
2.72	17	4.77	28.12	10.34	122	4.52	27.52
3.10	20	4.33	27.03	10.89	125	4.45	27.34
3.35	22	4.53	27.54	11.26	127	4.32	27.00
3.50	25	4.74	28.03	11.50	130	3.87	25.79
3.60	27	4.71	27.97	11.66	132	4.61	27.74
3.76	30	4.52	27.51	11.90	135	4.37	27.13
3.86	32	4.64	27.81	12.06	137	4.60	27.72
4.01	35	4.92	28.45	12.30	140	4.81	28.19
4.18	37	4.69	27.92	12.46	142	4.36	27.12
4.42	40	4.89	28.38	12.69	145	4.27	26.89
4.58	42	4.19	26.66	12.85	147	4.07	26.34
4.83	45	4.86	28.32	13.02	150	4.01	26.17
4.99	47	4.93	28.48	13.12	152	3.97	26.06
5.23	50	5.17	29.01	13.28	155	4.29	26.94
5.40	52	4.86	28.32	13.39	157	4.03	26.23
5.64	55	4.69	27.93	13.71	160	4.38	27.16
5.81	57	4.77	28.11	13.92	162	4.34	27.06
6.05	60	5.08	28.82	14.24	165	4.30	26.97
6.21	62	5.16	28.98	14.45	167	3.95	26.01
6.46	65	4.86	28.32	14.76	170	3.99	26.13
6.62	67	4.63	27.79	14.97	172	4.31	26.99
6.86	70	4.71	27.96	15.46	175	4.52	27.52
7.03	72	4.55	27.58	15.79	177	4.45	27.34
7.21	75	4.93	28.47	16.28	180	4.14	26.53
7.34	77	4.57	27.65	16.36	182	3.93	25.97
7.53	80	4.76	28.08	16.48	185	4.00	26.16
7.65	82	4.36	27.12	16.55	187	3.64	25.11
7.84	85	4.74	28.04	16.67	190	3.98	26.10
7.96	87	4.41	27.25	16.75	192	3.76	25.47
8.15	90	4.47	27.39	17.04	195	3.86	25.76
8.20	92	4.53	27.54	17.23	197	3.81	25.61
8.27	95	4.84	28.27	17.52	200	3.89	25.85
8.32	97	4.73	28.01	17.72	202	4.04	26.26
8.39	100	4.87	28.33	18.01	205	3.72	25.35
8.44	102	4.49	27.45	18.20	207	3.58	24.93
8.64	105	4.55	27.59	18.47	210	3.42	24.41

Age kyr BP	Depth (cm)	Mg/Ca	SST (^{o}C)	Age kyr BP	Depth (cm)	Mg/Ca	SST (^{o}C)
18.64	212	3.47	24.56	33.19	347	3.44	24.18
18.91	215	3.59	24.96	33.90	352	3.99	25.84
19.08	217	3.59	24.95	34.62	357	3.98	25.81
19.29	220	3.63	25.07	35.34	362	3.82	25.36
19.43	222	3.46	24.55	36.05	367	3.69	24.97
19.63	225	3.03	23.07	36.77	372	3.58	24.63
19.77	227	3.24	23.80	37.49	377	3.71	25.03
19.97	230	3.50	24.67	38.20	382	3.65	24.84
20.11	232	3.61	25.03	38.92	387	3.61	24.72
20.32	235	3.45	24.52	39.64	392	3.60	24.70
20.45	237	3.45	24.51	40.35	397	3.74	25.12
20.66	240	3.71	25.33	41.07	402	3.56	24.57
20.80	242	3.73	25.37	41.79	407	3.50	24.37
21.00	245	3.70	25.27	42.50	412	3.45	24.22
21.14	247	3.43	24.43	43.22	417	3.57	24.61
21.34	250	3.61	25.03	43.94	422	3.90	25.60
21.48	252	3.41	24.38	45.37	432	3.88	25.52
21.69	255	3.54	24.79	46.09	437	3.96	25.75
21.82	257	3.38	24.30	46.80	442	3.51	24.42
22.03	260	3.71	25.31	47.52	447	3.32	23.78
22.17	262	3.60	24.97	48.23	452	3.48	24.31
22.84	265	3.50	24.67	48.95	457	3.43	24.17
23.29	267	3.40	24.35	49.67	462	3.46	24.24
23.96	270	3.23	23.79	50.38	467	4.10	26.14
24.41	272	3.43	24.45	51.10	472	3.88	25.54
24.54	275	3.52	24.72	51.82	477	4.20	26.41
24.63	277	3.45	24.51	52.53	482	3.83	25.37
24.77	280	3.57	24.88	53.25	487	4.14	26.25
24.86	282	3.55	24.82	53.97	492	3.71	25.04
24.99	285	3.42	24.41	54.68	497	4.16	26.29
25.08	287	3.33	24.12	55.40	502	4.02	25.92
25.21	290	3.46	24.53	56.12	507	3.87	25.48
25.30	292	3.77	25.51	56.83	512	4.34	26.77
25.73	295	3.64	25.10	57.55	517	3.82	25.35
26.02	297	3.65	25.14	58.98	527	3.86	25.46
26.74	302	3.82	25.35	59.70	532	3.83	25.40
27.45	307	3.50	24.40	60.42	537	3.84	25.41
28.17	312	3.54	24.50	61.13	542	3.59	24.68
28.89	317	3.61	24.71	61.85	547	3.65	24.85
29.60	322	3.45	24.21	62.57	552	3.33	23.81
31.04	332	3.36	23.94	64.00	562	3.35	23.91
31.75	337	3.60	24.68	66.75	567	3.54	24.49
32.47	342	3.68	24.94	69.50	572	3.51	24.41

Age kyr BP	Depth (cm)	Mg/Ca	SST (^{o}C)	Age kyr BP	Depth (cm)	Mg/Ca	SST (^{o}C)
72.25	577	3.68	24.93	119.31	797	4.57	27.34
75.00	582	3.76	25.17	120.54	802	4.93	28.19
75.98	587	4.04	25.97	121.77	807	5.26	28.90
76.95	592	3.30	23.72	123.00	812	5.56	29.53
78.12	598	3.52	24.44	124.06	817	4.98	28.30
78.91	602	3.88	25.53	125.11	822	5.29	28.97
79.88	607	4.11	26.16	126.17	827	5.19	28.76
80.86	612	3.89	25.55	127.22	832	5.67	29.74
81.83	617	4.17	26.33	128.28	837	5.49	29.38
82.81	622	4.56	27.32	129.33	842	5.37	29.14
83.79	627	4.40	26.93	130.39	847	5.30	29.00
84.76	632	4.52	27.22	131.44	852	4.71	27.67
85.74	637	4.20	26.41	132.50	857	4.26	26.57
86.72	642	4.33	26.74	134.61	867	4.06	26.02
87.69	647	3.78	25.24	135.67	872	3.66	24.88
88.67	652	3.52	24.44	136.72	877	4.00	25.88
90.62	662	3.34	23.86	138.83	887	3.93	25.68
91.60	667	3.80	25.31	139.89	892	4.14	26.24
92.57	672	3.97	25.78	140.94	897	3.71	25.03
93.55	677	3.80	25.29	142.00	902	3.39	24.03
94.53	682	4.14	26.26	143.39	907	3.92	25.64
95.50	687	4.26	26.58	144.78	912	4.25	26.53
96.48	692	3.93	25.66	146.17	917	3.91	25.62
97.46	697	4.03	25.96	150.33	932	3.58	24.65
98.43	702	4.21	26.42	154.50	947	3.89	25.56
99.41	707	4.00	25.87	155.89	952	4.27	26.60
100.38	712	4.23	26.49	157.28	957	4.43	26.99
101.36	717	4.41	26.94	158.67	962	4.18	26.36
102.34	722	4.62	27.46	160.06	967	3.82	25.35
103.31	727	4.31	26.70	161.44	972	3.86	25.47
104.29	732	4.53	27.25	162.83	977	4.01	25.90
105.27	737	4.61	27.45	164.22	982	4.05	25.99
106.24	742	4.71	27.69	165.61	987	3.94	25.70
107.22	747	4.32	26.72	167.00	992	3.82	25.36
108.25	752	4.34	26.78	167.96	997	4.18	26.35
109.48	757	4.41	26.96	168.92	1002	4.07	26.07
110.70	762	4.21	26.44	169.88	1007	3.77	25.21
111.93	767	3.79	25.26	170.85	1012	3.88	25.54
113.16	772	4.02	25.92	171.81	1017	3.81	25.32
114.39	777	4.27	26.59	172.77	1022	3.81	25.32
115.62	782	3.96	25.76	173.73	1027	3.87	25.49
116.85	787	4.28	26.62	174.69	1032	3.59	24.65
118.08	792	4.37	26.85	175.65	1037	4.11	26.17

Age kyr BP	Depth (cm)	Mg/Ca	SST (^{o}C)	Age kyr BP	Depth (cm)	Mg/Ca	SST (^{o}C)
176.62	1042	4.02	25.93	228.15	1257	3.93	25.67
177.58	1047	4.09	26.11	229.20	1262	3.84	25.42
178.54	1052	4.09	26.10	230.25	1267	3.52	24.43
179.50	1057	3.79	25.27	231.30	1272	3.84	25.41
180.46	1062	3.77	25.22	232.35	1277	3.82	25.35
181.42	1067	4.38	26.87	233.40	1282	4.29	26.64
182.38	1072	4.61	27.44	234.45	1287	4.33	26.75
183.35	1077	4.55	27.30	235.50	1292	4.45	27.04
184.31	1082	3.53	24.47	236.55	1297	4.70	27.65
185.27	1087	3.41	24.10	237.60	1302	5.00	28.35
186.23	1092	3.44	24.20	238.65	1307	4.84	27.98
187.19	1097	3.41	24.09	239.70	1312	4.99	28.33
188.15	1102	3.78	25.24	240.75	1317	5.16	28.69
189.12	1107	3.76	25.19	241.80	1322	4.33	26.75
190.08	1112	3.66	24.88	242.85	1327	4.25	26.55
191.04	1117	3.75	25.15	243.90	1332	3.99	25.85
192.00	1122	3.77	25.21	244.95	1337	4.12	26.18
193.38	1127	3.99	25.84	246.00	1342	4.03	25.93
194.75	1132	3.88	25.52	246.81	1347	3.85	25.44
196.13	1137	4.17	26.33	247.62	1352	3.95	25.72
197.50	1142	4.42	26.98	249.24	1362	3.54	24.51
198.88	1147	4.54	27.28	250.06	1367	3.67	24.91
200.25	1152	4.73	27.72	250.87	1372	3.90	25.58
201.63	1157	4.74	27.74	251.68	1377	3.39	24.03
203.00	1162	4.49	27.14	252.49	1382	3.80	25.30
204.38	1167	4.60	27.41	253.30	1387	3.80	25.31
205.75	1172	4.28	26.63	254.11	1392	3.98	25.82
207.13	1177	4.64	27.52	254.92	1397	4.08	26.07
208.50	1182	4.34	26.76	255.73	1402	4.06	26.03
209.88	1187	4.45	27.05	256.54	1407	3.94	25.69
211.25	1192	4.52	27.23	257.36	1412	3.84	25.40
212.63	1197	4.97	28.28	258.17	1417	3.84	25.40
214.00	1202	4.80	27.89	258.98	1422	3.81	25.34
215.38	1207	4.99	28.32	259.79	1427	4.04	25.98
216.75	1212	4.80	27.89	260.60	1432	3.91	25.60
218.13	1217	4.82	27.94	262.30	1437	4.02	25.93
219.50	1222	5.15	28.66	264.00	1442	3.91	25.62
220.88	1227	4.85	28.01	265.70	1447	4.20	26.40
222.25	1232	4.26	26.58	267.40	1452	3.73	25.09
223.63	1237	4.17	26.32	269.10	1457	3.57	24.61
225.00	1242	4.50	27.18	270.80	1462	3.52	24.44
226.05	1247	3.83	25.39	272.50	1467	3.51	24.43
227.10	1252	3.93	25.67	274.20	1472	3.78	25.24

Age kyr BP	Depth (cm)	Mg/Ca	SST (^{o}C)	Age kyr BP	Depth (cm)	Mg/Ca	SST (^{o}C)
275.90	1477	3.57	24.59	320.23	1697	4.26	26.58
277.60	1482	3.63	24.80	321.31	1702	4.48	27.13
279.30	1487	3.56	24.57	322.38	1707	4.53	27.25
281.00	1492	3.58	24.62	323.46	1712	4.16	26.31
281.66	1497	3.35	23.90	324.54	1717	5.06	28.47
282.06	1500	3.71	25.02	325.62	1722	5.07	28.49
282.72	1505	3.59	24.66	326.69	1727	5.22	28.82
283.39	1510	4.38	26.88	327.77	1732	5.23	28.84
284.05	1515	4.34	26.78	328.85	1737	4.88	28.09
284.71	1520	4.68	27.61	329.92	1742	4.87	28.05
285.37	1525	4.63	27.50	331.00	1747	4.83	27.96
286.04	1530	4.49	27.16	332.08	1752	4.54	27.27
286.70	1535	4.57	27.36	333.15	1757	5.36	29.11
287.36	1540	4.84	27.98	334.23	1762	4.94	28.22
288.02	1545	4.47	27.10	335.31	1767	4.55	27.29
288.69	1550	4.22	26.45	336.38	1772	4.81	27.92
289.35	1555	4.05	25.99	337.46	1777	4.46	27.07
290.01	1560	3.79	25.28	338.54	1782	4.69	27.63
290.67	1565	3.78	25.25	339.62	1787	4.05	25.99
291.34	1570	3.59	24.65	340.69	1792	4.03	25.94
292.00	1575	3.49	24.34	341.77	1797	3.82	25.34
293.17	1580	3.70	25.00	342.85	1802	4.02	25.92
294.34	1585	4.03	25.95	343.92	1807	3.85	25.45
295.50	1590	3.99	25.84	345.00	1812	4.59	27.39
296.67	1595	3.74	25.13	346.26	1817	3.33	23.84
297.84	1600	3.72	25.05	347.52	1822	3.58	24.64
299.01	1605	3.99	25.83	348.78	1827	3.71	25.03
300.18	1610	3.87	25.49	350.04	1832	3.72	25.06
301.35	1615	4.05	26.00	351.30	1837	4.27	26.60
302.51	1620	4.45	27.05	352.56	1842	3.60	24.68
304.85	1630	4.33	26.75	353.81	1847	3.95	25.72
306.02	1635	4.19	26.38	355.07	1852	3.87	25.50
307.19	1640	4.38	26.87	356.33	1857	3.99	25.84
308.36	1645	4.34	26.78	357.59	1862	4.12	26.18
309.99	1652	4.61	27.44	358.73	1867	4.22	26.46
311.16	1657	4.72	27.70	359.35	1872	4.43	27.01
312.33	1662	4.55	27.30	359.98	1877	4.02	25.93
313.50	1667	4.67	27.59	360.60	1882	4.01	25.89
314.66	1672	4.43	27.00				
315.83	1677	4.41	26.95				
317.00	1682	4.11	26.15				
318.08	1687	4.09	26.11				
319.15	1692	4.27	26.59				

Table C. Calculated surface water oxygen isotope $\delta^{18}O_{SW}$ (‰, VSMOW)

Age kyr BP	Depth (cm)	$\delta^{18}O_{SW}$	Age kyr BP	Depth (cm)	$\delta^{18}O_{SW}$
0.89	0	0.87	8.96	110	0.32
1.02	2	0.24	9.28	115	0.32
1.22	5	0.09	9.97	120	0.73
1.47	7	-0.10	10.89	125	0.38
2.10	12	0.07	11.26	127	0.53
2.47	15	0.53	11.50	130	0.40
2.72	17	0.59	11.66	132	0.57
3.10	20	0.28	11.90	135	0.89
3.35	22	0.33	12.06	137	1.00
3.50	25	0.44	12.30	140	1.25
3.60	27	0.59	12.46	142	0.78
3.76	30	0.24	12.69	145	0.93
3.86	32	0.28	12.85	147	0.58
4.01	35	0.59	13.02	150	1.02
4.18	37	0.32	13.12	152	0.57
4.42	40	0.55	13.28	155	0.95
4.58	42	0.09	13.39	157	0.67
4.83	45	0.53	13.71	160	0.97
4.99	47	0.89	14.24	165	1.05
5.23	50	0.42	14.45	167	0.92
5.40	52	0.67	14.76	170	1.01
5.64	55	0.69	14.97	172	1.32
5.81	57	0.94	15.46	175	1.54
6.05	60	0.60	15.79	177	1.36
6.21	62	1.00	16.28	180	1.39
6.46	65	0.48	16.36	182	1.20
6.62	67	0.76	16.48	185	1.23
6.86	70	0.37	16.55	187	1.28
7.03	72	0.46	16.67	190	1.37
7.21	75	0.61	16.75	192	1.23
7.34	77	0.46	17.04	195	1.30
7.53	80	0.69	17.23	197	1.60
7.65	82	0.87	17.52	200	1.27
7.84	85	0.15	17.72	202	1.51
7.96	87	0.58	18.01	205	1.37
8.15	90	0.48	18.20	207	1.37
8.20	92	0.19	18.47	210	1.23
8.27	95	0.33	18.64	212	1.00
8.32	97	0.06	18.91	215	1.56
8.39	100	0.55	19.08	217	1.58
8.44	102	0.30	19.29	220	1.29
8.64	105	0.53	19.43	222	1.46

Age kyr BP	Depth (cm)	$\delta^{18}O_{SW}$	Age kyr BP	Depth (cm)	$\delta^{18}O_{SW}$
19.63	225	1.02	36.77	372	1.04
19.77	227	1.29	37.49	377	1.10
19.97	230	1.38	38.20	382	0.99
20.11	232	1.07	38.92	387	1.14
20.32	235	1.41	39.64	392	0.96
20.45	237	1.45	40.35	397	1.05
20.66	240	1.37	41.07	402	0.89
20.80	242	1.30	41.79	407	0.68
21.00	245	1.45	42.50	412	0.73
21.14	247	1.17	43.22	417	1.00
21.34	250	1.36	43.94	422	0.93
21.48	252	0.78	45.37	432	0.99
21.69	255	1.36	46.09	437	1.30
21.82	257	1.17	46.80	442	0.97
22.03	260	1.32	47.52	447	0.74
22.17	262	1.48	48.23	452	0.86
22.84	265	1.44	48.95	457	0.69
23.29	267	1.31	49.67	462	0.64
23.96	270	1.17	50.38	467	1.13
24.41	272	1.08	51.10	472	0.82
24.54	275	1.28	51.82	477	1.19
24.63	277	0.92	52.53	482	0.88
24.77	280	1.39	53.25	487	1.03
24.86	282	1.04	53.97	492	0.80
24.99	285	1.18	54.68	497	1.01
25.08	287	1.28	55.40	502	0.99
25.21	290	1.01	56.12	507	0.94
25.30	292	1.50	57.55	517	1.11
25.73	295	1.23	58.98	527	0.95
26.02	297	1.20	59.70	532	1.09
26.74	302	1.21	60.42	537	1.26
27.45	307	1.11	61.13	542	1.20
28.17	312	1.07	61.85	547	0.79
28.89	317	1.15	62.57	552	0.87
29.60	322	0.99	64.00	562	0.81
31.04	332	0.85	66.75	567	0.60
31.75	337	1.15	69.50	572	0.59
32.47	342	1.06	72.25	577	0.44
33.19	347	0.83	75.00	582	0.42
33.90	352	1.07	75.98	587	0.68
34.62	357	1.25	76.95	592	0.00
35.34	362	1.05	78.91	602	0.50
36.05	367	1.03	79.88	607	0.51

Age kyr BP	Depth (cm)	$\delta^{18}O_{SW}$	Age kyr BP	Depth (cm)	$\delta^{18}O_{SW}$
80.86	612	0.73	127.22	832	0.81
81.83	617	0.59	128.28	837	0.98
82.81	622	0.79	129.33	842	1.04
83.79	627	0.69	130.39	847	0.88
84.76	632	0.81	131.44	852	1.01
85.74	637	0.65	132.50	857	1.24
86.72	642	0.59	134.61	867	1.60
87.69	647	0.44	135.67	872	1.45
88.67	652	0.62	136.72	877	1.41
90.62	662	0.42	138.83	887	1.16
91.60	667	0.68	139.89	892	1.69
92.57	672	0.75	140.94	897	1.28
93.55	677	0.63	142.00	902	1.18
94.53	682	0.74	143.39	907	1.64
95.50	687	0.65	144.78	912	1.32
96.48	692	0.59	146.17	917	1.07
97.46	697	0.60	150.33	932	1.17
98.43	702	0.76	154.50	947	1.33
99.41	707	0.40	155.89	952	1.62
100.38	712	0.60	157.28	957	1.64
101.36	717	0.79	158.67	962	1.66
102.34	722	0.77	160.06	967	1.41
103.31	727	0.62	161.44	972	1.57
104.29	732	0.79	162.83	977	1.58
105.27	737	0.70	164.22	982	1.42
106.24	742	0.74	165.61	987	1.27
108.25	752	0.69	167.00	992	1.10
109.48	757	0.55	167.96	997	1.61
110.70	762	0.62	168.92	1002	1.58
111.93	767	0.52	169.88	1007	1.10
113.16	772	0.72	170.85	1012	1.38
114.39	777	0.76	171.81	1017	0.89
115.62	782	0.43	172.77	1022	1.12
116.85	787	0.60	173.73	1027	0.70
118.08	792	0.45	174.69	1032	0.90
119.31	797	0.65	175.65	1037	0.78
120.54	802	0.65	176.62	1042	1.11
121.77	807	0.72	177.58	1047	0.94
123.00	812	0.52	178.54	1052	1.14
124.06	817	0.43	179.50	1057	0.72
125.11	822	0.69	180.46	1062	1.04
126.17	827	0.70	181.42	1067	1.22
127.22	832	0.81	182.38	1072	1.28

Age kyr BP	Depth (cm)	$\delta^{18}O_{SW}$	Age kyr BP	Depth (cm)	$\delta^{18}O_{SW}$
183.35	1077	1.53	235.50	1292	0.78
184.31	1082	1.03	236.55	1297	0.78
185.27	1087	0.87	237.60	1302	0.88
186.23	1092	1.04	238.65	1307	0.66
187.19	1097	0.73	239.70	1312	0.82
188.15	1102	0.70	240.75	1317	1.39
189.12	1107	0.81	241.80	1322	1.18
190.08	1112	0.61	242.85	1327	1.17
191.04	1117	0.56	243.90	1332	1.19
192.00	1122	0.64	244.95	1337	1.22
193.38	1127	0.85	246.00	1342	1.26
194.75	1132	0.56	246.81	1347	1.23
196.13	1137	0.60	247.62	1352	1.20
197.50	1142	0.87	249.24	1362	1.22
198.88	1147	0.57	250.06	1367	0.99
200.25	1152	0.81	250.87	1372	1.29
201.63	1157	0.88	251.68	1377	1.18
203.00	1162	1.04	252.49	1382	1.22
204.38	1167	1.14	253.30	1387	1.28
205.75	1172	0.83	254.11	1392	1.35
207.13	1177	0.95	254.92	1397	1.29
208.50	1182	0.74	255.73	1402	1.16
209.88	1187	0.77	256.54	1407	1.08
211.25	1192	0.66	257.36	1412	1.06
212.63	1197	1.01	258.17	1417	1.16
214.00	1202	0.97	258.98	1422	0.90
215.38	1207	1.04	259.79	1427	1.25
216.75	1212	1.07	260.60	1432	1.08
218.13	1217	1.27	262.30	1437	1.01
219.50	1222	1.53	264.00	1442	1.32
220.88	1227	1.31	265.70	1447	1.36
222.25	1232	1.24	267.40	1452	1.14
223.63	1237	1.29	269.10	1457	1.20
225.00	1242	1.26	270.80	1462	1.10
226.05	1247	1.15	272.50	1467	1.05
227.10	1252	0.94	274.20	1472	0.96
228.15	1257	0.91	275.90	1477	0.96
229.20	1262	1.06	277.60	1482	1.00
230.25	1267	0.77	279.30	1487	0.68
231.30	1272	0.45	281.00	1492	0.78
232.35	1277	0.51	281.66	1497	0.32
233.40	1282	0.73	282.72	1505	0.75
234.45	1287	0.69	283.39	1510	0.73

Age kyr BP	Depth (cm)	$\delta^{18}O_{SW}$	Age kyr BP	Depth (cm)	$\delta^{18}O_{SW}$
284.05	1515	0.75	331.00	1747	0.75
284.71	1520	0.86	332.08	1752	0.36
285.37	1525	0.79	334.23	1762	0.88
286.04	1530	0.67	335.31	1767	0.63
286.70	1535	0.91	336.38	1772	1.36
287.36	1540	0.92	337.46	1777	1.29
288.02	1545	0.76	339.62	1787	1.41
288.69	1550	1.07	340.69	1792	1.53
289.35	1555	0.81	341.77	1797	1.28
290.01	1560	0.76	342.85	1802	1.84
290.67	1565	0.72	343.92	1807	1.34
291.34	1570	0.64	345.00	1812	1.85
292.00	1575	0.56	346.26	1817	1.03
293.17	1580	0.68	347.52	1822	1.48
294.34	1585	0.94	350.04	1832	1.31
295.50	1590	1.01	351.30	1837	1.58
296.67	1595	0.93	352.56	1842	1.16
297.84	1600	0.89	353.81	1847	1.34
299.01	1605	0.74	355.07	1852	1.24
300.18	1610	0.60	356.33	1857	1.22
301.35	1615	0.52	357.59	1862	1.55
302.51	1620	1.04	358.73	1867	1.41
304.85	1630	0.79	359.35	1872	1.63
306.02	1635	0.80	359.98	1877	1.13
307.19	1640	0.74	360.60	1882	0.98
309.99	1652	0.67			
311.16	1657	0.90			
312.33	1662	0.57			
313.50	1667	0.71			
314.66	1672	0.75			
315.83	1677	0.67			
317.00	1682	0.91			
318.08	1687	0.75			
319.15	1692	0.71			
320.23	1697	0.72			
321.31	1702	0.62			
322.38	1707	0.53			
323.46	1712	0.24			
324.54	1717	0.45			
325.62	1722	0.70			
327.77	1732	0.66			
328.85	1737	0.59			
329.92	1742	0.60			

Table D. *G. ruber* Nd/Ca (μmol/mol)

Age kyr BP	Depth (cm)	Nd/Ca	Age kyr BP	Depth (cm)	Nd/Ca	Age kyr BP	Depth (cm)	Nd/Ca
0.89	0	0.300	8.96	110	0.182	17.13	196	0.762
1.02	2	0.334	9.09	112	0.189	17.23	197	0.534
1.22	5	0.302	9.28	115	0.205	17.52	200	0.617
1.47	7	0.372	9.41	117	0.297	17.62	201	0.368
1.85	10	0.251	9.97	120	0.255	17.72	202	0.480
2.10	12	0.325	10.34	122	0.262	18.01	205	0.511
2.47	15	0.320	10.89	125	0.214	18.20	207	0.532
2.72	17	0.348	11.07	126	0.191	18.47	210	0.579
3.10	20	0.273	11.26	127	0.192	18.64	212	0.923
3.35	22	0.250	11.50	130	0.189	18.91	215	0.731
3.50	25	0.292	11.58	131	0.266	19.08	217	0.909
3.60	27	0.297	11.66	132	0.234	19.29	220	0.734
3.76	30	0.252	11.90	135	0.156	19.43	222	0.817
3.86	32	0.228	11.98	136	0.167	19.77	227	0.526
4.01	35	0.242	12.06	137	0.252	19.97	230	0.654
4.18	37	0.283	12.30	140	0.221	20.11	232	0.792
4.42	40	0.413	12.38	141	0.211	20.32	235	1.021
4.58	42	0.229	12.46	142	0.215	20.45	237	0.904
4.83	45	0.230	12.69	145	0.166	20.66	240	0.863
5.23	50	0.190	12.85	147	0.211	20.80	242	0.779
5.40	52	0.198	13.02	150	0.200	21.00	245	0.902
5.64	55	0.270	13.12	152	0.198	21.14	247	0.770
5.81	57	0.273	13.28	155	0.437	21.34	250	0.759
6.05	60	0.266	13.39	157	0.294	21.48	252	0.958
6.21	62	0.366	13.71	160	0.270	21.69	255	0.801
6.46	65	0.251	13.92	162	0.261	21.82	257	0.837
6.62	67	0.263	14.24	165	0.272	22.03	260	0.740
6.86	70	0.202	14.45	167	0.177	22.17	262	0.770
7.03	72	0.223	14.76	170	0.225	22.84	265	0.679
7.21	75	0.273	14.97	172	0.280	23.29	267	1.103
7.34	77	0.232	15.46	175	0.294	23.96	270	0.656
7.53	80	0.284	15.79	177	0.298	24.41	272	0.744
7.65	82	0.315	16.28	180	0.346	24.54	275	0.925
7.84	85	0.236	16.32	181	0.334	24.63	277	1.153
7.96	87	0.203	16.36	182	0.429	24.77	280	0.882
8.15	90	0.203	16.48	185	0.298	24.86	282	0.916
8.20	92	0.276	16.51	186	0.539	24.99	285	0.813
8.27	95	0.238	16.55	187	0.400	25.08	287	0.914
8.32	97	0.222	16.67	190	0.239	25.21	290	0.764
8.39	100	0.201	16.71	191	0.245	25.30	292	0.649
8.44	102	0.243	16.75	192	0.335	25.73	295	0.637
8.64	105	0.174	17.04	195	0.415	26.02	297	0.791

Age kyr BP	Depth (cm)	Nd/Ca	Age kyr BP	Depth (cm)	Nd/Ca	Age kyr BP	Depth (cm)	Nd/Ca
26.45	300	0.714	57.55	517	0.391	104.29	732	0.370
26.74	302	0.677	58.27	522	0.478	105.27	737	0.404
27.45	307	0.678	58.98	527	0.674	106.24	742	0.415
28.17	312	0.587	59.70	532	0.757	107.22	747	0.687
28.89	317	0.677	60.42	537	0.879	108.25	752	0.737
29.60	322	0.443	61.13	542	0.972	109.48	757	0.615
31.04	332	0.418	61.85	547	1.088	110.70	762	0.680
31.75	337	0.626	62.57	552	0.848	111.93	767	0.887
32.47	342	0.488	63.28	557	0.977	113.16	772	0.579
33.19	347	0.282	64.00	562	0.513	115.62	782	0.482
33.90	352	0.352	66.75	567	0.772	116.85	787	0.763
34.62	357	0.328	69.50	572	0.732	118.08	792	0.697
35.34	362	0.329	72.25	577	0.792	119.31	797	0.449
36.05	367	0.267	75.00	582	0.666	121.77	807	0.467
36.77	372	0.343	75.98	587	0.696	123.00	812	0.304
37.49	377	0.410	76.95	592	0.557	124.06	817	0.281
38.20	382	0.578	77.93	597	0.497	125.11	822	0.301
38.92	387	0.518	78.91	602	0.493	126.17	827	0.303
39.64	392	0.572	79.88	607	0.455	127.22	832	0.270
40.35	397	0.381	80.86	612	0.330	128.28	837	0.442
41.07	402	0.302	81.83	617	0.250	129.33	842	0.272
41.79	407	0.346	82.81	622	0.261	130.39	847	0.374
42.50	412	0.333	83.79	627	0.292	131.44	852	0.263
43.22	417	0.450	84.76	632	0.374	132.50	857	0.265
43.94	422	0.442	85.74	637	0.318	133.56	862	0.189
44.65	427	0.278	86.72	642	0.437	134.61	867	0.348
45.37	432	0.310	87.69	647	0.636	135.67	872	0.366
46.09	437	0.466	88.67	652	0.690	136.72	877	0.288
46.80	442	0.464	89.64	657	0.538	137.78	882	0.378
47.52	447	0.554	90.62	662	0.711	138.83	887	0.430
48.23	452	0.518	91.60	667	0.407	139.89	892	0.502
48.95	457	0.449	92.57	672	0.362	140.94	897	0.357
49.67	462	0.256	93.55	677	0.556	142.00	902	0.399
50.38	467	0.271	94.53	682	0.626	143.39	907	0.535
51.10	472	0.318	95.50	687	0.587	144.78	912	0.429
51.82	477	0.301	96.48	692	0.495	146.17	917	0.432
52.53	482	0.291	97.46	697	0.493	150.33	932	0.327
53.25	487	0.313	98.43	702	0.488	151.72	937	0.419
53.97	492	0.201	99.41	707	0.615	155.89	952	0.282
54.68	497	0.267	100.38	712	0.343	157.28	957	0.299
55.40	502	0.328	101.36	717	0.304	158.67	962	0.342
56.12	507	0.273	102.34	722	0.316	160.06	967	0.436
56.83	512	0.252	103.31	727	0.320	161.44	972	0.433

Age kyr BP	Depth (cm)	Nd/Ca	Age kyr BP	Depth (cm)	Nd/Ca	Age kyr BP	Depth (cm)	Nd/Ca
162.83	977	0.441	215.38	1207	0.175	260.60	1432	0.294
164.22	982	0.449	216.75	1212	0.325	262.30	1437	0.352
165.61	987	0.667	218.13	1217	0.213	264.00	1442	0.467
167.00	992	0.344	219.50	1222	0.243	265.70	1447	0.541
167.96	997	0.368	220.88	1227	0.198	267.40	1452	0.604
168.92	1002	0.416	222.25	1232	0.283	269.10	1457	0.775
169.88	1007	0.559	225.00	1242	0.556	270.80	1462	0.983
170.85	1012	0.549	226.05	1247	0.842	272.50	1467	0.995
171.81	1017	0.511	227.10	1252	0.702	274.20	1472	1.133
172.77	1022	0.445	228.15	1257	0.635	275.90	1477	1.270
173.73	1027	0.399	229.20	1262	0.727	277.60	1482	1.155
174.69	1032	0.550	230.25	1267	0.854	279.30	1487	0.792
175.65	1037	0.352	231.30	1272	0.675	281.66	1497	0.322
176.62	1042	0.325	232.35	1277	0.587	282.06	1500	0.608
177.58	1047	0.292	233.40	1282	0.479	282.72	1505	0.574
178.54	1052	0.299	234.45	1287	0.555	283.39	1510	0.329
179.50	1057	0.282	235.50	1292	0.353	284.05	1515	0.362
180.46	1062	0.304	236.55	1297	0.215	284.71	1520	0.315
181.42	1067	0.374	237.60	1302	0.231	285.37	1525	0.195
182.38	1072	0.409	238.65	1307	0.195	286.04	1530	0.208
183.35	1077	0.547	239.70	1312	0.234	286.70	1535	0.173
184.31	1082	0.815	240.75	1317	0.221	287.36	1540	0.341
185.27	1087	1.064	241.80	1322	0.274	288.02	1545	0.452
187.19	1097	0.890	242.85	1327	0.231	288.69	1550	0.544
188.15	1102	0.903	243.90	1332	0.289	289.35	1555	0.464
189.12	1107	0.919	244.95	1337	0.290	290.01	1560	0.481
190.08	1112	0.856	246.00	1342	0.281	290.67	1565	0.636
191.04	1117	0.883	246.81	1347	0.281	291.34	1570	0.644
192.00	1122	0.604	247.62	1352	0.444	292.00	1575	0.661
193.38	1127	0.598	249.24	1362	0.553	293.17	1580	0.580
194.75	1132	0.743	250.06	1367	0.458	294.34	1585	0.554
196.13	1137	0.564	250.87	1372	0.480	295.50	1590	0.544
197.50	1142	0.489	251.68	1377	0.435	296.67	1595	0.537
198.88	1147	0.309	252.49	1382	0.426	297.84	1600	0.526
200.25	1152	0.282	253.30	1387	0.344	299.01	1605	0.464
201.63	1157	0.254	254.11	1392	0.297	301.35	1615	0.413
203.00	1162	0.379	254.92	1397	0.336	302.51	1620	0.548
204.38	1167	0.373	255.73	1402	0.257	303.68	1625	0.468
205.75	1172	0.336	256.54	1407	0.286	304.85	1630	0.465
207.13	1177	0.338	257.36	1412	0.325	306.02	1635	0.463
208.50	1182	0.336	258.17	1417	0.300	307.19	1640	0.422
209.88	1187	0.225	258.98	1422	0.256	308.36	1645	0.376
211.25	1192	0.264	259.79	1427	0.301	309.99	1652	0.298

Age kyr BP	Depth (cm)	Nd/Ca	Age kyr BP	Depth (cm)	Nd/Ca
311.16	1657	0.319	359.35	1872	0.233
312.33	1662	0.285	359.98	1877	0.634
313.50	1667	0.282	360.60	1882	0.628
314.66	1672	0.283			
315.83	1677	0.480			
317.00	1682	0.549			
318.08	1687	0.544			
319.15	1692	0.462			
320.23	1697	0.472			
321.31	1702	0.508			
322.38	1707	0.330			
323.46	1712	0.265			
324.54	1717	0.294			
325.62	1722	0.288			
326.69	1727	0.218			
327.77	1732	0.264			
328.85	1737	0.216			
329.92	1742	0.207			
331.00	1747	0.245			
332.08	1752	0.161			
333.15	1757	0.278			
334.23	1762	0.441			
335.31	1767	0.317			
336.38	1772	0.294			
337.46	1777	0.284			
338.54	1782	0.210			
339.62	1787	0.141			
340.69	1792	0.208			
341.77	1797	0.230			
342.85	1802	0.498			
343.92	1807	0.649			
345.00	1812	0.482			
346.26	1817	0.794			
347.52	1822	0.593			
348.78	1827	0.261			
350.04	1832	0.425			
351.30	1837	0.382			
352.56	1842	0.411			
353.81	1847	0.286			
355.07	1852	0.304			
356.33	1857	0.289			
357.59	1862	0.334			
358.73	1867	0.366			

Table E. Composite benthic foraminifera $\delta^{18}O$ (‰, VPDB)
Uvigerina spp.

Age kyr BP	Depth (cm)	$\delta^{18}O$	Age kyr BP	Depth (cm)	$\delta^{18}O$	Age kyr BP	Depth (cm)	$\delta^{18}O$
13.39	157	4.44	67.80	562	4.32	113.31	781	3.99
15.79	177	4.70	71.40	572	4.47	113.64	782	3.42
16.36	182	4.81	72.48	575	3.77	114.62	785	3.62
19.43	222	4.86	74.28	580	3.99	114.95	786	3.67
20.11	232	4.77	75.00	582	3.82	115.27	787	3.75
20.45	237	4.74	76.90	592	3.99	116.25	790	3.49
20.66	240	4.60	78.79	602	4.02	116.58	791	3.42
20.80	242	4.60	80.69	612	3.88	116.91	792	3.54
21.00	245	4.51	82.59	622	3.71	117.89	795	3.61
21.14	247	4.68	86.95	645	3.87	118.22	796	3.26
21.48	252	4.56	87.90	650	3.92	118.55	797	3.38
21.82	257	4.57	88.28	652	3.94	120.18	802	3.10
24.54	275	4.70	88.85	655	3.98	121.16	805	3.30
24.63	277	4.68	89.80	660	4.04	121.49	806	3.30
25.97	297	4.48	90.75	665	3.79	121.82	807	3.19
27.99	312	4.52	92.08	672	3.74	122.80	810	3.04
29.33	322	4.47	93.97	682	3.71	123.45	812	2.95
30.67	332	4.56	95.87	692	3.77	124.44	815	3.19
32.01	342	4.49	97.77	702	3.56	125.09	817	2.98
33.35	352	4.42	99.67	712	3.62	126.07	820	2.97
34.69	362	4.33	101.56	722	3.62	130.00	832	3.37
36.04	372	4.26	105.36	742	3.78	133.67	865	4.46
37.38	382	4.31	106.88	750	3.91	134.44	872	4.45
38.72	392	4.39	107.07	751	3.96	134.78	875	4.59
40.06	402	4.42	107.26	752	3.88	135.00	877	4.65
41.40	412	4.24	107.83	755	3.84	136.39	882	4.64
42.74	422	4.19	108.02	756	3.79	139.17	892	4.66
44.08	432	4.15	108.21	757	3.88	140.57	897	4.54
45.43	442	4.13	108.77	760	3.94	141.96	902	4.41
46.77	452	4.40	108.96	761	3.87	144.74	912	4.58
48.11	462	4.26	109.15	762	3.94	150.30	932	4.40
49.45	472	4.25	109.72	765	3.88	151.70	937	4.46
50.79	482	4.31	109.91	766	3.86	158.65	962	4.57
52.13	492	4.20	110.10	767	3.97	161.43	972	4.49
55.89	520	4.00	110.67	770	3.93	164.22	982	4.59
56.16	522	4.25	110.86	771	3.96	167.00	992	4.29
56.56	525	4.05	111.05	772	3.79	170.85	1012	4.36
57.23	530	4.32	111.62	775	3.95	172.77	1022	4.42
58.08	535	4.33	111.81	776	3.67	174.69	1032	4.12
60.60	542	4.43	112.00	777	3.92	176.62	1042	4.17
64.20	552	4.40	112.98	780	3.69	178.54	1052	4.21

Age kyr BP	Depth (cm)	$\delta^{18}O$	Age kyr BP	Depth (cm)	$\delta^{18}O$
180.46	1062	4.13	274.09	1482	4.12
182.38	1072	4.22	276.79	1492	4.08
184.31	1082	4.31	280.30	1505	3.80
185.27	1087	4.31	283.00	1515	3.61
186.23	1092	4.35	284.82	1525	3.58
188.15	1102	4.21	286.64	1535	3.62
190.08	1112	4.10	288.45	1545	3.52
192.00	1122	3.69	289.36	1550	3.82
194.36	1132	3.91	290.27	1555	3.99
196.73	1142	3.67	291.18	1560	4.05
199.09	1152	3.58	293.00	1570	3.97
201.45	1162	3.52	294.07	1575	4.19
202.64	1167	3.49	296.21	1585	4.02
203.35	1170	3.57	298.36	1595	3.99
203.82	1172	3.63	300.50	1605	3.94
204.53	1175	3.62	301.57	1610	3.87
205.00	1177	3.71	302.64	1615	3.61
206.96	1182	3.94	305.86	1630	3.69
212.07	1195	3.92	306.93	1635	3.73
214.82	1202	3.41	308.43	1642	3.65
216.56	1207	3.27	310.57	1652	3.54
222.18	1227	4.03	312.71	1662	3.41
223.58	1232	4.04	314.86	1672	3.49
226.39	1242	4.07	317.00	1682	3.64
229.19	1252	4.05	319.90	1692	3.46
232.00	1262	4.07	322.80	1702	3.30
233.68	1272	3.79	325.71	1712	3.21
235.36	1282	3.64	328.61	1722	3.05
237.05	1292	3.64	331.51	1732	3.03
238.73	1302	3.34	332.96	1737	3.48
240.41	1312	3.32	334.33	1747	4.60
244.28	1335	4.02	341.00	1802	4.61
245.46	1342	4.30	343.25	1812	4.67
247.14	1352	4.39	345.50	1822	4.53
248.82	1362	4.37	347.75	1832	4.43
250.51	1372	4.39	350.00	1842	4.70
252.19	1382	4.49	353.54	1862	4.01
253.87	1392	4.21	357.07	1882	4.12
255.55	1402	4.17			
257.24	1412	4.31			
258.92	1422	4.31			
263.30	1442	4.27			
271.40	1472	4.32			

Cibicidoides wuellerstorfi

Age kyr BP	Depth (cm)	$\delta^{18}O$
52.54	495	3.28
54.55	510	3.45
55.22	515	3.39
83.16	625	3.05
84.11	630	2.96
128.36	827	2.80
210.11	1190	2.73
214.04	1200	2.67
216.00	1205	2.59
223.02	1230	3.22
241.76	1320	2.79
334.33	1747	2.64
336.75	1767	2.62
337.97	1777	3.68
339.18	1787	3.53

Bulimina spp.

Age kyr BP	Depth (cm)	$\delta^{18}O$
59.88	540	4.39
132.78	857	4.31
190.85	1116	4.07
206.18	1180	3.60
208.14	1185	3.72
212.86	1197	3.41
212.86	1197	3.38
340.15	1795	4.60